Inertial Measurement Units for Human Body Monitoring, Healthcare, and Sports

Lead Guest Editor: Alessandro Mengarelli
Guest Editors: Federica Verdini and Bernardo Innocenti

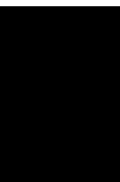# Inertial Measurement Units for Human Body Monitoring, Healthcare, and Sports

Inertial Measurement Units for Human Body Monitoring, Healthcare, and Sports

Lead Guest Editor: Alessandro Mengarelli
Guest Editors: Federica Verdini and Bernardo Innocenti

Contents

Research Article

Relationship between Lower Limb Kinematics and Upper Trunk Acceleration in Recreational Runners

Laura Simoni, Silvia Pancani ⓘ **, Federica Vannetti** ⓘ **, Claudio Macchi, and Guido Pasquini** ⓘ

Don Carlo Gnocchi Foundation IRCSS, 269 Via di Scandicci, 50143 Florence, Italy

Correspondence should be addressed to Silvia Pancani; spancani@dongnocchi.it

Upper trunk (UT) kinematics in runners and its relationship with lower limbs has been poorly investigated, although it is acknowledged that dynamic stability of the upper body is a primary objective of human locomotion. This study aimed to explore UT kinematics according to gender and level of training and in relation to lower limb run patterns described through the presence of: overstriding, crossover, excessive protonation, and pelvic drop. Lower body variables chosen to describe running pattern were those that are frequently modified during gait-retraining with the goal of reducing injury risk. Eighty-seven recreational runners (28 females and 59 males, age 41 ± 10 years) performed a one minute run test on a treadmill at self-selected speed. UT kinematics was measured using an inertial measurement unit, while run features were assessed through an optoelectronic system and video analysis. Accelerations and root-mean-square on mediolateral and anteroposterior axes, normalized using the vertical component of the acceleration, were estimated to describe UT stability. Results showed no significant differences in the normalized UT acceleration root-mean-square according to gender and level of training as well as according to the presence of overstriding, crossover, and excessive protonation. The only running strategy studied in this work that showed a significant relationship with UT stability was the presence of excessive pelvic drop. The latter was significantly associated ($p = 0.020$) to a decrease in the normalized acceleration root-mean-square along the mediolateral direction. Although the excessive pelvic drop seemed to have a positive effect in stabilizing the upper body, concerns remain on the effect of a poor control of the pelvis on the biomechanics of lower limbs. Results obtained confirm the hypothesis that the lower body is able to respond to varying impact load conditions to maintain UT stability.

1. Introduction

Running is one of the most popular recreational physical activities in the world, as it provides substantial health benefits at minimal expense [1]. Inertial measurement unit (IMU) is a sensor equipped with a triaxial accelerometer gyroscope and/or magnetometer, leading to a direct detection of the linear acceleration and angular velocity of the body segment to which they are attached. Accelerometers have been adopted in human joint kinematics studies since 1990s [2, 3] by attaching the sensors on foot, shank, thigh, and pelvis. Recent development and refinement in the technology have made IMUs less cumbersome, more economic, and ecological representing an alternative respect to the traditional 3D motion capture [4]. In recent years, the use of those sensors has been extended to the analysis of sport performances [5] and in particular of running gait [6]. Related research studies in the running field, employing an IMU system, focused mainly on lower limb kinematics [6] with several different purposes, such as describing the running pattern [7], investigating the epidemiology and risk factors for injuries [8], assessing the effect of biomechanical interventions on kinetic, kinematic, and spatiotemporal running variables during rehabilitation from running injuries [9], just to name a few. On the contrary, upper body biomechanics in runners has been poorly investigated, and reported measurements are mostly derived from triaxial accelerometers placed on the lower trunk, in the attempt to

describe the center of mass kinematics [1, 10]. However, it has been recognized that the dynamic stability of the upper body is a primary objective of human locomotion. Low and smooth accelerations of the upper body are considered as characteristics of a stable gait [1] that could be linked to lower energy consumption and reduced risk of injury [1, 11]. Upper trunk stability during walking and running results from attenuation mechanisms of the oscillations caused by the lower limb movements [12] and influences the transmission to the head of the shock provoked by the ground reaction force (GRF) [13]. During running gait, the collision of foot with ground generates the resultant GRF necessary for forward propulsion and support against gravity [1]. GRF provokes a shock from the lower to the upper body, along the kinetic chain [1, 13, 14] that is dissipated by the combination of passive (e.g., deformation of ligaments, muscle oscillation, increase in knee flexion, and limited protonation of the foot) and active mechanisms (e.g., increased muscle activation). Acceleration at any anatomical location depends on the shock level of attenuation at all points distal and from intensity and direction of GRF [1]. The pelvis and the spinal column play an important role in determining shock absorption. This attenuation manifests itself in the fact that the resultant acceleration tends to decrease going from tibia, to the pelvis, to head level. Level and number of repetition of this shock on musculoskeletal structures contribute to modify chronic running injury risks [1]. Even if it is recognized as a role of lower body kinematics in modulated shock transmission to the upper body [1, 15, 16] a thorough investigation on this topic have not been undertaken in running gait yet. Kawabata et al. measured lower and upper trunk (UT) accelerations in different phases of the running gait cycle, but they did not take into consideration lower limb movements [17]. So far, only a few attempts have been done to describe upper body kinematics and its relationship with lower limb movements. Mercer et al. assessed the characteristics of shock attenuation during high-speed running, concluding that shock attenuation increases linearly with running speed, and changes in running kinematics are characterized primarily by changes in the stride length [14]. Specific lower limb running pattern has been observed to alter intensity of the initial shock and intensity and direction of the GRF, having a certain influence on the level of shock transmitted to the upper body and its stability [18–20]. For example, the initial shock provoked by foot-ground collision during running can be modified by initial contact foot-strike pattern (rearfoot or forefoot) [19]. Some authors observed an influence of crossover gait and level of foot protonation on the mediolateral component of the GRF [21–24]. Other factors that are supposed to influence trunk stability during gait are gender and level of training, but studies exist only with regard to lower trunk level or walking gait [11, 24]. However, to the best of the authors knowledge, no study directly investigated the relationship between acceleration of the UT and gender, level of training, and lower limb and pelvis run pattern, described through the foot-strike pattern, presence of overstriding, crossover, excessive protonation (EPR), and pelvic drop (EPD), which have already been demonstrated to influence intensities and

direction of the GRF, shock transmission, and running-related injuries [7, 18–20, 25–28]. This study aims to fill this gap in the literature by characterizing UT kinematics by exploring differences in the UT kinematics according to gender and level of training and in relation to lower limb run pattern. The proposed analysis will be conducted by using an IMU placed on the UT.

2. Methods

2.1. Participants and Experimental Procedure. 87 recreational runners (28 females and 59 males) volunteered to participate in the study. Participants signed a written informed consent. The study was approved by the Don Gnocchi ethic committee. Inclusion criteria were being engaged in a running program (at least two sessions a week with a minimum continuous running time of 20 minutes per session), being free from injuries in the last two months and being free from chronic musculoskeletal diseases.

Subjects were requested to run on a treadmill following a previously developed protocol [28]. Five minutes of warm-up and familiarization with the treadmill and one minute of run test (approximately 150 running cycles) were carried out by each subject. Participants were asked to run at a self-selected speed [28, 29]. Self-selected speed was chosen to control for differences in running kinematics that could arise at a speed different from the habitual training one (either too low or too high) [17]. All participants wore conventional, neutral running shoes to avoid potential influence shoes which may have on gait mechanics [29].

2.2. Instrumentation. Running analysis was carried out by using a high-resolution IMU (Gyko, Microgate, Bolzano, Italy) in combination with a marker-less optical system (Optogait, Microgate, Bolzano, Italy) and video analysis. The IMU was equipped with a triaxial accelerometer, a triaxial gyroscope, and a triaxial magnetometer to measure linear acceleration, angular velocity, and magnetic field. The IMU was perpendicularly attached to an elastic harness provided with the system through automatic buttons. By using the manufacturer-provided harness, the IMU was positioned with the y-axis parallel to the back midline between the scapulae and the z-axis parallel to the line drawn between T1 to T5. This procedure was followed to approximately align the IMU to the anatomical axes, identified through anatomical landmarks and guided by the harness provided by the manufacturer. The sensor was oriented with the X-axis pointing backwards, representing the anterior-posterior direction (AP), the Y-axis pointing to the left representing the mediolateral direction (ML) and the Z-axis pointing downwards representing the vertical direction (V) (Figure 1). Data were sampled at a frequency of 1000 Hz.

The Optogait system is made up of two couples of transmitting and receiving bars. Each bar contains 96 LEDs that transmit on an infrared frequency with the same number of LEDs on the opposite bar. The system detects interruptions in the transmission between the bars. The first interruption of the LED signal during contact time is

FIGURE 1: Placement of the inertial measurement unit at the upper-trunk level and axis orientation.

defined as "Initial Contact" and the portion of contact time during which the foot interrupts the maximum number of LEDs is defined as "Midstance phase." Bars were placed on the sides of the treadmill tape, at the ground level, and fixed with adhesive tape to avoid movements caused by treadmill vibrations. The IMU and the Optogait systems were synchronized automatically by software provided by the manufacturer. In addition, the Optogait system was synchronized with two high-resolution cameras to film the frontal and sagittal planes of the participants. The videos were used to make frame-by-frame running video analysis provided by Kinovea software (version 0.8.15). Relevant landmarks for the videographic reference were marked using colored tape. Markers were placed on the low back at the level of the 5th lumbar (L5) vertebra and bilaterally by the external malleolus, the midline of the distal heel counter, the head of the fibula, the lateral condyle of the femur, the great trochanter, and the posterior iliac superior spine.

2.3. Data Analysis and Measured Parameters. Data processing was performed using custom procedures written in MATLAB R2017a (MATLAB, Mathworks Inc., Natick, MA, USA). The IMU reference frame was first rotated to have the Z-axis aligned with the gravity vector during the static postures at the beginning of each trial [30]. The acquired acceleration signal was lowpass-filtered using a 2nd order zero-lag Butterworth filter. The cutoff frequency value was set to 20 Hz, after having checked the frequency content of signals collected. The acceleration root-mean-square (aRMS) was then calculated along each axis to quantify the trunk kinematics.

RMS of the acceleration was computed for each separated axis using the following equation:

$$\text{aRMS} = \frac{\sqrt{x_1^2 + x_2^2 + \ldots + x_N^2}}{N}, \tag{1}$$

where x is the acceleration measured along the AP, V, or ML axis and N is the number of samples. In this analysis, aRMS was computed over the entire duration of the signal.

The RMS calculated along the V-axis was then used to normalize the RMS contribution along AP and ML axes by using the following formula:

$$\text{naRMS\_}i = \frac{\text{aRMSi}}{\text{RMS\_}V}, \tag{2}$$

where i is the respective axis: AP or ML. This calculation resulted in a unitless ratio for each axis and was performed to account for influence of running speed on trunk acceleration [31].

Lower body variables chosen to describe running pattern were those that are frequently modified during gait-retraining with the goal of reducing injury risk [27] and that can be easily identified through a frame-by-frame video analysis, namely, the presence of rearfoot strike, overstriding, crossover, EPR, and EPD. Rearfoot strike, overstriding, and crossover were assessed to describe the running pattern at initial contact, EPR, and EPD at midstance. Running gait phases were identified by the use of the Optogait system, and the presence or not of the selected running patterns was detected by video analysis with manual digitation. Criteria used to assess the presence of rearfoot strike, overstriding, crossover, EPR, and EPD by 2D video analysis referred to those used in literature [7, 18, 27, 28]. In particular, rearfoot refers to initial contact made by the heel in which the heel lands before the ball of the foot, a midfoot strike refers to an initial contact in which the heel and the ball of the foot land quasisimultaneously, while in a forefoot strike the ball of the foot lands before the heel [7]. Overstriding occurs when, at initial contact, the knee is completely extended, and the ipsilateral foot lands anteriorly to the pelvis [27]. Markers placed on the external malleolus, the head of the fibula, and the lateral condyle of the femur and the great trochanter were used to observe the complete extension of the knee and the foot placement compared with the pelvis (assumed to be on the same axis of the great trochanter). Crossover occurs when both feet land on the contralateral side of the body midline during a gait cycle [18]. The body midline was identified with the vertical line passing through the marker placed on the L5 vertebra. EPR and EPD describe running strategy during the midstance phase [27]. EPR is a triplanar motion of the subtalar joint characterized by a flattening of the medial arch and a hypermobile midfoot [27]. EPR was assessed by evaluating, through 2D video analysis, heel eversion, as reported by Souza et al. [27]. Presence of EPD was ascertained by evaluating the position of the iliac crest on the stance limb, which in EPD, is characterized by an excessive elevation relative to the contralateral iliac crest during the first half of the stance phase [27].

2.4. Statistical Analysis. Statistical analysis was performed using the STATA 10.0 Software, from Stata Corporation

(College Station, Texas, USA). Data were firstly tested for normality using the Shapiro–Wilk test and then analyzed accordingly. Since acceleration measured at the lower trunk level was observed to be influenced by the training status [11], with more trained subjects showing lower aRMS values, differences in normalized aRMS were investigated between subjects with different training levels. The criterion to be considered more trained runners was running more than 50 kilometers per week [10]. An independent t-test, with a p value of 0.05 as significance level, was used to compare the two groups. The magnitude of the difference was assessed through the effect size (d) which was interpreted as low, if <0.3, medium, if comprised between 0.3 and 0.5, or large, if >0.5. The same analysis was conducted to investigate differences in normalized aRMS between males and females and subjects with different running patterns.

Then, normalized aRMS on each axis was entered, as the dependent variable, into a multiple linear regression model in which variables previously shown to be associated with aRMS with a p value <0.05, was considered as independent variables, while age, sex, weight, and height were assumed as confounding factors.

3. Results

Participants' characteristics are given in Table 1. Runners were aged between 19 and 61 years with a larger number of males (59/87, 68%). More than half of the participants exhibited a rearfoot strike pattern (67%), a crossover behavior (54%), and an EPR (57%), whereas most of them were free from overstriding (94%) and from EPD (64%). Because of the low number of subjects presenting overstriding, the parameter was excluded from further analysis. Normalized aRMS values observed along the AP and ML axes were comparable.

Table 2 shows normalized aRMS values measured along each axis in the male and female groups. Mean normalized aRMS for males was 0.203 ± 0.051, 0.212 ± 0.033, respectively, along the AP and ML directions. Similar values were observed in females (AP: 0.194 ± 0.048 and ML: 0.207 ± 0.024, $p > 0.05$; detailed p values are reported in Table 2).

More trained runners ran on average 62 km per week. When normalized aRMS was assessed in this group, values obtained were 0.196 ± 0.045 along the AP direction and 0.216 ± 0.026 along the ML direction. Averaged kilometer ran per week was 31 for the less-trained participants. Trunk accelerations measured in this group were not significantly different ($p > 0.05$, detailed p values are given in Table 2) from those measured in the most-trained group, with a normalized aRMS value of 0.202 ± 0.053 and 0.208 ± 0.032 along the AP and ML axes, respectively. Since no significant differences in the normalized aRMS were observed between males and females and between more- and less-trained runners, data were pooled in further analyses. A significant difference was found in normalized aRMS measured along the ML direction between runners who exhibited a tendency towards crossover and those who did not ($p = 0.023$, $d = 0.5$, Table 3), with a higher acceleration value measured in the second group.

TABLE 1: Sample's characteristics.

Subjects' characteristics	Mean ± SD
Sex (%F)	31%
Age (yrs)	41 ± 10
Height (cm)	174 ± 8
Mass (kg)	69 ± 10
Running velocity (m/s)	10.6 ± 1.5
Initial contact characteristics	
Rearfoot (%Y)	67%
Overstriding (%Y)	6%
Crossover (%Y)	54%
Midstance characteristics	
Excessive pronation (%Y)	57%
Excessive pelvic drop (%Y)	36%
Upper trunk acceleration patterns	
Anteroposterior aRMS (g)	0.278 ± 0.067
Mediolateral aRMS (g)	0.294 ± 0.045
Vertical aRMS (g)	1.400 ± 0.094
Anteroposterior naRMS*	0.191 ± 0.046
Mediolateral naRMS*	0.201 ± 0.027

*Normalized acceleration root-mean-square.

Along the same axis, acceleration of the UT was significantly lower in runners who had EPD compared with those that did not ($p = 0.032$, $d = 0.5$). Even when sociodemographic variables (age, sex, weight, and height) were included in the analysis as confounding factors, the presence of EPD remained significantly associated to a decrease in the aRMS along the ML direction ($p = 0.020$, Table 4).

4. Discussion

The aims of this study were to assess whether, in recreational runners, UT loading response and stance might be affected by sex, level of training, and lower body running pattern. The aim was accomplished by using an IMU, and a quantitative assessment of UT kinematics was obtained.

In our sample, no differences were found in terms of the aRMS on the AP and ML planes between men and women. The result is in agreement with findings observed for walking gait in a study of Mazzà et al., aiming to investigate gender differences in gait patterns [24]. Mazzà et al., by examining shock attenuation during gait, found similar values for the UT aRMS in men and women, when the gait was performed both at comfortable and fast speed.

In our group of runners, the level of training did not affect the measured aRMS (Table 2). Different from what observed in this study, Mc Gregor et al. reported significant differences in lower trunk acceleration when comparing a group of more-trained runners (semiprofessional athletes) with a group of recreational runners [11]. Discrepancies observed in the two studies may in part be the result of the different locations of the sensor (upper vs. lower trunk) and the consequent different shock attenuations provided by the intervertebral disks. However, more likely, the cause of different results obtained lays in the higher gap in training present between the two groups studied by Mc Gregor compared with the groups investigated in this study, with the latter including only recreational runners [11]. Indeed, more

Table 2: Normalized acceleration root-mean-square (naRMS) values measured along each axis in the male and female group and in the more trained and less trained ones.

		Males $n = 59$	Females $n = 27$	p	More trained $n = 30$	Less trained $n = 57$	p
	v (m/s)	3.1 ± 0.4	2.7 ± 0.3	**<0.001**	3.1 ± 0.5	2.9 ± 0.4	**0.004**
	km/sett	41.1 ± 19.2	41.9 ± 15.8	**0.856**	61.7 ± 11.4	30.7 ± 9.6	**<0.001**
UT acceleration variables							
Anteroposterior naRMS*		0.203 ± 0.051	0.194 ± 0.048	0.420	0.196 ± 0.045	0.202 ± 0.053	0.606
Mediolateral naRMS*		0.212 ± 0.033	0.207 ± 0.024	0.461	0.216 ± 0.026	0.208 ± 0.032	0.231

*Normalized acceleration root-mean-square.

Table 3: Normalized acceleration root-mean-square (naRMS) values of lower limbs parameters measured along each axis.

	Rearfoot		p	Crossover		p	Excessive pronation		p	Excessive pelvic drop		p
	Yes	No		Yes	No		Yes	No		Yes	No	
UT acceleration variables												
	$n = 58$	$n = 29$		$n = 43$	$n = 37$		$n = 45$	$n = 34$		$n = 29$	$n = 52$	
Anteroposterior naRMS* median (interquartile range)	0.211 (0.07)	0.186 (0.08)	0.115	0.186 (0.08)	0.216 (0.07)	0.053	0.196 (0.07)	0.210 (0.08)	0.759	0.181 (0.09)	0.206 (0.06)	0.344
Mediolateral naRMS* median (interquartile range)	0.214 (0.04)	0.210 (0.02)	0.089	0.202 (0.02)	0.217 (0.04)	**0.023**	0.213 (0.04)	0.203 (0.05)	0.109	0.202 (0.03)	0.214 (0.04)	**0.032**

*Normalized acceleration root-mean-square.

Table 4: Multiple linear regression describing the relationship between excessive pelvic drop and crossover with mediolateral naRMS, adjusted for age, sex, weight, and height.

Final model: obs = 86; prob > chi^2 < 0.036; R-square 0.170			
	Unstandardized coefficients	Standard error	p
naRMS* mediolateral			
Constant	0.301	0.114	0.010
Sex	−0.013	0.010	0.217
Age	0.000	0.000	0.517
Height	−0.001	0.001	0.473
Weight	0.000	0.001	0.798
Crossover	−0.011	0.006	0.103
Excessive pelvic drop	−0.016	0.007	**0.020**

*Normalized acceleration root-mean-square.

trained athletes develop a greater capacity to stabilize the trunk segments during running; however, this difference seems to become significant only in presence of an advanced level of training (professional and semiprofessional athletes).

Runners involved in this study did not show differences in UT aRMS, neither in the AP nor in the ML plane, in presence of different lower limb strategies with regard to the contact phase. The only running strategy that showed a significant relationship with UT stability was the EPD. To the best of the authors' knowledge, there are no studies in literature that have investigated possible correlations between running patterns and UT accelerations; thus, a direct comparison of results across studies is not possible.

Concerning different strike patterns, Gruber et al. investigated a group of habitual rearfoot runners and a group of habitual forefoot runners with the purpose of determining differences in the head and tibial acceleration signal power and shock attenuation [19]. What arose was that rearfoot strikers had significantly higher peak accelerations at the

tibia level in comparison with forefoot strikers, while accelerations at the head level were not different between the two groups. Authors concluded that the body has the capacity to manage a range of impulsive loads derived by the shock generated from the GRF, in order to protect the head from excessive acceleration and to guarantee the stability of the oculovestibular system, which seems to be in accordance with results obtained in this study [19, 32]. In fact, none of the lower limb running patterns analyzed in the present study did not influence UT accelerations, even if literature shows that they influence direction and/or intensity of the resultant GRF.

This principle might apply also to EPR, and this might be the reason why a relationship between EPR and UT stability was not detected in our runners. A certain degree of protonation is physiological, and it contributes to loading absorption [33]. However, literature is not in agreement on the effect of physiological and excessive protonation on the ML component of the GRF.

The only running strategy studied in this work that showed a significant relationship with UT stability was the EPD. Running patterns presenting EPD seemed to be associated to lower ML aRMS at the UT level during the entire gait cycle. Previous investigations confirmed this finding by observing an association between excessive pelvic drop and the reduction of shoulder and head displacements during the weight acceptance phase of running [20, 34, 35]. It is conceivable that pelvis and spinal column play a determinant role in managing and absorbing the shock derived from GRF, even if lower limb running pattern influences its direction and intensity. Our study supports the hypothesis of Lim at al. that hip can be used by runners to meet upper body stability demands [13]. Moreover, Mazzà et al., in a study on walking gait, observed that the spinal column at all levels plays an important role in attenuating the shock provoked by the GRF, transmitted from lower limbs to the head, and this attenuation is already effective at the shoulder level (Mazzà). The same mechanism it is probably working for running pattern, and further studies are needed to corroborate this hypothesis.

Although the EPD seems to have a positive effect in stabilizing the upper body, concerns remain on the effect of a poor control of the pelvis on the biomechanics of lower limbs. As pointed out by Powers et al., in activities characterized by a single foot contact phase, such as running, the presence of EPD might cause the GRF vector passing lateral with respect to the knee joint center [34]. The valgus moment that originates in this case places a tensile strain on the medial soft tissue restraints of the knee, which represents one of the districts more prone to injuries in recreational runners [34, 36].

Future studies should investigate whether the possible protective role of pelvis drop on UT and oculovestibular system stability, has a negative effect on lower limb kinematics and might, eventually, lead to a higher risk of injuries.

The authors acknowledge that the use of a treadmill represents one of the limitations of this study. The main reason for testing athletes on a treadmill was the need to evaluate the protonation and pelvic drop parameters which otherwise would have been difficult to detect through a video analysis performed overground. An additional limitation is represented by the absence of a functional calibration and the manual alignment of the IMU with the anatomical axes. Although having followed the manufacturer's instructions and having performed a tilt correction of the acceleration signal through the gravity vector, a perfect alignment with the anatomical axes can not be guaranteed.

Moreover, kinematic differences between overground and treadmill running were deemed as acceptable for the purposes of this study, according to data reported in literature [14, 30].

Further investigations conducted in an ecological setting would surely add an important contribution to the results obtained in this study.

5. Conclusions

In our sample of recreational runners, UT stability did not appear to be affected by the gender, the level of training, and lower limb strategies during contact phase. However, it was found to be related to the compensation mechanisms of the pelvis on the ML plane. Results obtained confirm the hypothesis that the lower body is able to respond to varying impact load conditions to maintain UT stability.

Data Availability

The data used to support the findings of this study are available from the corresponding author upon request.

Conflicts of Interest

The authors declare no conflicts of interest.

References

[1] T. R. Lindsay, J. A. Yaggie, and S. J. McGregor, "Contributions of lower extremity kinematics to trunk accelerations during moderate treadmill running," *Journal of NeuroEngineering and Rehabilitation*, vol. 11, no. 1, p. 162, 2014.

[2] A. T. M. Willemsen, C. Frigo, and H. B. K. Boom, "Lower extremity angle measurement with accelerometers-error and sensitivity analysis," *IEEE Transactions on Biomedical Engineering*, vol. 38, no. 12, pp. 1186–1193, 1991.

[3] A. Heyn, R. E. Mayagoitia, A. V. Nene, and P. Veltink, "The kinematics of the swing phase obtained from accelerometer and gyroscope measurements," in *Proceedings of 18th Annual International Conference of the IEEE Engineering in Medicine and Biology Society*, pp. 463-464, Amsterdam, The Netherlands, November 1996.

[4] D. Fong and Y.-Y. Chan, "The use of wearable inertial motion sensors in human lower limb biomechanics studies: a systematic review," *Sensors*, vol. 10, no. 12, pp. 11556–11565, 2010.

[5] V. Camomilla, E. Bergamini, S. Fantozzi, and G. Vannozzi, "Trends supporting the in-field use of wearable inertial sensors for sport performance evaluation: a systematic review," *Sensors*, vol. 18, no. 3, p. 873, 2018.

[6] M. Norris, R. Anderson, and I. C. Kenny, "Method analysis of accelerometers and gyroscopes in running gait: a systematic review," *Proceedings of the Institution of Mechanical Engineers, Part P: Journal of Sports Engineering and Technology*, vol. 228, no. 1, pp. 3–15, 2014.

[7] M. Giandolini, T. Poupard, P. Gimenez et al., "A simple field method to identify foot strike pattern during running," *Journal of Biomechanics*, vol. 47, no. 7, pp. 1588–1593, 2014.

[8] M. B. Samozino, C. L. MacLean, and J. E. Taunton, "A review of anthropometric, biomechanical, neuromuscular and training related factors associated with injury in runners," *International Sportmed Journal*, vol. 7, no. 2, pp. 120–137, 2006.

[9] C. Napier, C. K. Cochrane, J. E. Taunton, and M. A. Hunt, "Gait modifications to change lower extremity gait biomechanics in runners: a systematic review," *British Journal of Sports Medicine*, vol. 49, no. 21, pp. 1382–1388, 2015.

[10] K. H. Schütte, J. Aeles, T. O. De Beéck, B. C. van der Zwaard, R. Venter, and B. Vanwanseele, "Surface effects on dynamic stability and loading during outdoor running using wireless trunk accelerometry," *Gait & Posture*, vol. 48, pp. 220–225, 2016.

[11] S. J. McGregor, M. A. Busa, J. A. Yaggie, and E. M. Bollt, "High resolution MEMS accelerometers to estimate VO2 and

compare running mechanics between highly trained inter-collegiate and untrained runners," *PLoS One*, vol. 4, no. 10, Article ID e7355, 2009.

[12] C. Mazza, M. Iosa, F. Pecoraro, and A. Cappozzo, "Control of the upper body accelerations in young and elderly women during level walking," *Journal of NeuroEngineering and Rehabilitation*, vol. 5, p. 30, 2008.

[13] J. Lim, M. A. Busa, R. E. A. van Emmerik, and J. Hamill, "Adaptive changes in running kinematics as a function of head stability demands and their effect on shock transmission," *Journal of Biomechanics*, vol. 52, pp. 122–129, 2017.

[14] J. A. Mercer, J. S. Dufek, B. C. Mangus, M. D. Rubley, K. Bhanot, and J. M. Aldridge, "A description of shock attenuation for children running," *Journal of Athletic Training*, vol. 45, no. 3, pp. 259–264, 2010.

[15] R. J. Butler, H. P. Crowell, and I. M. Davis, "Lower extremity stiffness: implications for performance and injury," *Clinical Biomechanics*, vol. 18, no. 6, pp. 511–517, 2003.

[16] S. A. Meardon and T. R. Derrick, "Effect of step width manipulation on tibial stress during running," *Journal of Biomechanics*, vol. 47, no. 11, pp. 2738–2744, 2014.

[17] M. Kawabata, K. Goto, C. Fukusaki et al., "Acceleration patterns in the lower and upper trunk during running," *Journal of Sports Sciences*, vol. 31, no. 16, pp. 1841–1853, 2013.

[18] I. S. Ishii and P. R. Cavanagh, "Relationship between foot placement and mediolateral ground reaction forces during running," *Clinical Biomechanics*, vol. 9, no. 2, pp. 117–123, 1994.

[19] A. H. Gruber, W. B. Edwards, J. Hamill, T. R. Derrick, and K. A. Boyer, "A comparison of the ground reaction force frequency content during rearfoot and non-rearfoot running patterns," *Gait & Posture*, vol. 56, pp. 54–59, 2017.

[20] T. F. Novacheck, "The biomechanics of running," *Gait & Posture*, vol. 7, no. 1, pp. 77–95, 1998.

[21] J. Hamill and B. T. Bates, "A kinetic evaluation of the effects of in vivo loading on running shoes," *Journal of Orthopaedic & Sports Physical Therapy*, vol. 10, no. 2, pp. 47–53, 1988.

[22] G. Giakas, V. Baltzopoulos, P. H. Dangerfield, J. C. Dorgan, and S. Dalmira, "Comparison of gait patterns between healthy and scoliotic patients using time and frequency domain analysis of ground reaction forces," *Spine*, vol. 21, no. 19, pp. 2235–2242, 1996.

[23] R. A. Brindle, C. E. Milner, S. Zhang, and E. C. Fitzhugh, "Changing step width alters lower extremity biomechanics during running," *Gait & Posture*, vol. 39, no. 1, pp. 124–128, 2014.

[24] C. Mazzà, M. Iosa, P. Picerno, and A. Cappozzo, "Gender differences in the control of the upper body accelerations during level walking," *Gait & Posture*, vol. 29, no. 2, pp. 300–303, 2009.

[25] T. R. Derrick, "The effects of knee contact angle on impact forces and accelerations," *Medicine & Science in Sports & Exercise*, vol. 36, pp. 832–837, 2004.

[26] B. Hintermann and B. M. Nigg, "Pronation in runners," *Sports Medicine*, vol. 26, no. 3, pp. 169–176, 1998.

[27] R. B. Souza, "An evidence-based videotaped running biomechanics analysis," *Physical Medicine and Rehabilitation Clinics of North America*, vol. 27, no. 1, pp. 217–236, 2016.

[28] J. M. Hart, D. C. Kerrigan, J. M. Fritz, and C. D. Ingersoll, "Jogging kinematics after lumbar paraspinal muscle fatigue," *Journal of Athletic Training*, vol. 44, no. 5, pp. 475–481, 2009.

[29] T. S. A. Soares, C. F. d. Oliveira, F. Pizzuto, R. Manuel Garganta, J. P. Vila-Boas, and M. C. d. A. Paiva, "Acute kinematics changes in marathon runners using different

footwear," *Journal of Sports Sciences*, vol. 36, no. 7, pp. 766–770, 2018.

[30] J. Favre, B. M. Jolles, O. Siegrist, and K. Aminian, "Quaternion-based fusion of gyroscopes and accelerometers to improve 3D angle measurement," *Electronics Letters*, vol. 42, no. 11, pp. 612–614, 2006.

[31] M. Iosa, A. Fusco, G Morone et al., "Assessment of upper-body dynamic stability during walking in patients with subacute stroke," *Journal of Rehabilitation Research & Development*, vol. 49, no. 3, 2012.

[32] M. A. Busa, J. Lim, R. E. A. van Emmerik, and J. Hamill, "Head and tibial acceleration as a function of stride frequency and visual feedback during running," *PLoS One*, vol. 11, no. 6, Article ID e0157297, 2016.

[33] J. B. Morley, L. M. Decker, T. Dierks, D. Blanke, J. A. French, and N. Stergiou, "Effects of varying amounts of pronation on the mediolateral ground reaction forces during barefoot versus shod running," *Journal of Applied Biomechanics*, vol. 26, no. 2, pp. 205–214, 2010.

[34] C. M. Powers, "The influence of abnormal hip mechanics on knee injury: a biomechanical perspective," *Journal of Orthopaedic & Sports Physical Therapy*, vol. 40, no. 2, pp. 42–51, 2010.

[35] A. G. Schache, P. D. Blanch, D. A. Rath, T. V. Wrigley, R. Starr, and K. L. Bennell, "A comparison of overground and treadmill running for measuring the three-dimensional kinematics of the lumbo-pelvic-hip complex," *Clinical Biomechanics*, vol. 16, no. 8, pp. 667–680, 2001.

[36] J. E. Taunton, M. B. Ryan, D. B. Clement, D. C. McKenzie, D. R. Lloyd-Smith, and B. D. Zumbo, "A retrospective case-control analysis of 2002 running injuries," *British Journal of Sports Medicine*, vol. 36, no. 2, pp. 95–101, 2002.

Research Article

Design of a Remote Real-Time Monitoring System for Multiple Physiological Parameters Based on Smartphone

Noman Q. Al-Naggar ⬤, Husam Mohammed Al-Hammadi, Adel Mohammed Al-Fusail, and Zakarya Ali AL-Shaebi

Department of Biomedical Engineering at Faculty of Engineering, University of Science and Technology, Sana'a, Yemen

Correspondence should be addressed to Noman Q. Al-Naggar; noman_qaed@yahoo.com

Background. Utilization of the widely used wearable sensor and smartphone technology for remote monitoring represents a healthcare breakthrough. This study aims to design a remote real-time monitoring system for multiple physiological parameters (electrocardiogram, heart rate, respiratory rate, blood oxygen saturation, and temperature) based on smartphones, considering high performance, autoalarm generation, warning transmission, and security through more than one method. *Methods.* Data on monitoring parameters were acquired by the integrated circuits of wearable sensors and collected by an Arduino Mega 250 R3. The collected data were transmitted via a Wi-Fi interface to a smartphone. A patient application was developed to analyze, process, and display the data in numerical and graphical forms. The abnormality threshold values of parameters were identified and analyzed to generate an autoalarm in the system and transmitted with data to a doctor application via a third-generation (3G) mobile network and Wi-Fi. The performance of the proposed system was verified and evaluated. The proposed system was designed to meet main (sensing, processing, displaying, real-time transmission, autoalarm generation, and threshold value identification) and auxiliary requirements (compatibility, comfort, low power consumption and cost, small size, and suitability for ambulatory applications). *Results.* System performance is reliable, with a sufficient average accuracy measurement (99.26%). The system demonstrates an average time delay of 14 s in transmitting data to a doctor application via Wi-Fi compared with an average time of 68 s via a 3G mobile network. The proposed system achieves low power consumption against time (4 h 21 m 30 s) and the main and auxiliary requirements for remotely monitoring multiple parameters simultaneously with secure data. *Conclusions.* The proposed system can offer economic benefits for remotely monitoring patients living alone or in rural areas, thereby improving medical services, if manufactured in large quantities.

1. Introduction

The practice of remotely monitoring physiological parameters has become prevalent. Smartphones and wearable sensors (WS) are widely available and can provide real-time monitoring of critical parameters for healthcare providers and patients. Thus, integrating and combining WS and smartphone technology (WSST) in a system can reduce the challenges in monitoring life parameters of patients with complex health conditions regardless of their location (e.g., remote or rural areas) [1–3]. The use of WSST can likewise

improve telemedicine and healthcare services and provide progressive services to patients with chronic conditions [1, 4].

Numerous innovations have been developed for real-time monitoring and/or store-and-forward telemedicine services using ubiquitous connectivity tools and simple mobile phone or WS applications. WSST has developed over time owing to the creation of various built-in applications and communication tools, such as GPS and third-generation (3G) and fourth-generation phone network Internet [5, 6]. WSST development has been accompanied by the increasing

number of smartphone users, which was predicted to grow from 2.1 billion in 2016 to approximately 2.5 billion in 2019, as well as the growing number of applications being developed for real-time monitoring and health diagnosis [3, 7].

Remote monitoring systems have improved progressively to meet the needs of the elderly as well as to reduce the number of deaths from chronic diseases, such as cardiac arrhythmia, high blood pressure, and diabetes [8]. Therefore, numerous studies have been conducted to monitor multiple physiological parameters responsible for such diseases [1, 9–14]. However, other studies have focused on developing WSST to monitor a specific disease [15–18].

Several studies have emphasized the use of developed WSST in health applications given the positive static data measurement characteristics of WSST, such as reliability and accuracy in continuous or real-time monitoring [19–21]. Other studies have focused on the disadvantages of WSST, such as high power consumption, the generation of false alarms, long-term health monitoring efficiency, and large-scale utilization [1, 3, 20]. A few studies have also discussed a combination of mobile technologies or monitoring issues [3, 22, 23].

The limitations of such designed systems include measurement of a single parameter, analysis, and data transmission and reception method/time [15–18]. Improvements in this field have mostly tried to overcome these limitations in ambulatory applications, specifically, the monitoring of only one vital parameter, battery life, cost-effectiveness, monitoring functions, a monomethod for warning transmission, and data security.

The current study integrates the specialized WSST to design a remote real-time monitoring system for multiple physiological parameters based on smartphones with developed health applications that can monitor and display measured critical parameters, including an electrocardiogram (ECG), heart rate (HR), respiratory rate (RR), blood oxygen saturation (SpO_2), and temperature. The proposed system should meet main requirements such as sensing, processing, displaying, and real-time transmission and should have the capability to generate an autoalarm based on the analysis threshold values of multiple monitoring parameters. Moreover, it should ensure the dispatch of warning messages via two transmittal methods, namely, short message service (SMS) and the Internet, and identify a patient's location via GPS. The system should also meet auxiliary requirements such as compatibility, comfort, low power consumption and cost, and small size. Furthermore, the developed application should enable users to record, save, and transmit real-time data in video and text forms.

In this study, a WS acquires the body data, which are first sent to an Arduino Mega 2560 R3 and then to a smartphone through a Wi-Fi interface. The data are collected in a smartphone using a developed patient application that analyzes, processes, and displays the data before transmitting them to the developed doctor application. The patient application consists of two working modes. The first mode continuously transmits data, while the second mode transmits data only when abnormality is detected. Thus, the second mode saves phone or device power as well as the time of doctors/operators. The application prompts an autoalarm when an abnormal value is detected based on a previously identified threshold and sends a warning message to the doctor application (doctors/operators). The developed application is designed with adequate security to protect patient information. A special power bank is also designed to ensure the long feeding power of the system and smartphone.

System performance and reliability are evaluated for accuracy measurement, power consumption test against time, and average time delay. The average accuracy measurement of the collected parameters is 99.26%, and the system achieves low power consumption against time (4 h 21 m 30 s) for feeding measured circuits. Moreover, the result shows that the average time delay of data transmission to the doctor application via Wi-Fi is 14 s, whereas that via a 3G mobile network is 68 s.

The results demonstrate the reliability and acceptability of the system as well as the achievement of main and auxiliary requirements. Therefore, the current system is recommended not only for rural areas, particularly in developing countries, but also for hospitals and specific health centers and to provide first aid, primary diagnosis, and treatment. The system will also offer economic benefits if manufactured in a large scale.

2. Materials and Methods

The proposed design was achieved through a combination of WS circuits and smartphone technologies via an Arduino circuit (as shown in Figure 1). The WS circuits acquired and computed the body data using an Arduino, which performed primary data collection. An electronic interface connected the Arduino circuits to the smartphone application to monitor, analyze, process, and transmit the data. The data were ensured and secured for intended persons only.

Figure 1 shows an overview of the designed system architecture, in which Figure 1(a) shows a block diagram of the hardware components and their connectivity sequence and Figure 1(b) demonstrates the data transmission network of the monitoring parameters.

2.1. Hardware Components.
All hardware components were carefully selected to meet the requirements of the proposed design, namely, low power consumption, suitability for ambulatory applications, accuracy, reliability, affordability, and availability. Auxiliary requirements such as easy handling, comfort, minimal weigh, and long-term battery power (power consumption) were also considered, as these features could solve and overcome the limits and challenges of this field [3]. The hardware components are elucidated as follows.

2.1.1. ECG and HR Circuits.
These circuits were used to acquire the first measuring parameter (i.e., an ECG) from which the second parameter (i.e., HR) was calculated using a

(a)

(b)
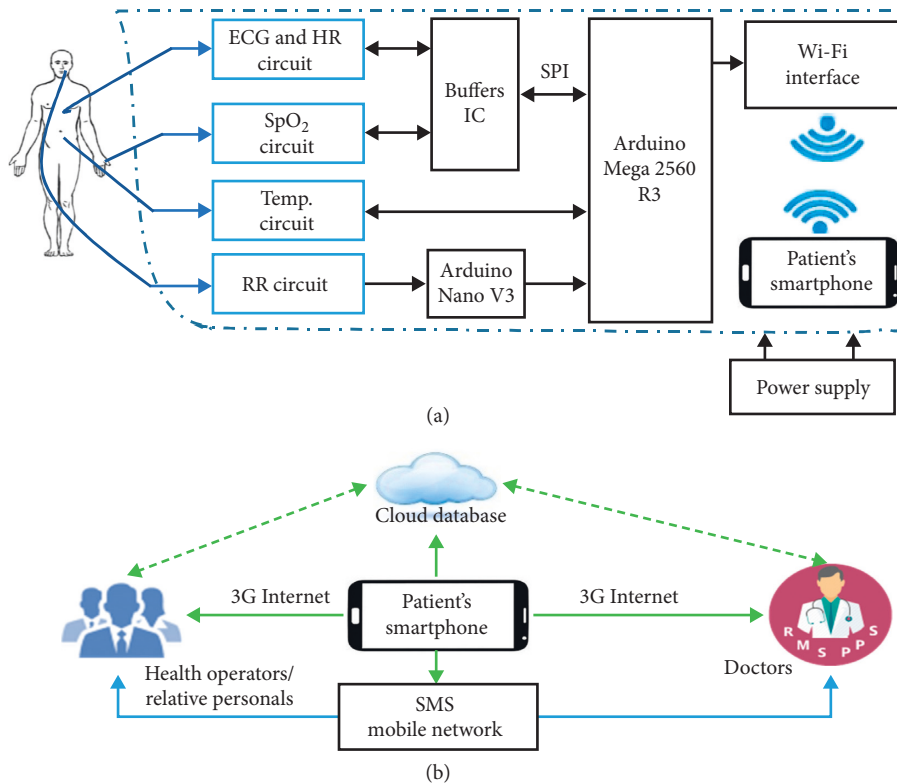
FIGURE 1: Overview of designed system architecture: (a) circuit diagram connectivity between WS, Arduino board, Wi-Fi module, and smartphone; (b) overview of data transmission network.

MAX30003 circuit [24], which reduces movement artifacts during continuous monitoring and is common in telemetry monitoring [8].

The ECG circuit removed motion artifacts using an instrumentation amplifier that has a two-pole active anti-aliasing filter with a 600 Hz−3 dB frequency. The high-pass filter options included a first-order infinite impulse response (IR) Butterworth filter with a 0.4 Hz corner frequency, which was selected to correspond to ambulatory applications. The low-pass filter options included a 12-tap linear phase (constant group delay) finite IR filter with a 40 Hz corner frequency. The amplification process in this study used 20 V/ V.

The raw data of the ECG signals were saved in the memory of the ECG circuit and then sent as a sequence to the Arduino (Mega 2560 R3) using a DM74LS125A integrated circuit (IC) through a high-speed interface to prevent interference between the data of the ECG signal and other signals.

(1) HR Extraction. HR was defined by calculating the *R-R* duration/interval time among QRS complexes of consecutive ECG waveforms within 1 minute intervals, where *R* was the first upward deflection wave after the P wave, the QRS complex was a series of waveforms following the P wave in the ECG waveforms, and the R-R interval was the elapsed time between two consecutive R waves [25, 26].

In this work, R waves were extracted by an Android program from the recorded ECG waveforms as the maximum. Next, identical maximum points ($R − R$ interval, ms)

were calculated, averaged, and divided into 1 minute intervals ($60 × 1000$ ms). Hence, HR was calculated in beats per minute (bpm) as follows:

$$\mathrm{HR}(\mathrm{bpm}) = \frac{60 * 1000}{R − R \, \mathrm{interval}\,(\mathrm{ms})}. \tag{1}$$

2.1.2. SpO$_2$ Circuit. The SpO$_2$ signal was acquired by a finger probe using an AFE 4490 from Texas Instruments [27], which utilized a pulse oximeter technique (light-emitting diodes). The signal presented a voltage to the 22-bit analog-to-digital converter (ADC), which was fed to a data processor to digitize and send the display signal.

2.1.3. Temperature Circuit. The body temperature signal was acquired through skin temperature using a MAX30205 temperature sensor, which provided a digital output using an ADC and operated within the 0°C to +50°C temperature range. The completed temperature reading operation was updated for a new temperature measurement. During this process, changes in temperature were discounted until the peer reading was completed. The updated temperature register was sent to the Arduino Mega 2560 R3 to process and display the signal.

2.1.4. RR Circuit. RR was acquired by a circuit that consisted of a 10 K-negative temperature coefficient thermistor fitted into a nebulizer mask with a voltage divider configuration.

Thermistor resistance decreased during exhalation owing to comparatively hot air and increased during inhalation. The obtained signal from resistance was converted into a voltage and fed into a 0.0884–0.8942 Hz bandpass filter. The output of the filter was amplified 100 times and sent to the Arduino Mega 2560 R3 through an Arduino Nano, as shown in Figure 1.

2.1.5. Power Supply Circuit Bank.

The power supply circuit was designed to meet the requirements of the power bank for the proposed system, such as low cost and effective long-time consumption.

Figure 2 illustrates the components of the designed circuit bank, which consisted of a charger/discharger IC (TP4056 chip), an IC converter, an LCD screen, and a lithium-ion battery. A TP4056 chip was used to control the charging and discharging of the battery, which was supplied by a control switch through an "on" and "off" function. A DC-DC boost IC converter chip was used to cater to a stable 5 V DC supply at outlets to ensure a supply of not less than 3.7 V DC from the battery. The LCD screen showed the percentage of the remaining capacity and the working status. A USB outlet 2 (OT 2) was used as an option for charging smartphones (if needed), and an outlet 1 (OT 1) was used to feed the circuits via constant current and voltage (5 V). The actual capacity of the battery was 3678 mAh, and actual recharging time was 1 h 50 m 15 s. The designed features/specifications of the power supply circuit bank are demonstrated in Table 1.

2.1.6. Arduino Mega 2560 R3.

An Arduino Mega 2560 R3 was selected owing to its memory capacity, multiple and various input/output pins, data-processing speed, various WS connection modes, and simple computer connection via a USB cable. Moreover, it included an option to send signals wirelessly or via a USB cable.

2.2. Patient Data Collection and Transmission

2.2.1. Patient Data Collection.

The acquired data from multiple WS were collected in the Arduino Mega 2560 R3, which was the primary platform for data collection and preparation for transmission to Android devices. The Arduino was connected to a tablet or a smartphone via a USB cable and a computer to display the acquired data during the tests. However, this capability enabled monitoring parameters in sideway locations.

2.2.2. Patient Data Transmission.

Patient data were transmitted from the Arduino Mega 2560 R3 to an Android smartphone using a Wi-Fi ESP8266 circuit through serial communication (RX/TX lines), which was capable of either hosting an application or offloading all Wi-Fi networking functions from another application processor. The Wi-Fi ESP8266 circuit was used rather than Bluetooth owing to the former's standby power consumption of <1.0 mW and
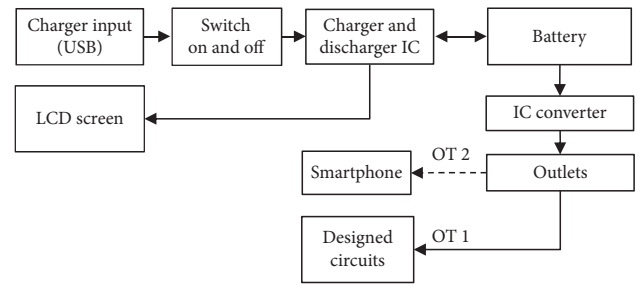
Figure 2: Block diagram of the power supply circuit bank.

waking-up and packet transmission of <2 ms and capability to send a variety of data.

A smartphone's Wi-Fi was forced to fast switch (833 μs) between two operations automatically to receive and transmit data to the doctor application. The system did not lose its capability for real-time transmission because of the delay from switching.

2.3. Android Health Application Design.

The application design considered features that help increase the probability of saving patient lives as well as modern attributes, thereby presenting advantages over other designs in recent studies [2, 21]. The current application consisted of patient and doctor applications.

2.3.1. Patient Application.

A health application was created in the proposed system in the Android studio interface to simplify the procedures of the intended features. The Android applications were written using the Java programming language. The primary data collected in the patient application were converted into integer values (secondary data) and compared with the threshold values of each parameter. The application continuously scanned for updating parameter values simultaneously and visualized the values in the adaptation window of the smartphone. The application worked in the following modes:

(i) The first mode monitored and displayed parameter values simultaneously in real time through a smartphone, with a possibility of transmitting these values to intended trends.

(ii) The second mode transmitted data when abnormal/threshold values were detected. That is, the system monitored and sensed parameter value abnormalities and then transmitted these data to intended trends.

Selection of the second mode helped arrange/save time for personnel working with related proposed systems. Moreover, this mode saved a considerable amount of energy; thus, it provided more advantages than those in previous works [1, 2, 8, 10, 14]. The developed application also included the following features:

(i) Provided a platform for monitoring and displaying measured parameters based on primary analysis and diagnosis

TABLE 1: Specifications of the designed power supply.

Parameter	Specifications
Battery type	Lithium ion
Capacity	4000 mAh
Connectivity	Two output ports (2 A feed system, 1 A USB to feed phone)
Voltage required input	USB 5 V, 2 A
Time required to recharge	1 hour 50 minutes
Battery life with full charge	4 hour 30 minutes

(ii) Saved recorded data with respect to time to review activities during movements and exercises

(iii) Transmitted data in video (graphic and numerical data) or numerical forms to responsible individuals (doctor application)

(iv) Offered more than one option for monitoring and transmitting data

(v) Sent patient locations via GPS using Wi-Fi or 3G as well as a warning to other personal operators via mobile or/and Internet networks using SMS or/and WhatsApp, respectively

2.3.2. Doctor Application. The second component of the health application was created in Android and provided a screen window to show the transmitted data from the patient application. This component permitted doctors or responsible persons from an insurance company or medical center to monitor a patient's situation and provide first aid and diagnosis for critical cases. The web portal requires a user name and ID/password to protect privacy. The web interface provided data in video form (graphic and numerical data) recorded from the patient application and/or numerical data for multiple patients to display on smartphone/Android devices.

2.3.3. Application User Management. The application interfaces and icons were designed in a simplified manner to be managed and used easily by anyone, as shown in Figure 3. The menu interface of the patient application is shown in Figure 4.

2.4. Autoalarm System. The designed system generated an autoalarm in the two working modes of the health application when it sensed abnormalities in one or more of the monitored parameters and would transmit data using two warning methods.

2.4.1. Wi-Fi/3G Warning Method. This method was used in both application modes to transmit data to the web interfaces of intended trends. The 3G network was dominant in smartphones for transmitting and receiving data via Wi-Fi from the Arduino owing to the default Wi-Fi system, as shown in Figure 5.

Wi-Fi was reconnected automatically for $833\,\mu s$ to receive data from the Arduino to send to the doctor application. In case of available Wi-Fi NAN, such as in rural areas and locations far from health facilities, the system used 3G Internet provided by a mobile phone network. The autoalarm generated through the system was received on the web interface and perceived through sound and vibration to notify doctors or operators with identified locations via GPS.

2.4.2. Mobile Network Warning Method. This method was used to send SMS warning messages to centers such as RMSPPS servers, families, or doctors. The message was shown as "I have detected an abnormality condition; for more details, visit your account on the doctor application." Phone numbers of the operator's server/insurance company and doctors were identified previously in the system.

Figure 6 shows the sequence of the application working mechanism, threshold value identification, and data transmission. The default mode in the application was mode 1, whereas mode 2 in the dashed line was considered as a user option.

2.5. Determining Threshold Values. The autoalarm feature of the proposed system was based on the threshold value determination of monitored physiological parameters, such as HR, which reflects certain cases of ECG abnormalities and is considered as an indicator of a motion function [28]. In this study, HR was extracted and calculated from ECG waveforms on the basis of an algorithm proposed in [25], and the HR threshold values were determined based on works [13, 26].

RR threshold values have been defined in different ranges depending on the acquisition method and age of a patient [29] and are considered as an indicator of various symptoms, such as cardiac arrest, coughing, decreased alertness, poor feeding, grunting, and fever [30–32]. The mean observed RR was 14.2 (±4.17 precision (SD)) breaths per minute for adults [29], which was less than the mean RR 15.1 (±4.05 SD) breaths per minute measured by respiratory inductive plethysmograph [32]. In this study, the normal RR for monitoring elderly and adult subjects (between the ages of 20 and 50 years) at rest was from 12 breaths per minute to 16 breaths per minute. The common RR abnormality limits are shown in Table 2 [30, 33].

Temperature and SpO_2 estimation values were determined as ranges that have been defined for pathologies [1, 13]. Table 2 shows a summary of the threshold values of intended parameters.

(a)   (b)
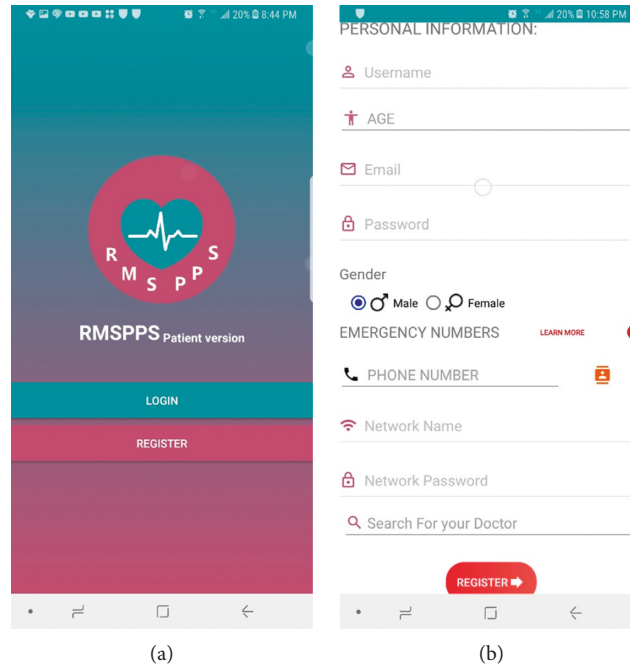
FIGURE 3: First windows of the patient application: (a) log-in and registration screen option; (b) patient information registration screen (e.g., name, age, gender, and the emergency number of the intended person).

(a)   (b)
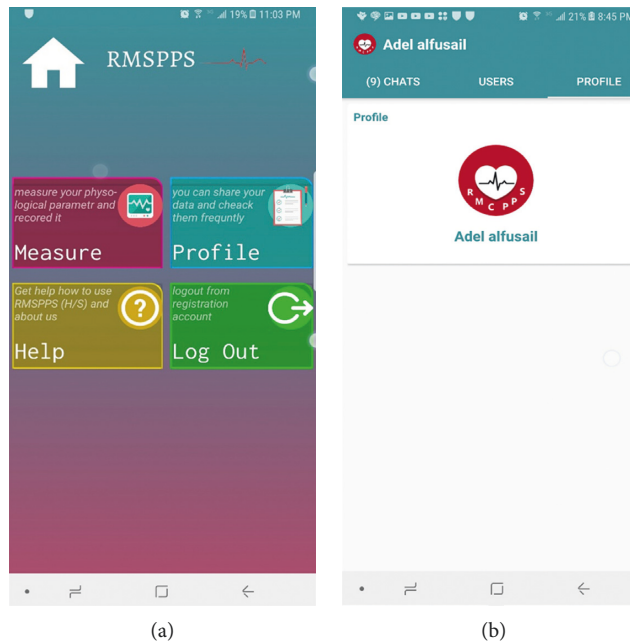
FIGURE 4: The menu interface of the patient application: (a) home screen of the patient application; (b) the patient account page.

2.6. System Test. The proposed system was subjected to numerous tests to determine the accuracy and reliability of remote monitoring and data transmission in real time. The system primarily evaluated the achievement of designed and functional requirements at each implementation step. Quality performance of the system was measured by calculation accuracy. Accuracy was determined by the

agreement between the measured (experimental) values of the proposed system and the true value of the qualified equipment (patient monitor model TR6628-9500, Eastern Europe Co.) in the biomedical engineering laboratories at the University of Science and Technology, Yemen. Equation (2) demonstrates the percent error calculation, and equation (3) shows the percent accuracy calculation:
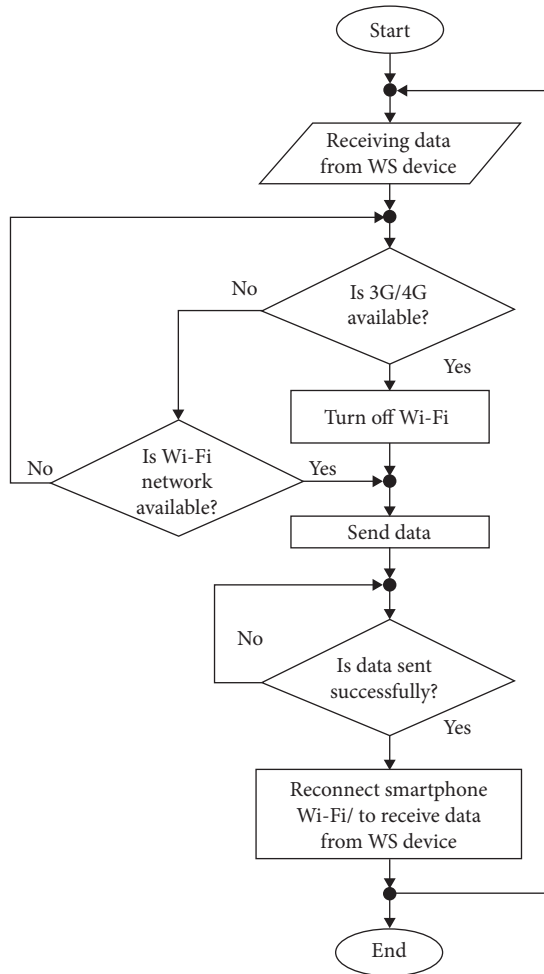
Figure 5: Smartphone Wi-Fi connection-reconnection sequence.

$$\text{percent error} = \frac{\text{measured value} - \text{true value}}{\text{true value}} * 100, \quad (2)$$

$$\text{percent accuracy} = 100\% - \text{percent of error.} \quad (3)$$

The accuracy measurement of each sensor was calculated by averaging the obtained accuracy values of five measurement processes. Then, the total accuracy of the entire WS was calculated as the average of the total WS measurement accuracy, as shown in Tables 3 and 4.

System reliability was tested and held in different time periods. Power consumption for long-term use was evaluated through battery life charge time (LCT) for three cases, namely, supplying only the working circuits, charging the circuit and smartphone simultaneously (versatility), and supplying only the smartphone (an auxiliary), as shown in Table 5. Likewise, reliability of the system for data transmission delay time was checked with Wi-Fi and 3G. The system held seven connection/disconnection trials, considering several connection conditions, such as weak Internet, coverage area, and cloud server type (see Table 6).

3. Results

The obtained results illustrated the achievement of the current system in monitoring critical parameters related to common diseases, such as HR, ECG, SpO_2, and temperature, which were measured using a combined WS and Arduino circuits and a developed application in Android devices, such as smartphones. The patient application met the requirements of receiving, processing, analyzing, and transmitting data to intended trends as well as displaying them in the doctor application/web interface. The results are organized to show the main achievements.

Figure 7 shows the interface display for monitoring data, which was represented in graphic and numerical forms. These features promoted readability for healthcare personnel, such as patients, doctors, nurses, and operators. The exterior interface was designed like a patient's monitor, reflecting the same functions and information but through a portable device.

The results revealed the success of the autoalarm generation system in case of abnormalities and in sending a warning SMS via the system to the doctor application through sound and vibration as well as a written flag to attract a doctor's attention.

Figure 8 shows several capabilities of the designed system, in which Figure 8(a) illustrates an example of an SMS received via a mobile network. Therefore, the system was useful for tracking patients, particularly when Internet connection was unavailable. The system transmitted data and/or video recordings of acquired abnormal cases to doctors/operators and displayed them via the doctor application and WhatsApp, as depicted in Figures 8(b) and 8(d). Figure 8(c) demonstrates the system's capability to determine locations via GPS.

Tables 3 and 4 show the results of the accuracy measurement evaluation by comparing the values of our system with a standard device. The accuracy measurement was calculated as the average accuracy of each measured parameter, and all the accuracy measurements were averaged as the accuracy measurement of the entire system (99.25%).

The results of the power consumption test against time showed sufficient LCT in the case of supplying the circuits (4 h 21 m 30 s). However, in the versatility case, LCT was low and approximately 45% of time, as shown in Table 5.

Table 6 demonstrates the results of the time needed to connect stages and transmit data through the system for Wi-Fi and 3G. The average time for data transmission to the doctor application was 18 s via Wi-Fi and 70 s via 3G. The average time delay was less (14 s) with a Wi-Fi network compared with a 3G network (68 s). Therefore, the system can serve its purpose, and the alarm response time depended on the smartphone model and Internet speed.

The final specifications and features of our system are concluded in Table 7, and the final design is shown in Figure 9.
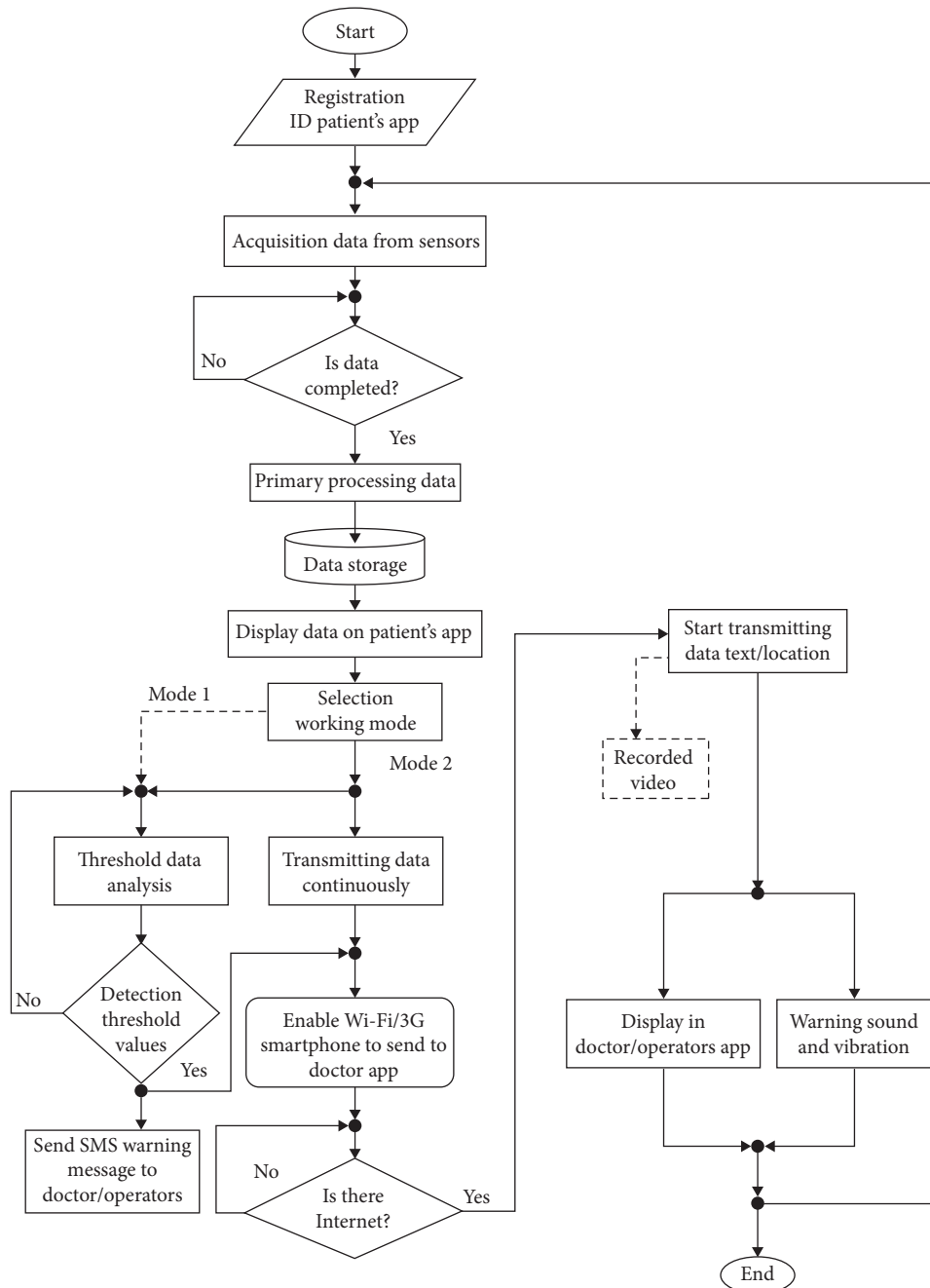
Figure 6: Flowchart of the working mechanism of the designed system.

4. Discussion

The results of the proposed system appear clearly and correctly without interference in the monitored parameter data in the patient and doctor applications.

The provided features in the interface display in graphic and numerical forms (Figure 7), distinguish the proposed system, and overcome the challenges in previous works in this field [1, 2, 8, 10, 21]. Moreover, the system includes other capabilities that improve primary diagnosis to offer first aid, particularly for simultaneous critical cases of multiple patients. These capabilities include generating an autoalarm

and transmitting data in multiple forms. The system also exhibits general features, such as sending data to social media (WhatsApp) and determining patient location via GPS.

The system demonstrates a satisfactory time delay (14 s) for data transmission via Wi-Fi compared with the recent presented system (30 s) [1]. The time needed to transmit data via 3G is 68 s owing to the low speed used in the tested area, which can be improved. A 3G mobile network can provide the proposed system with long real-time monitoring to achieve an extensive coverage area. The low and acceptable power consumption against time (4 h 21 m 30 s) is an

TABLE 2: Threshold values of monitoring parameters.

Parameter	Rhythm/pathology	Threshold values
SpO$_2$ (%)	Normal	96 to 99
	Pulmonary or cardiovascular chronic diseases	Drop rapidly
	Acute respiratory failure	<90% + 3 to 4%
RR (breaths per minute (bpm))	Normal	12–16
	Cardiac arrest	≥27
	Lower respiratory tract infections	>24
	Tachypnea	>12–16
	Bradypnea	<12–16
Temperature (°C)	Normothermia or euthermia	37.0
	Fever	≥37.8
	Hypothermia	≤35.0
HR (beats per minute (bpm))	Normal	60 to 100
	Bradycardia	<60
	Tachycardia	>100

TABLE 3: Accuracy measurement of SpO$_2$, HR, and ECG.

Subject	Parameter					
	SpO$_2$ %		Heart rate (bpm)		ECG (R-R ms)	
	MV*	TV*	MV	TV	MV	TV
1	96	96	77	76	632	630
2	95	94	100	98	568	563
3	98	96	99	98	581	585
4	96	97	45	45	627	632
5	95	94	89	88	639	635
Average accuracy (%)	98.36		98.89		99.93	

*MV, measured value; TV, true value.

TABLE 4: Accuracy measurement of RR and temperature.

Subject	Parameter			
	Respiratory rate (rpm)		Temperature (°C)	
	Measured value	True value	Measured value	True value
1	14	14	32	33
2	16	15	35	34
3	14	15	35	33.5
4	15	16	36	35
5	15	15	34.5	35.5
Average accuracy (%)	100.00		99.11	

TABLE 5: Power consumption test.

Test type	Description	Time
Battery LCT	Supplies the circuits only	4 h 21 m 30 s
	Supplies the circuits and smartphone (versatility)	2 h 15 m 20 s
	Supplies the smartphone only	3 h 50 m 05 s

TABLE 6: Performance test of transmission time.

Performance parameter	Wi-Fi	3G
Average connecting time (s)	71	117
Average transmitting time to doctor app (s)	18	70
Average time loss ratio (s)	4	2
Average time delay (s)	14	68

important feature that distinguishes our system. Thus, the use of less time for transmitting data, with a potential for improvement, and the long operation time make our system superior to other systems in the related work in this field [1, 10, 14].

The results of the combined WSST and developed application meet the main requirements for remotely

FIGURE 7: Interface display of monitoring parameters (application display).

(a)

(b)

(c)

(d)
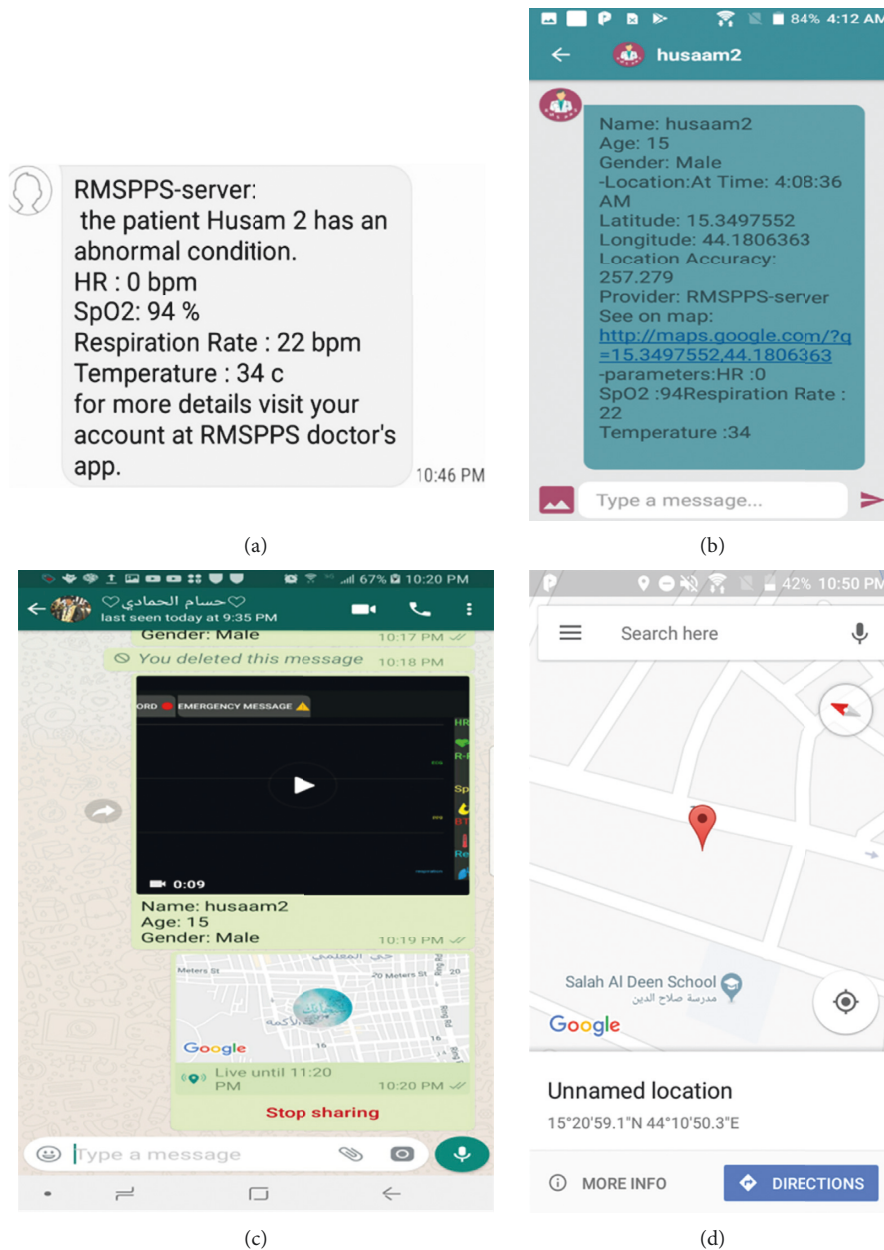
FIGURE 8: Several capabilities of the designed system: (a) example of receiving an SMS; (b) transmitted data in the doctor application; (c) receiving a video recording and a message in WhatsApp; (d) sending a patient's location to a doctor/operator.

TABLE 7: Final specifications of the designed system.

WS/parameter	Specifications
General	(i) Rechargeable battery (ii) Compatible with most android devices (iii) Small size, portable, and easy to use (iv) Comfortable for adult and old patients (v) Multiple parameters: ECG, HR, SpO$_2$, temperature, and RR (vi) The ability of recording a video and data text of signals (vii) Sending autoalarm to the doctor/centers in different tools
ECG and HR	(i) ECG: single lead without the need for a third right-leg drive (DRL) electrode (ii) Heart rate detected by R to R distance (iii) Frequency range: 15.625 mHz up to 256 Hz (iv) ECG calibration: ±0.25 mV (v) Arrhythmia analysis: yes
SpO$_2$	(i) Display: waveforms and digits (ii) Real-time display of PPG (photoplethysmogram) (iii) Measurement range: 1–100% (iv) Resolution: 1% (v) Accuracy: 2% (80–100%) (vi) Pulse rate range: 20–300 bpm
RR (respiratory rate)	(i) Method: air flow temperature (ii) Measurement range: 5~50 rpm (iii) Accuracy: ±1 bpm (iv) Resolution: 2 bpm
Temperature	(i) Measurement range: 0~50°C (ii) 0.1°C accuracy (37°C to 39°C) (iii) Resolution: 0.1°C
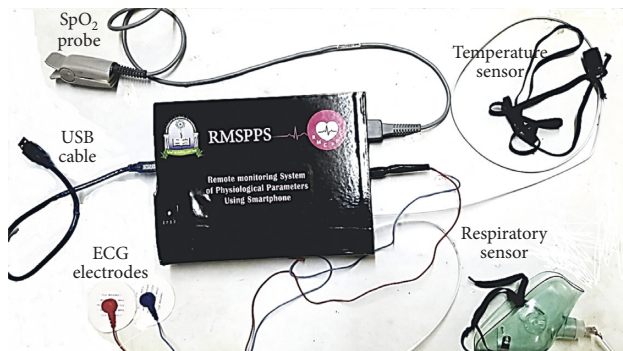
FIGURE 9: Final external view of the designed system.

monitoring physiological parameters. These requirements include a remarkable achievement in design and efficiency improvement in terms of accurate real-time sensing, transmuting, and displaying as well as low power consumption. Moreover, the system achieves auxiliary requirements such as comfort, compatibility, ease of use, minimal weight, small size, and affordability, which are considered more than the stated requirements in such systems [3].

Despite its features and advantages, the system should be further developed and adapted for iPhone operating systems. That is, the application is compatible only with Android devices, specifically Android operating systems starting from version 5.1.1. A blood pressure monitoring parameter should be added to the current five parameters of the system for the full monitoring of critical cases. In this study, our emphasis on the use of Wi-Fi rather than Bluetooth for sending data to smartphones is justified owing to the former's data transmission speed and minimal power consumption. Thus, the two features distinguish the system and meet the essential requirements for real-time monitoring.

5. Conclusion

The use of WSST in a remote monitoring system can advance healthcare services, particularly for the elderly who live alone or in rural areas with limited access to medical services or institutions. In this study, a remote monitoring system is designed based on smartphones to perform real-time monitoring and to provide primary analysis, diagnosis, and treatment (i.e., first aid) simultaneously. The proposed system helps reduce the death rate from chronic and common diseases related to the monitoring of critical parameters, such as ECG-HR, SpO$_2$, RR, and temperature.

The system also possesses features that render it superior to other systems in the field, such as application capabilities, option modes, autoalarm generation, alarm transmission via two methods, secured data transmission, and appropriate forms for displaying such data for multiple patients simultaneously. Moreover, the system meets the main and auxiliary requirements.

Consequently, the designed system presents a solution not only for rural areas in developing countries but also for all types of healthcare facilities. Furthermore, the system would be economically beneficial if manufactured in large quantities because it would lead to the development of widespread health service networks in developing countries as well as rural areas.

In the future, the system can add a blood pressure signal to the monitoring parameters, as it relates to critical cases. Moreover, the system will need to overcome its limits, such as adaptation to iPhone operating system devices, given the wide range of people using such devices.

Data Availability

The Arduino code and the Android applications that are used to support the findings of this study have been deposited in the RMSPPS repository on GitHub website (https://github.com/adelalfusail/RMSPPS).

Conflicts of Interest

The authors declare that they have no conflicts of interest.

References

[1] P. Kakria, N. K. Tripathi, and P. Kitipawang, "A real-time health monitoring system for remote cardiac patients using smartphone and wearable sensors," *International Journal of Telemedicine and Applications*, vol. 2015, Article ID 373474, 11 pages, 2015.

[2] X. Liang, J. Zhao, S. Shetty, J. Liu, and D. Li, "Integrating blockchain for data sharing and collaboration in mobile healthcare applications," in *Proceedings of the 2017 IEEE 28th Annual International Symposium on Personal, Indoor, and Mobile Radio Communications (PIMRC)*, pp. 1–5, IEEE, Montreal, Canada, October 2017.

[3] S. Patel, H. Park, P. Bonato, L. Chan, and M. Rodgers, "A review of wearable sensors and systems with application in rehabilitation," *Journal of Neuroengineering and Rehabilitation*, vol. 9, no. 1, p. 21, 2012.

[4] S. Meystre, "The current state of telemonitoring: a comment on the literature," *Telemedicine and e-Health*, vol. 11, no. 1, pp. 63–69, 2005.

[5] P. Bonato, "Wearable sensors and systems," *IEEE Engineering in Medicine and Biology Magazine*, vol. 29, no. 3, pp. 25–36, 2010.

[6] N. Petr, "Smartphones for in-home diagnostics in telemedicine," *International Journal of Medical and Biological Sciences*, vol. 6, pp. 36–40, 2012.

[7] Number of mobile phone users worldwide from 2015 to 2020 (in billions), 2018, https://www.statista.com/statistics/274774/forecast-of-mobile-phone-users-worldwide/.

[8] J. Gómez, B. Oviedo, and E. Zhuma, "Patient monitoring system based on internet of things," *Procedia Computer Science*, vol. 83, pp. 90–97, 2016.

[9] A. Al-Naji, A. G. Perera, and J. Chahl, "Remote monitoring of cardiorespiratory signals from a hovering unmanned aerial vehicle," *Biomedical Engineering Online*, vol. 16, no. 1, p. 101, 2017.

[10] H. Li and T. Pan, "Development of physiological parameters monitoring system using the internet of things," *International*

[11] C. G. Scully, J. Lee, J. Meyer et al., "Physiological parameter monitoring from optical recordings with a mobile phone," *IEEE Transactions on Biomedical Engineering*, vol. 59, no. 2, pp. 303–306, 2012.

[12] N. S. Shivakumar and M. Sasikala, "Design of vital sign monitor based on wireless sensor networks and telemedicine technology," in *Proceedings of the 2014 International Conference on Green Computing Communication and Electrical Engineering (ICGCCEE)*, pp. 1–5, IEEE, Coimbatore, India, March 2014.

[13] P. Sundaram, "Patient monitoring system using android technology," *International Journal of Computer Science and Mobile Computing*, vol. 2, no. 5, pp. 191–201, 2013.

[14] J. Wang, Y. Zhang, Y. Han et al., "Design of a real-time emergency monitoring platform based on wireless communication technology," in *Proceedings of the 2016 8th International Conference on Intelligent Human-Machine Systems and Cybernetics (IHMSC)*, pp. 191–194, IEEE, Hangzhou, China, August 2016.

[15] G. Gaoan and Z. Zhenmin, "Heart rate measurement via smart phone acceleration sensor," in *Proceedings of the 2014 International Conference on Smart Computing (SMART-COMP)*, pp. 295–300, IEEE, Hong Kong, China, November 2014.

[16] R. Kirtana and Y. Lokeswari, "An IoT based remote HRV monitoring system for hypertensive patients," in *Proceedings of the 2017 International Conference on Computer, Communication and Signal Processing (ICCCSP)*, pp. 1–6, IEEE, Chennai, India, January 2017.

[17] K. S. Tan, R. Saatchi, H. Elphick, and D. Burke, "Real-time vision based respiration monitoring system," in *Proceedings of the 2010 7th International Symposium on Communication Systems Networks and Digital Signal Processing (CSNDSP)*, pp. 770–774, IEEE, Newcastle upon Tyne, UK, July 2010.

[18] C. Worringham, A. Rojek, and I. Stewart, "Development and feasibility of a smartphone, ECG and GPS based system for remotely monitoring exercise in cardiac rehabilitation," *PLoS One*, vol. 6, no. 2, Article ID e14669, 2011.

[19] P. Jelekäinen, "GSM-PKI solution enabling secure mobile communications," *International Journal of Medical Informatics*, vol. 73, no. 3, pp. 317–320, 2004.

[20] E. Jovanov, P. Gelabert, B. Wheelock, R. Adhami, and P. Smith, "Real time portable heart monitoring using low power dsp," in *Proceedings of the International Conference on Signal Processing Applications and Technology (ICSPAT)*, pp. 16–19, Dallas, TX, USA, October 2000.

[21] A. Walinjkar, "A composite and wearable sensor kit for location-aware healthcare monitoring and real-time trauma scoring for survival prediction," *Applied System Innovation*, vol. 1, no. 3, p. 35, 2018.

[22] E. Jovanov, D. Raskovic, J. Price, J. Chapman, A. Moore, and A. Krishnamurthy, "Patient monitoring using personal area networks of wireless intelligent sensors," *Biomedical Sciences Instrumentation*, vol. 37, pp. 373–378, 2001.

[23] T. Martin, E. Jovanov, and D. Raskovic, "Issues in wearable computing for medical monitoring applications: a case study of a wearable ECG monitoring device," in *Proceedings of the Fourth International Symposium on Wearable Computers*, pp. 43–49, IEEE, Atlanta, GA, USA, August 2000.

[24] Ultra-Low Power, "Single-channel integrated biopotential (ECG, R-to-R detection) AFE," 2018, https://datasheets.maximintegrated.com/en/ds/MAX30003.pdf.

[25] M. Li and Y. Kim, "Design of a wireless sensor system with the algorithms of heart rate and agility index for athlete evaluation," *Sensors*, vol. 17, no. 10, p. 2373, 2017.

[26] T. P. Utomo and N. Nuryani, "QRS peak detection for heart rate monitoring on Android smartphone," *Journal of Physics: Conference Series*, vol. 909, Article ID 012006, 2017.

[27] AFE4490 Integrated Analog Front-End for Pulse Oximeters, 2018, http://www.ti.com/lit/ds/symlink/afe4490.pdf.

[28] L. Sheng, C. Wei, G. Lihua, and C. Yuquan, "Study of algorithm for heart rate detection based on bipolar motion ECG," in *Proceedings of the 2011 Third International Conference on Measuring Technology and Mechatronics Automation (ICMTMA)*, vol. 3, pp. 389–392, IEEE, Shangshai, China, January 2011.

[29] A. Herbert, *Analysis of Respiratory Rate and the Respiratory Cycle in Infants and Children Using an Optical Sensor*, Department of Child Health, University of Queensland, Brisbane, Australia, 1995.

[30] S. Bose, K. Prabu, and D. S. Kumar, "Real-time breath rate monitor based health security system using non-invasive biosensor," in *Proceedings of the 2012 Third International Conference on Computing Communication & Networking Technologies (ICCCNT)*, pp. 1–6, IEEE, Coimbatore, India, July 2012.

[31] C. J. Morley, A. J. Thornton, M. A. Fowler, T. J. Cole, and P. H. Hewson, "Respiratory rate and severity of illness in babies under 6 months old," *Archives of Disease in Childhood*, vol. 65, no. 8, pp. 834–837, 1990.

[32] M. J. Tobin, T. S. Chadha, G. Jenouri, S. J. Birch, H. B. Gazeroglu, and M. A. Sackner, "Breathing patterns," *Chest*, vol. 84, no. 2, pp. 202–205, 1983.

[33] K. M. Rao and B. G. Sudarshan, "Design and development of real time respiratory rate monitor using non-invasive biosensor," *International Journal of Research in Engineering and Technology*, vol. 4, no. 6, pp. 437–442, 2015.

Research Article

Comparison of a Low-Cost Miniature Inertial Sensor Module and a Fiber-Optic Gyroscope for Clinical Balance and Gait Assessments

Daniel Roetenberg [iD],[1] **Claudia Höller,**[1] **Kevin Mattmüller,**[2] **Markus Degen,**[2] **and John H. Allum** [iD][3]

[1]*Hocoma AG, Volketswil, Switzerland*
[2]*FHNW University of Applied Sciences and Arts Northwestern Switzerland, School of Life Sciences, Muttenz, Switzerland*
[3]*Department of ORL, University of Basel Hospital, Basel, Switzerland*

Correspondence should be addressed to John H. Allum; john.allum@usb.ch

Objective. To investigate whether a microelectromechanical system (MEMS) inertial sensor module is as accurate as fiber-optic gyroscopes when classifying subjects as normal for clinical stance and gait balance tasks. *Methods.* Data of ten healthy subjects were recorded simultaneously with a fiber-optic gyroscope (FOG) system of SwayStar™ and a MEMS sensor system incorporated in the Valedo® system. Data from a sequence of clinical balance tasks with different angle and angular velocity ranges were assessed. Paired *t*-tests were performed to determine significant differences between measurement systems. Cohen's kappa test was used to determine the classification of normal balance control between the two sensor systems when comparing the results to a reference database recorded with the FOG system. Potential cross-talk errors in roll and pitch angles when neglecting yaw axis rotations were evaluated by comparing 2D FOG and 3D MEMS recordings. *Results.* Statistically significant ($\alpha = 0.05$) differences were found in some balance tasks, for example, "walking eight tandem steps" and various angular measures ($p < 0.03$). However, these differences were within a few percent (<2.7%) of the reference values. Tasks with high dynamic velocity ranges showed significant differences ($p = 0.002$) between 2D FOG and 3D MEMS roll angles but no difference between 2D FOG and 2D MEMS roll angles. An almost perfect agreement could be obtained for both 2D FOG and 2D MEMS ($\kappa = 0.97$) and 2D FOG and 3D MEMS measures ($\kappa = 0.87$) when comparing measurements of all subjects and tasks. *Conclusion.* MEMS motion sensors can be used for assessing balance during clinical stance and gait tasks. MEMS provides measurements comparable to values obtained with a highly accurate FOG. When assessing pitch and roll trunk sway measures without accounting for the effect of yaw, it is recommended to use angle and angular velocity measures for stance, and only angular velocity measures for gait because roll and pitch velocity measurements are not influenced by yaw rotations, and angle errors are low for stance.

1. Introduction

Technological advances and clinical research have shown that body-worn sensors measuring angular velocity (gyroscopes) and/or the acceleration of the trunk can accurately quantify balance during stance and gait tasks [1, 2], enabling detection of potential fallers [3] and discrimination between clinically different balance disorders [4].

The sensors used for these purposes must be accurate over different ranges of angular velocity, low velocity ranges (<0.5°/s) for stance tests on a firm surface [4], and high velocity ranges (>100°/s) for more dynamic tasks such as rising from a stool. To detect possible deviations of body sway compared to normal reference ranges when standing with eyes open or closed on a firm surface, tests typically used clinically, highly accurate, low-noise, and low-drift sensors are required [5]. In contrast, when performing a comparison of body dynamics to those of healthy subjects, observed when rising from a stool and then walking forward, a sensor with a large working range and high resolution is required [6]. Tasks with intermediate ranges of sway amplitudes, such as those of normal walking, require a mix of

these requirements in order to identify elderly "fallers" [7]. The question is whether technologic improvements in microelectromechanical system (MEMS) motion sensors forming the basis of low-cost (approximately 10 times cheaper) and lightweight inertial measurement units (IMUs) are able to replace relatively more expensive, heavier, but more accurate (drift 10 times less) fiber-optic gyroscopes (FOGs) used for assessing a wide spectrum of balance tasks [2, 4].

A further method to reduce the costs of balance measuring devices is to use a sensor system measuring only roll and pitch motion thereby ignoring yaw motion (Figure 1(b)) under the assumption that motion about the yaw axis has a negligible influence on roll and pitch measures for most clinical stance and gait tests, except those involving turning. As this approach is often used with FOG systems, a confirmation of the negligible influence of yaw would permit interchange of reference value databases [5] collected with both devices.

In this study, we investigated whether a 2D or 3D MEMS motion sensor could be used as a cheaper lightweight alternative to measuring balance control in the form of angular sway velocity at the lower trunk with accurate FOGs. As small sensors can be placed easily at other locations on the body, an affirmative result would pave the way for the use of such sensors in different body locations and provide the basis for a comprehensive body-mounted motion analysis system. Our primary hypothesis was that a MEMS system would provide a comparable level of accuracy (kappa > 0.8) in classifying normal balance test results as a FOG system. We did not compare the MEMS motion to optical motion capture system because, unlike the 2 systems we compared in this study, motion capture systems are not portable and not quick to start, requiring the attachment of several optical "markers."

2. Methods

2.1. Measurement Systems. A fiber-optic gyroscope system SwayStar, manufactured by Balance International Innovations GmbH (Switzerland), was used as this is supplied with an extensive healthy control reference database of several clinical stance and gait balance tasks for subjects in the age range of 6 to 80 years [5]. This system measures the angular velocities of the trunk in sensor coordinates near the center of mass (around L3–L5) by means of two orthogonally placed fiber-optic gyroscopes (FOG). These record trunk sway velocities in sensor coordinates in the pitch and roll directions (Figure 1(b)). Rotations about the yaw axis are not measured with this system. Data were sampled at 100 Hz and sent unfiltered via a wireless Bluetooth connection to the PC, where the data were low-pass-filtered at 30 Hz. Angular deviations in the roll and pitch direction were calculated using trapezoid integration of angular velocity recordings from the sensors after any velocity spikes (due to a communication error) in the data were removed with a 3-sample filter examining differences between angular accelerations over the 3 samples and then low-pass-filtering with a low-pass finite impulse response

filter with a cutoff of 30 Hz. Spikes were removed by examining if the neighboring accelerations were of different sign and exceeded the mean plus 1.5 standard deviations of all accelerations in the recording, and then the sample with a spike was replaced with a linearly extrapolation value from the neighboring samples. The sensors have a specified drift of 6°/hr, a noise level (random walk) of 0.04°/s per $\sqrt{hr}$, and a maximum range of ±256°/s sampled with a resolution of 16 bits at 100 Hz. The dimensions of the sensor box mounted on a converted motorcycle belt are 15 cm × 11 cm × 9 cm, and the weight with the sensors is approximately 750 grams.

For the microelectromechanical system (MEMS), one sensor system from the Valedo® products, developed and manufactured by Hocoma AG (Switzerland), was used. The standard application of these sensors is to measure pelvic and spinal movements in order to assess movement parameters and to provide training as part of a physiotherapy plan [8]. The dimensions of each sensor are 4.2 cm × 3.2 cm × 1.6 cm, and the weight is 18 grams. The sensor module consists of a 3D MEMS gyroscope, 3D accelerometer, and 3D magnetometer, together with an onboard microprocessor, battery, and Bluetooth Low Energy (BLE) module. The gyroscope has a typical drift of 30°/hr and a noise level of 0.02°/s per $\sqrt{Hz}$, and samples have a resolution of 14 bits at 1000 Hz. The internal microprocessor runs an extended Kalman filter fusing the data of all three sensing elements outputting drift-free orientation [9]. The data of the magnetometers were not taken into account in the Kalman filter sensor fusion to eliminate any effect of magnetic disturbances [10]. Data from the sensor were transferred to the client (PC) by means of the BLE Notify operation at a rate of 50 Hz. Sampled data consisted of the orientation of the sensor module in quaternion format with respect to an earth-fixed reference system.

To obtain 3D angular velocity, the received quaternion samples were differentiated with respect to time [11]. Differentiation of the quaternion reduces the effect of gyroscope offset fluctuations and drift in comparison with the directly measured gyroscope signals because the orientation output is corrected by the sensor fusion scheme. The disadvantage is that noise in the orientation samples can cause spikes in the angular velocity derivatives. Therefore, a Hampel filter was applied using the MATLAB (MathWorks) application. This removed spikes by replacing each sample with the median of six surrounding samples [12]. Because the implemented Bluetooth protocol did not ensure that all data packages were received, occasional missing data were linearly interpolated. After the interpolation stage, the data were filtered by means of a second-order low-pass Butterworth filter with a cutoff frequency at the Nyquist frequency of 25 Hz.

The lower trunk angles measured with the MEMS system were calculated using two methods. The first technique involved applying the 3D Tilt/Twist extraction based on the orientation of the sensor [13]. The second was based on the time integration of the roll and pitch angular velocities, yielding 2D sensor-based angles, as used by the SwayStar system. When rotations around the vertical axis (yaw) are not taken into account, these will result in cross-talk between

(a)

(b)
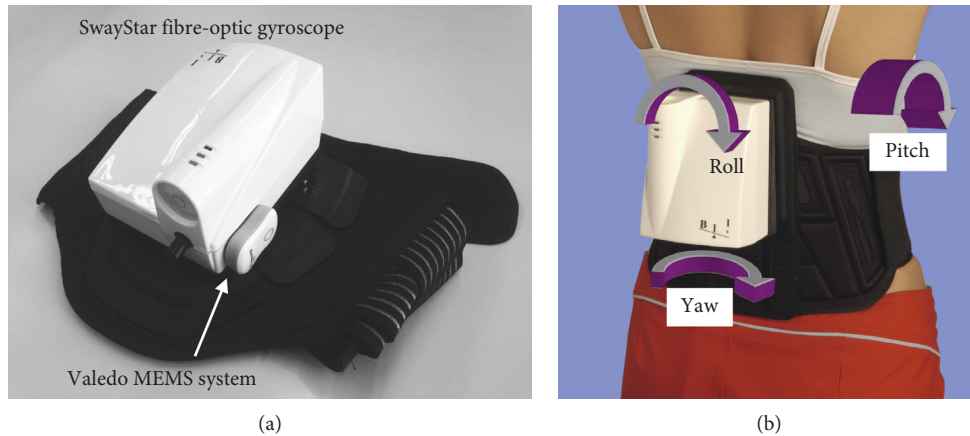
FIGURE 1: (a) SwayStar (FOG) mounted on a converted motorcycle belt with a Valedo (MEMS) sensor attached to its side. (b) The SwayStar system mounted on a subject. The SwayStar motion measurement axes (pitch and roll) are, as shown, sensor-based.

the roll and pitch angles because rotations are not commutative. The effect of this cross-talk was investigated by analyzing the differences between the 2D and 3D angle calculation methods of the 3D MEMs with the 2D angle calculation of the FOG sensor system. Cross-talk does not occur for the angular velocity measures as these are local derivatives.

From the two sets of sampled sensor data, the following measures were extracted for analysis: peak-to-peak range (difference between maximum and minimum value during the task) and 90% range (difference between 95% and 5% percentile values when the peak-to-peak range of sampled values was divided into 40 bins and a histogram of the task recording samples built after assigning samples to these bins), for both angular velocities and angles in the pitch (sagittal plane) and roll (lateral plane) direction. Therefore, the data extraction yielded the following 8 measures:

   (i) Peak-to-peak range, roll, angle

  (ii) 90% range, roll, angle

 (iii) Peak-to-peak range, pitch, angle

 (iv) 90% range, pitch, angle

  (v) Peak-to-peak range, roll, angular velocity

 (vi) 90% range, roll, angular velocity

(vii) Peak-to-peak range, pitch, angular velocity

(viii) 90% range, pitch, angular velocity

2.2. Experimental Procedures. During the clinical stance and gait tasks, a Valedo (MEMS) sensor was held on the side of the SwayStar (FOG) sensor as shown in Figure 1(a) using double-sided adhesive tape. The mechanical alignment between Valedo and SwayStar coordinate systems was determined using an optimization algorithm as described by Chardonnes et al. [14]. We considered this a better clinical comparison of the devices than mounting both devices to a gyro test-table. Time synchronization between the recordings of the two measurement systems was performed by finding the delay of maximum cross-correlation between the two angular velocity signals of both systems for each trial and correcting sample times for this delay.

Data of 10 young healthy subjects (8 male, 2 female, age: 19–34 years) were recorded with the FOG and MEMS sensor systems simultaneously. We planned to compare between Valedo and SwayStar sensor measurements for 10 subjects and then if several trends for differences were observed to expand the data set to 20 subjects. As described below, the results showed either statistically significant differences or no differences, with a few trends. Therefore, an expansion of the data set was not considered necessary. The 9 tasks evaluated with both sensor systems are listed below in the order these were performed, that is, in the same order as for the reference database [5]. These tasks are considered to represent the full dynamic range of clinically relevant balance assessments [2, 5]. All standing tasks had a predefined duration of 20 seconds. The recording of the walking tasks was ended when the subject completed the task, for example, reached 3 meters or walked 8 tandem steps:

   (i) Standing on two legs with eyes open, on a normal (firm) surface

  (ii) Standing on two legs with eyes closed, on a foam surface

 (iii) Standing on one leg with eyes closed, on a normal surface

 (iv) Walking 8 tandem steps with eyes open

  (v) Getting up from a stool and walking 3 meters

 (vi) Walking 3 meters while pitching the head up and down

(vii) Walking 3 meters with eyes closed

(viii) Walking up and down a set of stairs (2 steps up and 2 down)

 (ix) Walking 8 meters with eyes open

If subjects were not able to complete a task (due to loss of balance which mostly occurred for the "standing on one leg, eyes closed," task for which the mean duration for healthy

young subjects is 12 sec [5]), the task was not repeated; however, the data were removed from the analysis. The total time required to record the tasks was approximately 10 minutes per subject. The study was approved by the local ethical committee responsible for the University of Basel Hospital (approval EKNZ 2015-071).

3. Analysis

For the data comparison, the differences between the FOG and MEMS measurements were expressed as absolute values as well as percentage values. The 8 extracted measures from both sensor systems were compared with reference data from 88 age- and gender-matched healthy subjects recorded by Hegeman et al. [5] (using SwayStar). Pearson's correlation coefficient r was calculated to evaluate the correlation of the peak-to-peak measures between the two sensor systems (task specific as well as for all tasks). Paired t-tests were performed to determine whether there was a significant difference between means obtained from the 2 devices for the same task measure. For this comparison, all eight measures of all 10 subjects and 9 tasks were normalized relative to the mean value of the normal reference database to account for the differences in magnitudes between tasks: for example, between the differences in the magnitudes of pitch velocity for the task of standing on 2 legs with eyes open and the task of getting up off a stool. Quoted p values in the results are before any Bonferroni correction for multiple corrections. The comparisons were made across all tasks and for each task separately. Data from the FOG and MEMS were also compared to the clinically relevant 95% limit of the reference database, looking for values less or greater than this limit. Cohen's kappa test was performed in order to assess the interrater classification accuracy (the number of measures classified as within and outside the normal reference range for the Valedo system compared to the SwayStar system) between the two sensor systems. As both sensor systems measure the movements and outcome variables independently, we therefore considered the systems as independent raters.

4. Results

Results of 3 of the 9 tasks performed are presented here in detail. These 3 tasks cover the range from low body dynamics (represented by "standing on two legs with eyes open") to high dynamics ("get up and go, and then walk 3 meters"). All graphs and tables present both the 2D MEMS and 3D MEMS data. In the sections "2D data processing" and "2D vs. 3D data processing," the comparison between the 2D and 3D angle calculations is described in further detail for all tasks.

4.1. Stance Task: Standing on Two Legs with Eyes Open. Figure 2 shows the angular velocity and angle traces for a typical recording for the task "standing on two legs with eyes open on a normal surface."

In Figure 2, the difference in angles between the two 2D recordings at the end of the 20 seconds recording is less than 0.1 degree. The Pearson correlation coefficient r between the 2D MEMS and 2D FOG values of the peak-to-peak values of all subjects is higher than 0.98 for both the angular velocity and angle signals in the pitch and roll planes. The 3D MEMS roll angle has a correlation coefficient of 0.851 with the roll angle of the FOG; the corresponding pitch angle correlation is 0.968. Angular velocity results in both roll and pitch are highly correlated with $r > 0.99$.

Table 1 compares the reference values of the matching age group [5] with the results for FOG and MEMS systems as well as the mean differences between the systems for recordings of all subjects performing the task "standing on two legs with eyes open." The FOG versus 2D MEMS and FOG versus 3D MEMS sensor values are listed as absolute and relative values (the error between both systems as a percentage of the mean reference data). The p value of the paired t-test is listed in the table. It can be observed that only roll angle (90% range) and pitch angular velocity (90% range) data are significantly different between the FOG and 2D MEMS measures, whereas the corresponding peak-to-peak values do not show any significant differences. Furthermore, with a Bonferroni correction for multiple comparisons, only pitch angular velocity (90% range) remains significant. There were no significant differences between FOG and 3D MEMS angle values (Table 1).

Note that the differences in 3D are only presented in Table 1 for the angle values; the pitch and roll angular velocities are equal for 2D and 3D. For yaw angles and angular velocities, no FOG reference values are available.

For the other stance tasks, the following was observed: "Standing on two legs with eyes closed, on a foam surface" showed significant differences between FOG and 2D MEMS for both roll and pitch angular velocities (roll: $p = 0.002$; pitch: $p < 0.001$, MEMS lower values), as well as the angle in roll plane ($p = 0.02$). The task "standing on one leg with eyes closed, on a normal surface" showed no significant differences.

4.2. Gait Tasks: Get Up and Go 3 Meters. Figure 3 shows a typical recording of the angular velocity and angle traces for "get up and go 3 meters" task (a dynamic gait task). Similar to the stance task shown in Figure 2, the biggest deviation can be observed in the 3D MEMS roll angle. The subject rotated axially when getting up and during walking. This yaw rotation is not recorded with the 2D FOG and causes a different projection in the roll plane when compared with the 3D MEMS angles. Across the test population, this difference is significant (Table 2). The MEMS angular velocities and 2D roll and pitch angles of all subjects have a very high correlation (>0.97) with the FOG data. The 3D MEMS roll angle has a correlation of 0.911 with the FOG data, and for the 3D pitch angle, the corresponding correlation is 0.999.

Table 2 shows the reference values of the matching age group in comparison with the FOG and 2D MEMS and 3D MEMS for recordings of all subjects. The relative error between the 2D FOG and the 2D MEMS compared to the mean reference values is 5.73% for the 90% roll angle range but this would not be significant after Bonferroni correction.

(a)

(b)

FIGURE 2: Angular velocity data (a) and angles (b) in the lateral/roll plane (upper), sagittal/pitch plane (middle), and the axial/yaw plane (lower) of the FOG and MEMS sensors for standing on two legs with eyes open on a normal surface task. The red lines depict the 2D FOG data, the green lines the 2D MEMS, and the blue lines the 3D MEMS angle calculations. Note that the velocity traces overlay. The pitch angle 2D traces for FOG and MEMS 2D also overlay. For the yaw angular velocity and yaw angle, only the MEMS data are available.

TABLE 1: FOG to MEMS comparison results for the task "standing on two legs with eyes open" of all recordings.

Value	PtP Ro A (°)	90 Ro A (°)	PtP Pi A (°)	90 Pi A (°)	PtP Ro V (°/s)	90 Ro V (°/s)	PtP Pi V (°/s)	90 Pi V (°/s)
Mean normal reference	0.493	0.368	1.250	1.004	1.742	0.604	3.311	1.336
FOG mean	0.450	0.322	1.352	1.108	1.553	0.609	2.884	1.404
FOG SD	0.364	0.258	0.481	0.412	0.759	0.261	0.980	0.544
MEMS 2D mean	0.427	0.298	1.337	1.102	1.525	0.595	2.763	1.368
MEMS 2D SD	0.338	0.261	0.484	0.408	0.783	0.266	0.967	0.536
Error between 2D FOG and 2D MEMS relative to mean normal reference	4.66%	6.46%	1.20%	0.63%	1.61%	2.34%	3.67%	2.68%
p value (paired t-test)	0.242	0.044*	0.528	0.739	0.635	0.073	0.079	<0.001*
MEMS 3D mean	0.420	0.307	1.299	1.068				
MEMS 3D SD	0.229	0.171	0.338	0.325				
Error between 2D FOG and 3D MEMS relative to mean normal reference	6.16%	4.03%	4.26%	3.97%				
p value (paired t-test)	0.654	0.769	0.273	0.340				

PtP: peak-to-peak range, 90 : 90% range (95%–5% percentiles); Ro: roll; Pi: pitch; A: angle in degrees; V: angular velocity in degrees/seconds. *Significant difference between the absolute values of FOG and 2D/3D MEMS before any Bonferroni correction. The mean normal reference values are taken from an age-matched group [5].
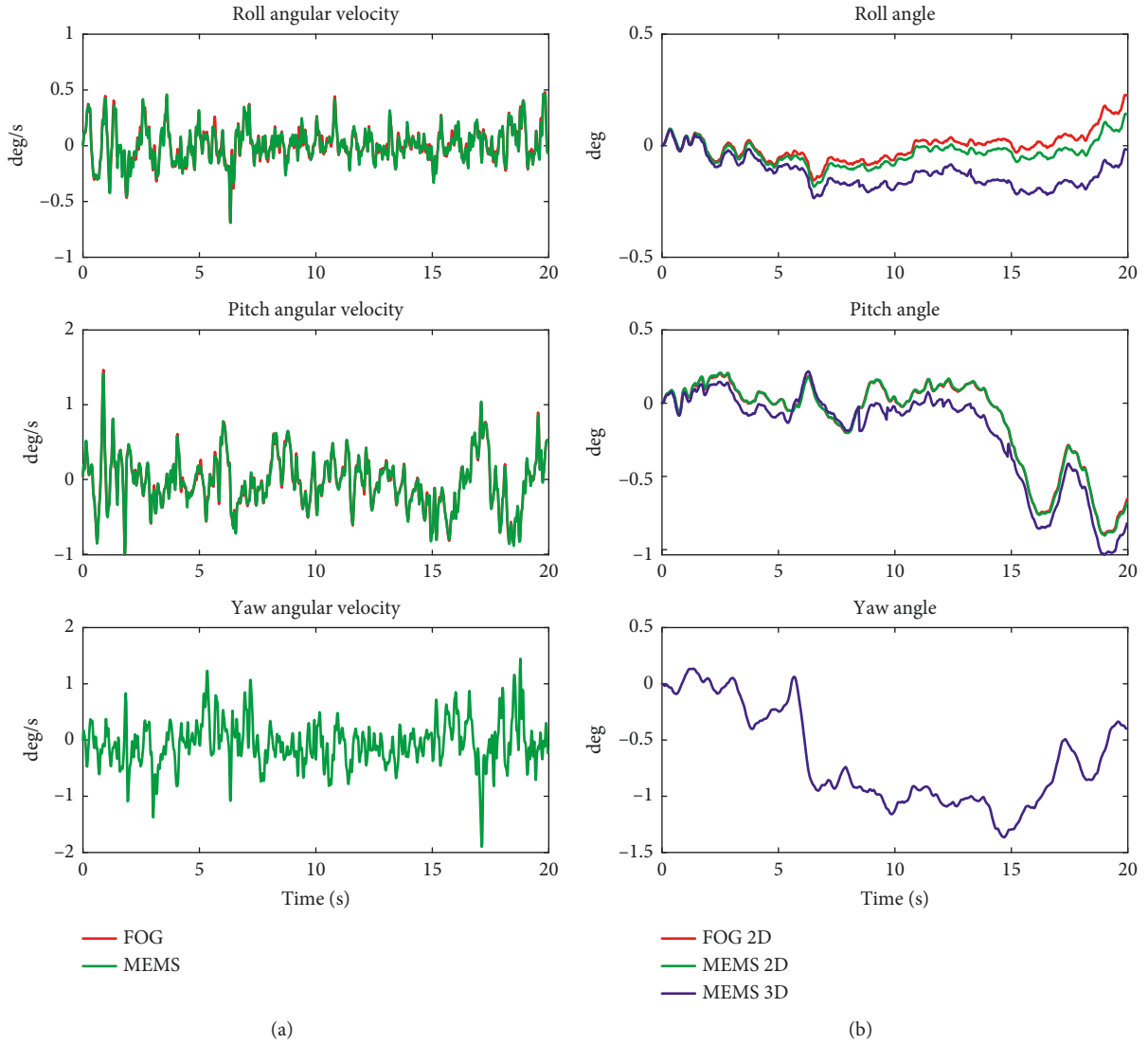
Figure 3: Angular velocity data (a) and angles (b) in the roll plane (upper) and pitch plane (middle) and yaw plane (lower) of the FOG and MEMS sensors for the "get up and go 3 meters" task. The red lines illustrate the 2D FOG data, the green lines the 2D MEMS, and the blue lines the 3D MEMS angle calculations. Note that the velocity traces overlay. The 2D FOG and 2D MEMS roll traces overlay. The pitch angle 2D traces for FOG and MEMS also overlay with the 3D MEMS traces. For the yaw angular velocity and yaw angle, only the MEMS data are available.

Table 2: FOG to MEMS comparison results for the task "get up and go 3 meters."

Value	PtP Ro A (°)	90 Ro A (°)	PtP Pi A (°)	90 Pi	PtP Ro V (°/s)	90 Ro V (°/s)	PtP Pi V (°/s)	90 Pi V (°/s)
Mean normal reference	6.451	5.201	45.95	41.90	53.78	29.61	191.7	126.5
FOG mean	5.646	4.347	34.59	31.44	50.61	28.16	139.6	93.18
FOG SD	1.931	1.252	5.858	5.615	23.13	9.960	33.03	27.74
MEMS 2D mean	5.927	4.645	34.57	31.55	48.08	27.78	137.3	92.60
MEMS 2D SD	1.966	1.428	5.876	5.599	21.78	9.768	32.48	26.97
Error between 2D FOG and 2D MEMS relative to mean normal reference	4.35%	5.73%	0.04%	0.26%	4.69%	1.25%	1.18%	0.46%
p value (paired t-test)	0.077	0.024*	0.614	0.167	0.278	0.260	<0.001*	0.343
MEMS 3D mean	6.746	5.323	34.54	31.50				
MEMS 3D SD	1.962	1.532	5.997	5.722				
Error between 2D FOG and 3D MEMS relative to mean normal reference	17.0%	18.7%	0.12%	0.15%				
p value (paired t-test)	0.002*	0.002*	0.512	0.572				

PtP: peak-to-peak range, 90: 90% range (95%–5% percentiles); Ro: roll; Pi: pitch; A: angle in degrees; V: angular velocity in degrees/seconds. Note that the differences in 3D are only presented for the angle values; the pitch and roll angular velocities are equal for 2D and 3D. *Significant difference between the absolute values of FOG and 2D/3D MEMS before any Bonferroni correction.

The difference between the 2D FOG and 3D MEMS roll angle measures is, however, much larger, 18.7%, and more significant ($p = 0.002$) (Table 2). Thus, the roll angle is underestimated by the 2D systems. Peak-to-peak pitch velocity was underestimated by the MEMS system.

For the other gait tasks listed below, the differences between the 2D FOG and 3D MEMS roll angles were not significant:

    (i) Walking 3 meters while pitching the head up and down (not significant (ns) with $p = 0.187$)

    (ii) Walking 3 meters with eyes closed (ns, $p = 0.945$)

    (iii) Walking up and down a set of stairs (ns, $p = 0.824$)

    (iv) Walking 8 meters with eyes open (ns, $p = 0.469$)

For the pitch angles, no significant differences were observed.

4.3. Semi-Gait Task: Walking 8 Tandem Steps with Eyes Open. Figure 4 shows angular velocity and angle traces of a typical recording for "walking 8 tandem steps with eyes open." This is a classical clinical task with body motion alternating between tandem stance and gait. The FOG and 2D MEMS data show very high correlations ($r > 0.99$ for both pitch and roll angle and angular velocity); FOG and 3D MEMS data all show $r > 0.93$.

Table 3 shows the reference values with the comparison of the FOG and MEMS for the task "Walking 8 tandem steps with eyes open" for all recordings. It can be seen that there were no significant differences for pitch and roll angles. However, the 90% angular velocities in both planes differ with respect to those of the MEMS system, which underestimated these measures.

4.4. Classification Accuracy between the Sensor Systems

4.4.1. 2D Data Processing. For all tasks, except trials were subjects lost their balance control, the eight extracted measures for both the 2D FOG and 2D MEMS were checked for lying within or outside the normal reference range defined by the 95% limits of the reference database. If the data are within the reference 95% range, clinically, the recording would be considered normal [5].

Because of the loss of balance, six recordings were not taken into account in the analyses (6 ∗ 8 = 48 variables). Four of these records were due to subjects losing their balance prior to task completion (20 secs) for the task, "Standing on one leg with eyes closed." The lower 5% limit of duration for this task is 14.7 secs [5].

Table 4 presents the resulting contingencies. Based on these values, Cohen's kappa was calculated and yielded a result of $\kappa = 0.969$. This is usually interpreted as an almost perfect agreement [15].

The single measurement that was inside the range as measured by the MEMS but outside with the FOG was a peak-to-peak value of the angular velocity (no differences were detected for the corresponding 90% range values because single peaks or outliers are filtered out when calculating the 90% range value.). Note that as we compared with 95% reference range values, some values outside the normal range are to be expected.

4.4.2. 2D vs. 3D Data Processing. The 3D angles and angular velocity measures measured with the MEMS and 2D FOG measures were compared with the reference database and the FOG similar to the 2D MEMS comparisons presented in the previous paragraph. For stance tasks that have low ranges, the differences between the 2D and 3D calculations were in the same range as the noise level of the MEMS sensors because the tasks involved limited axial rotation. Thus, divergences in comparison with the reference database were not expected. In contrast, in some recordings of the "get up and go 3 meters" and walking tasks, axial rotation caused a significant "cross-talk" between roll and pitch angles that resulted in a slightly higher number (6) of false-negatives when comparing the angles with the normal reference values. Nonetheless, the Kappa value is 0.868, which is also considered as an almost perfect agreement [15].

In Figure 5(a), the regressions between the 2D FOG and 2D MEMS, and 2D FOG and 3D MEMS peak-to-peak roll angles are plotted. In Figure 5(b), 2D FOG and MEMS roll angular velocities (peak-to-peak) are plotted. Data are for all subjects and recordings. The correlation coefficient r value for the 2D MEMS angle is 0.991. The 3D MEMS angles have an r value of 0.922. The angular velocity r value is 0.994. All results are highly significant ($p < 0.001$). Similar regression results could be observed for pitch angle and pitch angular velocities ($r > 0.98$). The classification matrixes described in Tables 4 and 5, and the regressions of Figure 5 indicate that the differences between the two measurement systems are small from a clinical viewpoint across all tasks, including those not described in detail above. Otherwise, for example, the regressions of Figure 5 would be less significant.

5. Discussion

In this study, we have tested whether low-cost MEMS motion sensors can provide comparable accuracy as highly accurate fiber-optic gyroscopes to assess balance tasks, which require low noise, minimum drift, and a high resolution across the range of angular sway and sway velocity induced by the balance tasks. We could also assess whether cross-talk errors on pitch and roll angular measures due to not recording yaw angular velocity are significant. If comparable in accuracy and with insignificant cross-talk errors, then MEMS motion sensors can be used to compare extracted balance measures with reference values obtained with highly accurate fiber-optic gyroscopes recording pitch and roll angular velocities. Our main findings were, firstly, that except for the get up and go test, there were no significant differences between 2D FOG and 3D MEMS roll and pitch angle measures. Secondly, angular velocities were slightly underestimated with the MEMS system. Thus, the analyses of the 2D MEMS data showed almost perfect agreement with the FOG data with an interrater classification accuracy of $\kappa = 0.969$ when comparing the measures
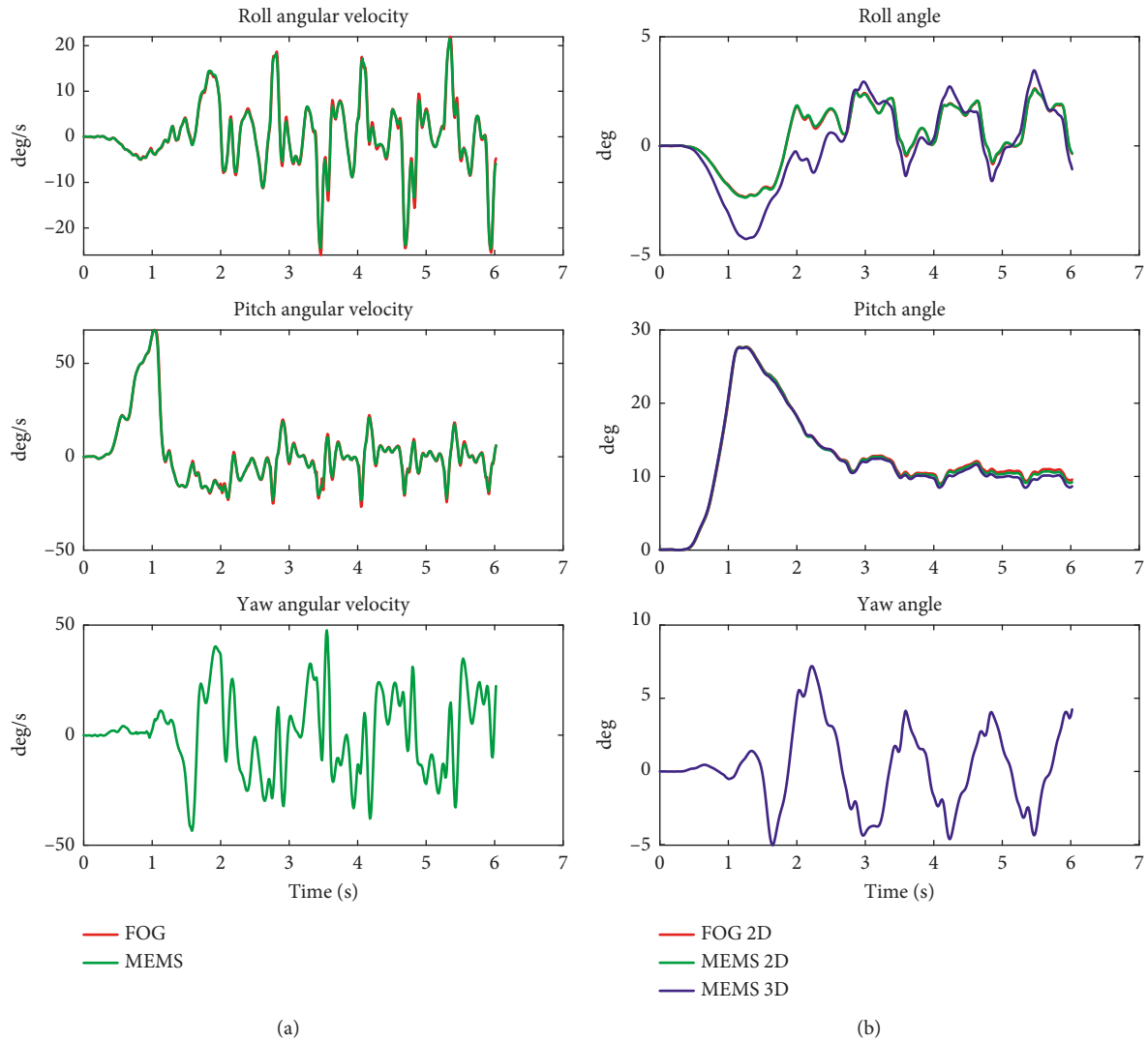
(a)

(b)
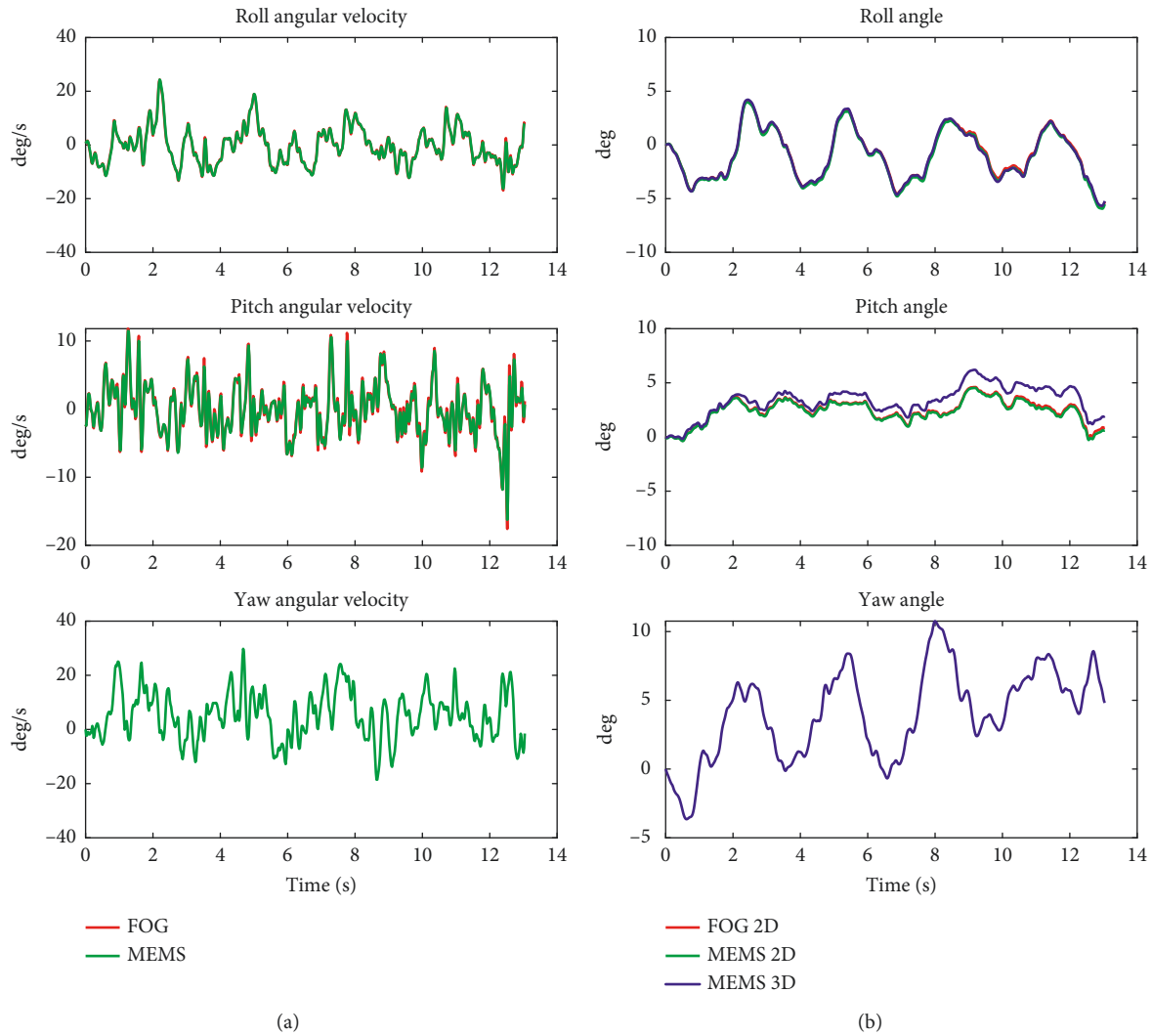
FIGURE 4: Angular velocity data (a) and angles (b) in the roll plane (upper) and pitch plane (middle) and yaw plane (lower) of the FOG and MEMS sensors for walking 8 tandem steps with eyes open task. The red lines represent the 2D FOG, the green lines the 2D MEMS, and the blue lines the 3D MEMS angle calculations. Note that roll angle traces overlay as do pitch angle FOG and MEMS 2D traces. All velocity traces overlay. The yaw angle is only available for MEMS 3D.

TABLE 3: FOG to MEMS comparison results for the task "walking 8 tandem steps with eyes open."

Value	PtP Ro A (°)	90 Ro A (°)	PtP Pi A (°)	90 Pi A (°)	PtP Ro V (°/s)	90 Ro V (°/s)	PtP Pi V (°/s)	90 Pi V (°/s)
Mean normal reference	6.324	4.714	6.920	5.160	33.86	18.49	37.92	21.03
FOG mean	5.200	3.718	5.706	4.126	35.93	19.21	31.90	17.14
FOG SD	1.904	1.494	1.328	1.181	12.47	5.055	5.813	3.407
MEMS 2D mean	5.134	3.657	5.717	4.127	34.18	18.76	30.66	16.59
MEMS 2D SD	1.919	1.524	1.336	1.189	11.46	4.963	5.076	3.156
Error between 2D FOG and 2D MEMS relative to mean normal reference	1.04%	1.29%	0.16%	0.01%	5.17%	2.48%	3.28%	2.62%
p value (paired t-test)	0.202	0.155	0.675	0.984	0.051	<0.001*	0.216	0.003*
MEMS 3D mean	5.126	3.641	5.957	4.229				
MEMS 3D SD	1.968	1.534	1.132	1.113				
Error between 2D FOG and 3D MEMS relative to mean normal reference	1.17%	1.64%	3.63%	1.98%				
p value (paired t-test)	0.496	0.447	0.132	0.412				

PtP: peak-to-peak range, 90 : 90% range (95%–5% percentiles); Ro: roll; Pi: pitch; A: angle in degrees; V: angular velocity in degrees/seconds. *Significant difference between the absolute values of FOG and 2D/3D MEMS before any Bonferroni correction.

TABLE 4: Contingency table for agreement on values lying within or outside the range of 95% limit of the reference data.

MEMS 2D	FOG 2D	
	Inside range	Outside range
Inside range	637	1
Outside range	1	33

TABLE 5: Contingency table for agreement on values lying within or outside the range of 95% limit of reference data.

MEMS 3D	FOG 2D	
	Inside range	Outside range
Inside range	636	6
Outside range	2	28
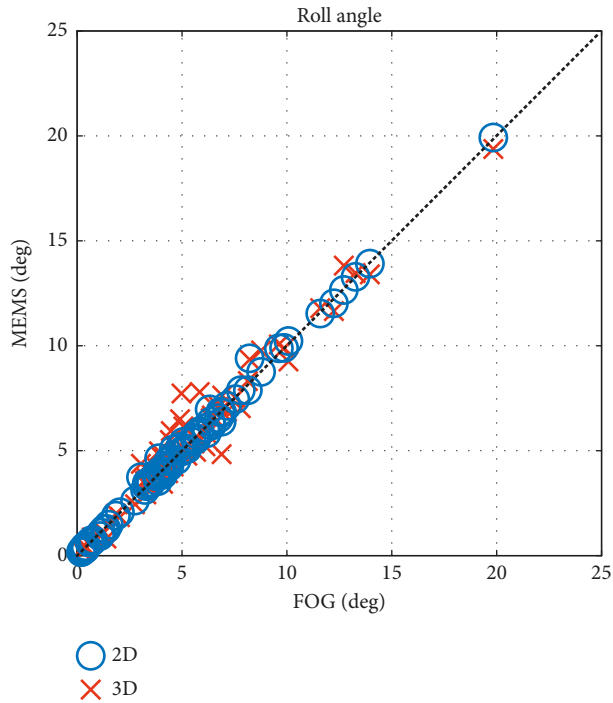
(a)
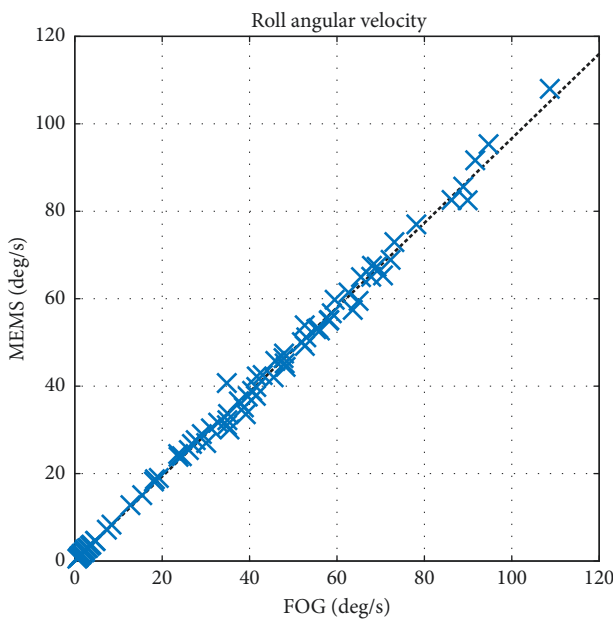
(b)

FIGURE 5: (a) Regression of peak-to-peak roll angle FOG vs MEMS 2D (blue circles) and MEMS 3D (red crosses). (b) Peak-to-peak roll angular velocity FOG vs MEMS.

with those of a normal reference data set [5]. In summary, although as described above, for some tasks and some measures statically significant differences were found, further analysis showed that all these differences were within a few percent of the reference values and therefore assumed not to be clinically relevant. Therefore, with the proposed MEMS signal processing pipeline, consisting of outlier rejection, interpolation and filtering, resulting in an average correlation of over $r = 0.95$, the MEMS data can be compared for classification purposes (as normal values or not) to reference values collected with a 2D FOG system.

Statistically significant differences were found between the 3D MEMS roll angles in comparison with the 2D FOG values for the most dynamic gait task "get up and go 3 m," that is, with the greatest range of pitch angular velocity (over 100 deg/s, Table 2). The observed differences between the contingency tables based on 3D MEMS and 2D FOG were due to cross-talk errors of axial rotations and not to noise. When comparing the two contingencies tables (Tables 4 and 5), this happened in less than 1% of all recordings. Specifically, the errors occurred almost exclusively with the get up and go task, which had large jaw and pitch axial rotations (Figure 3). Thus, employing balance tasks with little yaw rotation would avoid this problem. Nonetheless using the third orthogonal, yaw sensing axis of the MEMS opens the possibility of measuring trunk sway during many other clinically relevant balance assessments tasks involving turning (e.g., those of Dite and Temple [16] and Salarian et al. [17]).

Angular velocities measured with the MEMS sensors were obtained by differentiating the processed quaternion output with respect to time. Even if the small differences noted (less than 3% of normal reference values) are not clinically relevant, angular velocities tended to be underestimated by the MEMS. A cause of this difference could be related to mechanical misalignment of the two sensor systems, which is estimated to be around 1 degree [14]. Another cause is likely to be noise and spikes in the MEMS angular velocity data and probably both noise and spikes could be reduced further by modifying the signal processing used here. For example, the bias-corrected gyroscope signal could be sent by the sensor in addition to the quaternion. This, however, would require a modification to the currently used Bluetooth protocol. Additionally, data from multiple MEMS sensor modules could be fused to reduce noise levels. This would require a proper mechanical alignment and time synchronization between the modules. Another alternative would be to improve the filtering of the angular velocity spikes in comparison with the Hampel filter used here.

One of the drawbacks of our study is the limited range of subject ages (19–34 years) we considered. We have compared the accuracy of the two systems in relation to the healthy control reference database of Hegeman et al. [5]. As Hegeman et al. [5] have shown that there are no differences in balance control between the 10 young adults of aged 19–34 years we tested and those aged 35–60, we can argue that our comparison is applicable to patients with the age range 19–60 years, but possibly not for patients less than 19 and persons older than 60 years. Both of the latter groups have sway greater than middle-aged persons [5].

There are three analytical and clinical areas, which should be considered for future studies. As indicated above, the MEMS system tends to underestimate values of pitch and roll velocities. Thus, the cause of this difference should be examined and established if this underestimate is due to signal processing or sensor alignment. If these causes are ruled out, then attention should be placed on examining patient groups with ataxia that are known to have higher velocity trunk sway during gait trials with tandem steps or eyes closed [18]. Underestimates of velocities might prove to be clinically relevant for these patient groups. A third area concerns children younger than 6 years for whom there is no SwayStar reference data [5]. The lighter weight of the MEMS system compared to the FOG system is crucial when considering measurements of this age group.

In this study, the MEMS sensors were attached directly onto the FOG system, which was mounted on a converted motorcycle kidney belt. Therefore, both sensor systems measured the same angular movements of the pelvis and lower back. This ensured that movement of the skin during the tasks had no effect in comparing the measurements in the pitch and roll planes between the sensors systems. MEMS sensors can be mounted with double-sided adhesive tape directly on the skin or with an elasticated belt around the waist. These later methods of mounting can cause distinctive soft tissue artefacts compared to the relatively rigid converted motorcycle belt used for the FOG. Additionally, the significant difference in weight between the two sensor systems can influence the effect of soft tissue movements on the outcome measures. For walking tasks, typical roll and pitch soft tissue errors are of the order of 1–2 degrees [19] and therefore at least equal to 20% of the roll angle amplitudes we measured during gait tasks when the yaw contribution was ignored (Figures 3 and 4; Tables 2 and 3). Given the effect of soft tissue artefacts during dynamic gait balance tasks, and our results indicating that the effect of yaw angle on roll angle estimates was much greater during routine clinical gait tasks compared to stance tasks, we consider it advantageous to concentrate on recording angular velocity measures when using body-mounted sensors to quantify gait balance control pathologies, as roll and pitch velocity measures are not influenced by yaw rotations. In this respect, many current patient classification techniques rely on angle measures for stance and velocity measures for gait [2, 4, 7].

In conclusion, except for tests that involve large yaw movements, there were no significant differences between 2D FOG and 3D MEMS roll and pitch angle measures, although angular velocities were slightly underestimated with the MEMS system. Therefore, 2D MEMS data showed almost perfect agreement with the 2D FOG data. In summary, although for some tasks and some measures statically significant differences were found, further analysis showed that all these differences were within a few percent of the reference values and therefore these differences were assumed not to be clinically relevant. Future studies could consider placing two MEMS sensors side-by-side on a belt, thereby reducing skin artifacts and providing increased accuracy.

Data Availability

The data used to support the findings of this study are available from the corresponding author upon request.

Ethical Approval

This study was approved by the local ethical committee responsible for the University of Basel Hospital, Ethical Committee of North-Central Switzerland (approval EKNZ 2015-071).

Conflicts of Interest

D. Roetenberg and C. Höller are employees of Hocoma AG producing the Valedo inertial sensors used in this study. J. H. J. Allum is a consultant for the company Balance International Innovation GmbH producing the SwayStar equipment used in this study.

Acknowledgments

References

[1] R. I. Spain, R. J. St. George, A. Salarian et al., "Body-worn motion sensors detect balance and gait deficits in people with multiple sclerosis who have normal walking speed," *Gait & Posture*, vol. 35, no. 4, pp. 573–578, 2012.

[2] J. H. Allum and M. G. Carpenter, "A speedy solution for balance and gait analysis: angular velocity measured at the centre of body mass," *Current Opinion in Neurology*, vol. 18, no. 1, pp. 15–21, 2005.

[3] B. R. Greene, E. P. Doheny, C. Walsh, C. Cunningham, L. Crosby, and R. A. Kenny, "Evaluation of falls risk in community-dwelling older adults using body-worn sensors," *Gerontology*, vol. 58, no. 5, pp. 472–480, 2012.

[4] J. Vonk, C. G. C. Horlings, and J. H. J. Allum, "Differentiating malingering balance disorder patients from healthy controls, compensated unilateral vestibular loss, and whiplash patients using stance and gait posturography," *Audiology and Neurotology*, vol. 15, no. 4, pp. 261–272, 2010.

[5] J. Hegeman, E. Y. Shapkova, F. Honegger, and J. H. Allum, "Effect of age and height on trunk sway during stance and gait," *Journal of Vestibular Research*, vol. 17, no. 2-3, pp. 75–87, 2007.

[6] D. Kaski, R. O. Dominguez, J. H. Allum, and A. M. Bronstein, "Improving gait and balance in patients with Leukoaraiosis using transcranial direct current stimulation and physical training," *Neurorehabilitation and Neural Repair*, vol. 27, no. 9, pp. 864–871, 2013.

[7] E. W. de Hoon, J. H. Allum, M. G. Carpenter et al., "Quantitative assessment of the stops walking while talking test in the elderly," *Archives of Physical Medicine and Rehabilitation*, vol. 84, no. 6, pp. 838–842, 2003.

[8] C. M. Bauer, F. M. Rast, M. J. Ernst et al., "Concurrent validity and reliability of a novel wireless inertial measurement system to assess trunk movement," *Journal of Electromyography and Kinesiology*, vol. 25, no. 5, pp. 782–790, 2015.

[9] M. Schepers, H. Luinge, G. Bellusci, and P. Slycke, *XKF3—Low-Power, Optimal Estimation of 3D Orientation Using Inertial and Magnetic Sensing—AN-5084*, Fairchild Semiconductor Cooperation, Sunnyvale, CA, USA, 2015.

[10] D. Roetenberg, H. J. Luinge, C. T. M. Baten, and P. H. Veltink, "Compensation of magnetic disturbances improves inertial and magnetic sensing of human body segment orientation," *IEEE Transactions on Neural Systems and Rehabilitation Engineering*, vol. 13, no. 3, pp. 395–405, 2005.

[11] J. Hol, "Sensor fusion and calibration of inertial sensors, vision, ultra-wideband and GPS," Ph. D. thesis, Linköping University, Linköping, Sweden, 2011.

[12] F. R. Hampel, "The influence curve and its role in robust estimation," *Journal of the American Statistical Association*, vol. 69, no. 346, pp. 383–393, 1974.

[13] N. R. Crawford, G. T. Yamaguchi, and C. A. Dickman, "A new technique for determining 3-D joint angles: the tilt/twist method," *Clinical Biomechanics*, vol. 14, no. 3, pp. 153–165, 1999.

[14] J. Chardonnes, J. Favre, and K. Aminian, "An effortless procedure to align the local frame of an inertial measurement unit to the local frame of another motion capture system," *Journal of Biomechanics*, vol. 45, no. 13, pp. 2297–2300, 2012.

[15] J. Cohen, "A coefficient of agreement for nominal scales," *Educational and Psychological Measurement*, vol. 20, no. 1, pp. 37–46, 1960.

[16] W. Dite and V. A. Temple, "Development of a clinical measure of turning for older adults," *American Journal of Physical Medicine & Rehabilitation*, vol. 81, no. 11, pp. 857–866, 2002.

[17] A. Salarian, C. Zampieri, F. Horak, P. Carlson-Kuhta, J. Nutt, and K. Aminian, "Analyzing 180° turns using an inertial system reveals early signs of progression of Parkinson's disease," in *Proceedings of the 2009 Annual International Conference of the IEEE Engineering in Medicine and Biology Society*, September 2009.

[18] B. P. C. Van de Warrenburg, M. Bakker, B. P. H. Kremer, B. R. Bloem, and J. H. J. Allum, "Trunk sway in patients with spinocerebellar ataxia," *Movement Disorders*, vol. 20, no. 8, pp. 1006–1013, 2005.

[19] N. M. Fiorentino, P. R. Atkins, M. J. Kutschke, J. M. Goebel, K. B. Foreman, and A. E. Anderson, "Soft tissue artifact causes significant errors in the calculation of joint angles and range of motion at the hip," *Gait & Posture*, vol. 55, pp. 184–190, 2017.

Research Article

Design and Validation of Multichannel Wireless Wearable SEMG System for Real-Time Training Performance Monitoring

Serkan Örücü [1] **and Murat Selek** [2]

¹*Ermenek Vocational School, Karamanoğlu Mehmetbey University, Karaman 70400, Turkey*
²*Vocational School of Technical Sciences, Konya Technical University, Konya 42130, Turkey*

Correspondence should be addressed to Serkan Örücü; srknorucu@kmu.edu.tr

Monitoring of training performance and physical activity has become indispensable these days for athletes. Wireless technologies have started to be widely used in the monitoring of muscle activation, in the sport performance of athletes, and in the examination of training efficiency. The monitorability of performance simultaneously in the process of training is especially a necessity for athletes at the beginner level to carry out healthy training in sports like weightlifting and bodybuilding. For this purpose, a new system consisting of 4 channel wireless wearable SEMG circuit and analysis software has been proposed to detect dynamic muscle contractions and to be used in real-time training performance monitoring and analysis. The analysis software, the Haar wavelet filter with threshold cutting, can provide performance analysis by using the methods of moving RMS and %MVC. The validity of the data obtained from the system was investigated and compared with a biomedical system. In this comparison, 90.95% ± 3.35 for left biceps brachii (BB) and 90.75% ± 3.75 for right BB were obtained. The output of the power and %MVC analysis of the system was tested during the training of the participants at the gym, and the training efficiency was measured as 96.87% ± 2.74.

1. Introduction

In recent years, the monitoring of athlete performance has become indispensable for the health of athletes. Wireless technologies have started to be widely used in order to obtain data for the purpose of examining training efficiency in the monitoring of muscle activation and sport performance of athletes [1, 2]. It is possible to collect information about athlete performance and rehabilitation, about preventing muscle fatigue or injuries through posttraining analysis of SEMG signal obtained during the training [3–5]. Recording of SEMG signals in related muscles during training can be extremely useful in increasing performance and preventing disabilities [6].

Traits of SEMG signals obtained during training (frequency, severity, etc.) change depending on the muscle group measured and the severity of contraction [7–9]. In these measurements, surface-type electrodes are used to determine and examine the activity of muscles during contraction and relaxation of muscles. When academic studies related to this subject are analysed, there are some wearable biometric systems developed for the purpose of the monitoring of performance during training. Some of these systems are intended for recording parameters like heart rate, respiration, location, and velocity or for estimating the levels of muscle fatigue [10–13]. Some of them have been produced for the measurement of the SEMG signals in laboratorial environment [14]. Another proportion of them has been designed for the purpose of perceiving dynamic muscle contraction during isolated training through the SEMG [15]. The last proportion has carried out low-cost experimental SEMG systems and matched the key features of the system with the existing systems [16–18].

The most reliable method used in the adequacy and examination of muscle activation in physiological studies is the amplitude analysis carried out on SEMG signals, known as MVC (maximum voluntary contraction) normalization

[19]. Data with MVC normalization enable understanding of what capacity the muscle works, how effective level muscles have reached through training and how much effort a training requires from an athlete [20].

The simultaneous monitorability of athlete performance during the process of training is a must for athletes at the beginner level to being able to carry out healthy training in sports like weightlifting and bodybuilding [21, 22]. This feature enables performance evaluation to be carried out momentarily during the time when there is no trainer or until the motor skills of the athlete concerning movement develop enough. A SEMG system, to be used during the training for this purpose [7, 23–25] has to

(i) Be able to provide the required SEMG data necessary for monitoring training efficiency in performance analysis

(ii) Be able to filter the noise of movement during isotonic exercises and noise and distortions in SEMG signals appearing as a result of other factors

(iii) Its procedures like calibration, etc., have to continue for a short time

(iv) The data obtained have to be at a close accuracy to biomedical systems

(v) Has to be simultaneously usable in a training environment

For use in the industrial field, various systems are available for SEMG data collection and processing. To investigate these, WB-EMG [26], BiometricsDatalog [27], Myo Armband [28], DelsysTrignio [29], BITalino [30], Mbody3 [31], Mpower [32], MyoTrac [33], MyoWare [34], Shimmer [35], and hospital [36] are such systems. The systems specified in [26], [27], and [29] and the systems which we measure in hospital [36] are not wearable during training. The system specified in [44] is wearable and supports wireless transmission but its production is stopped. In terms of the electrodes used, and CMRR, there is no difference in all of these products and they comply with the SENIAM criteria. The systems [26], [27], and [30] do not have noise and data processing filters, and the systems in [28] and [29] use a Notch filter and a band-stop filter with narrow-bandwidth in hardware. The system in [26, 34] is designed for single-channel use but does not support multichannel monitoring. The systems in [31–34] are wearable and do not include contraction detection and simultaneous MVC analysis although they can monitor multiple muscle groups. A summary of these comparisons is presented in Table 1.

When the table is analysed, it is seen that all of these systems can simultaneously observe biopotential changes in muscle or muscle groups monitored during training, but none of them include real-time MVC normalization and contraction detection procedures for performance analysis during training.

That these features can be monitored simultaneously during the training process may be useful especially for beginner athletes to perform a healthy training in sports like weightlifting and bodybuilding, for the performance evaluation of the athlete until the motor skills of the movement are improved and at necessary moments in preventing the injury process by intervening in training.

Based on these elements, a new wireless wearable SEMG data collection system has been introduced which enables performance monitoring and analysis at training time with its real-time MVC normalization and contraction detection processes. The SEMG circuit used in our system is designed by us to be used in future studies and to be developed according to our needs.

In the presented system, digital filtering is also used in addition to hardware filtering in SEMG circuit. These numerical filters are Haar wavelet filters with Threshold cutting based on (TCHW) and linear Kalman [37, 38]. Each numerical filtering method is tested together with hardware filtering. Results obtained from here will be determinative in deciding the filtering structure that can be used in future stages of the system design. Subsequently, filtered data are processed through moving RMS method containing the methods of moving average (MA) and root mean square (RMS), scaled through MVC normalization, and a training support system that can carry out real-time performance analysis and monitoring.

2. Materials and Methods

2.1. Isotonic Contraction. Isotonic contraction encompasses exercises where muscle tendons get shortened to generate movement. Any kind of movement, ranging from weightlifting to rowing and running, is in this category [39]. In sport, an isotonic exercise is a training where the most amount of strength is exerted on a particular muscle or muscle group to increase that muscle mass or performance in general. Due to the fact that human activity and athletic performance necessitate these kinds of movement, isotonic exercises form the basis of a lot of training protocols [40]. It is possible to observe pathological changes or efficiency obtained from the training through an examination of SEMG signals generated in muscles during these exercises [41].

2.2. SEMG Circuit Design. The SEMG circuit design details are given below. The circuit consisting of 4 channels could monitor the biopotential change of 4 different muscle groups at the same time. So, it is possible to monitor biopotential changes occurring in muscles in symmetrical movements that affect multiple muscle groups (e.g., the Bench Press movement affects pectoralis major and triceps muscles). The circuit has in each channel, respectively, one instrumentation amplifier, a inverting amplifier, a low-pass filter, a high-pass filter, and a full-wave rectifier. The circuit has a diode for input protection, a pointer indicating that the circuit is working, and a start-up button. During working, the LD1117 regulator was used for the Bluetooth feed and the 7805 regulator for the +5 volt and −5 volt op-amp feed (Figure 1(a)). The SEMG signals we want to process are

TABLE 1: Comparison of the SEMG acquisition systems.

System	Signal type	Number of channels	Gain	ADC resolution (bits)	Wearable	Filter type	Contraction detection	Real-time MVC norm.	CMRR	Connection type
Proposed system	SEMG	4	4400	12	Yes	Hardware + software	Yes	Yes	>90	Bluetooth
WB-EMG	SEMG	1	100–10000	12	No	No	No	No	>90	Bluetooth
Biometrics datalog	SEMG	8	1000	14	No	No	No	No	>90	Bluetooth
Myo armband	SEMG	8	≥1000	8	Yes	Notch	No	No	>90	Bluetooth
Delsys Trignio	SEMG	16	909	16	No	Notch	No	No	>90	RF
BITalino	SEMG	Up to 6	1000	6–10	Yes	No	No	No	>90	Bluetooth
Mbody3	SEMG	Up to 6	≥1000	24	Yes	Hardware + software	No	No	>90	Bluetooth
Mpower	SEMG	4	≥1000	—	Yes	Hardware + software	No	No	>90	Bluetooth
MyoTrac	SEMG	2	≥1000	14	Yes	Butterworth	No	No	>90	Bluetooth
MyoWare	SEMG	1	≥1000	—	Yes	No	No	No	>90	Bluetooth
Shimmer	SEMG	Up to 60	≥1000	16	Yes	Hardware + software	No	No	>90	Bluetooth
Hospital	SEMG	8	1–10000	24	No	Hardware + software	Yes	No	>90	Usb

MUAP signals whose amplitude is between 0 and 1.5 mVolt (RMS). To process this electrical signal, it must firstly be amplified. In the system, this amplification is done by increasing the difference between the two electrodes in bipolar mode. While the obtained common signal is amplified in this mode, the background noise is also suppressed. Two of the probes activated from each channel are connected to the circuit's soil, like the reference probe [42] which is placed in a more electrically remote area (preferably a neutral or close to the bone region) while going to the amplifier and filter circuits over INA 128P, which operates in a single differential mode. In the first step, amplification was performed by using the INA 128P differential amplifier (Figure 1(b)).

As stated in [43], the reason why we use INA 128P is that the amplitude of the SEMG signal is low and that the amplifier to be used due to other factors like noise must have a high input impedance and a high common mode rejection rate (CMRR > 95 dB). This amplifier has the required features with CMRR >120 dB and 10 GΩ input impedance. When we set the gain value for the 60 Hz input signal to $G = 74.52$ using INA 128P in our system, approximately 108 dB CMRR was obtained as stated in the technical document in [44]. The reason for selecting a 60 Hz input signal in the system design is that the SEMG signal is dominant in the range of 50 Hz to 150 Hz. To obtain a processable signal amplitude in the second stage, TL072 was used as shown in Figure 1(c) as an active inverting amplifier. At this stage was the amplifier gain approximately $G = 59$ and the CMRR approximately 100 dB by using the 60 Hz input signal as stated in [45].

In SEMG applications, analogue (hardware) and digital (software) filters are used to remove unwanted component noises and process the necessary parts in the SEMG signal [46]. Analogue filters remove anything above or below a selected cut frequency, while digital filters make this process more precise as they can be programmed [47]. This certainty is due to the fact that the features of digital filters can be changed depending on the input signal parameters [48]. In these applications, analogue filters are used to eliminate noise from the signal in signal amplification and processing circuits, to provide noise immunity, and to obtain the necessary parts of the frequency band [49]. On the contrary, digital filters are used to filter signal residues named artifact after motion and to analyse SEMG signal (feature extraction, time-frequency analysis, contraction detection, performance analysis, etc.) [41, 50].

In the circuit, analogue filtering is performed by low- and high-pass filters. Ideal SEMG signals are observed between 50 Hz and 500 Hz and should be filtered from frequency components outside this range [51]. For this, the signal from the output of the instrumentation amplifier is first filtered so that the gain is 1 in the high-pass filter (HPF) using TL072 with a cutoff frequency of about 48 Hz (Figure 1(d)). The components of the EMG signal above 500 Hz are filtered through a 2nd order Sallen–Key low-pass filter (LPF) using TL072. Through this section, resistance and capacitor values are designed so that the cutoff frequency is approximately 482 Hz, the quality factor is 0.5, and the gain is 1 (Figure 1(e)). The reason we prefer the Sallen–Key topology we use in the circuit is that this filter has the ability to produce a quadratic low-pass reaction with better selectivity (higher pole) and various possible approaches (Butterworth, Chebyshev, Thomson-Bessel, etc.) [43, 47, 49]. This will help us in our future work.

Then, the whole SEMG signal was moved to the positive level using the full-wave rectifier (Figure 1(f)). With this process, it is possible to analyse the low-frequency oscillations by overcoming the high-pass nature of the SEMG signal [52]. Thus, it is aimed to use the circuit except for the training efficiency, also in the fields of prosthesis control and ergonomics.

The Pic16F1786 microcontroller with connected full-wave rectifier outputs contains 11 12 bit A/D (Analogue/Digital) converters. The data obtained from the rectifier of each channel
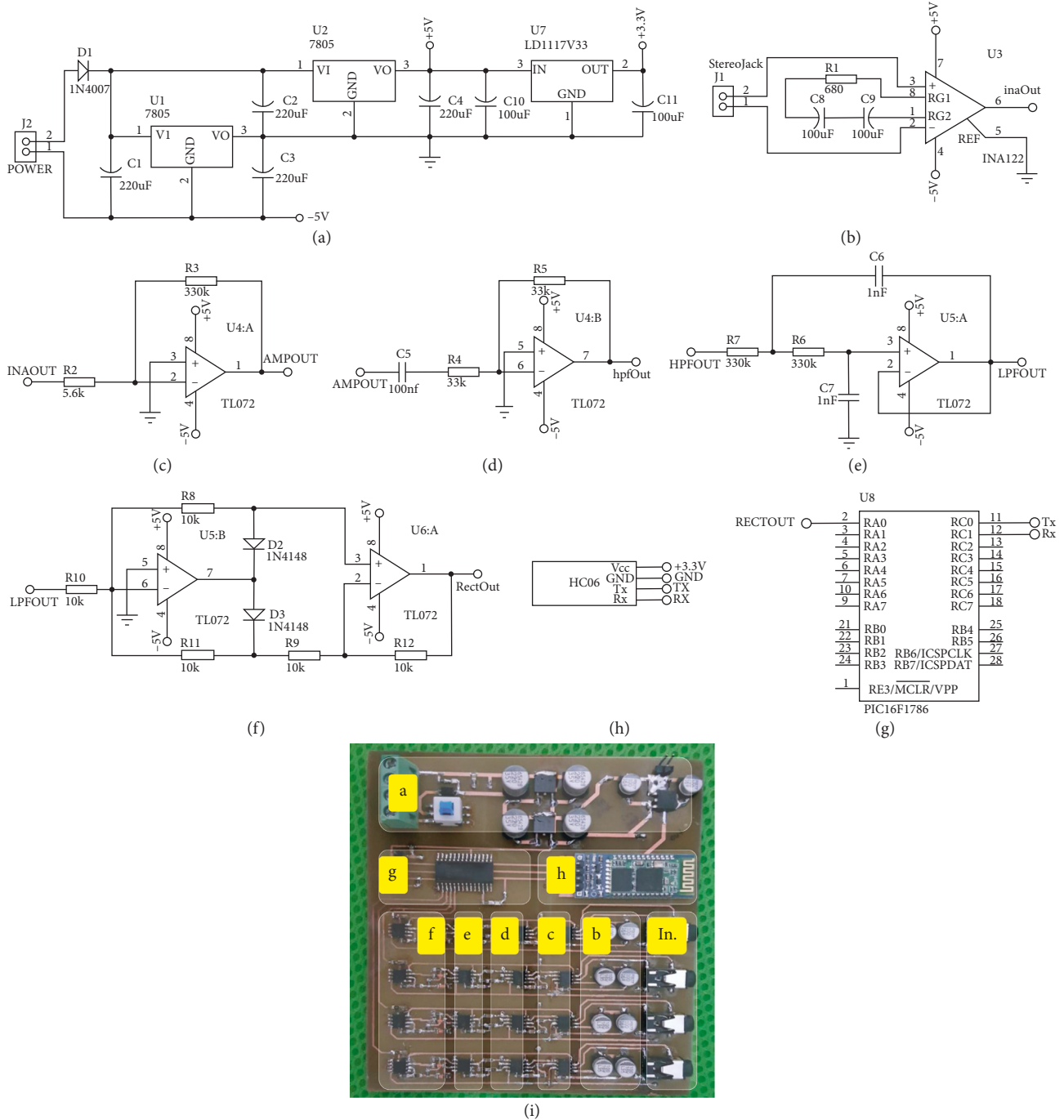
Figure 1: Block diagram and mounted state of the SEMG circuit. (a) Regulator circuit. (b) Instrumentation amplifier. (c) Inverting amplifier. (d) 1st-order HPF. (e) 2nd-order Sallen–Key LPF. (f) Full-wave rectifier. (g) PIC 16F1786. (h) Bluetooth module. (i) Mounted state of the SEMG circuit.

in the circuit are connected, respectively, to the RA0-RA3 inputs of this controller. This microcontroller performs the A/D conversion in 20 ms time intervals through the program we write. The converted channel data are turned into a string, and this sends data from the RC0 output to the Bluetooth module (Figure 1(g)). The transmitted data have a resolution of 2.4 μV in each step. Data sent at 4800 bps speed via the HC-06 Bluetooth module (Figure 1(h)) are

received and processed by the data collection program written in the C# language. The digitalized SEMG data in the data collection program are processed through digital filters. The PCB (printed circuit board) of the circuit is designed to be 10 cm × 10 cm in size, and as stated in [53], the PCB tracks are intended to be exposed to as little noise as possible. The mounted state of the circuit shown in Figure 1(i) is boxed and placed inside a wearable belt. The necessary

energy for the operation of the circuit was obtained from 1000 mAh lithium batteries. It is intended to minimize power line interference (PLI) without the need for any insulation, as stated in [54] using battery in the system.

2.3. Participants and Setup. Five males and two females voluntarily participated in our study and have at least 2 years of experience in strength training. The information of the participants is shown in Table 2.

The participants were informed about the content of our study, and a signed consent form was obtained from all of them. All exercises and measurements were made under the supervision of a specialized trainer. As described in the recommendations of the European initiative known as SENIAM (surface electromyography for noninvasive muscle evaluation of muscles) by selecting 10 mm diameter electrodes shown in Figure 2 for SEMG, the bipolar configuration is located 1–2 cm away from the centre of the muscle and the reference electrode is placed in a region that is electrically neutral according to the action [51]. The connection between the electrodes and the circuit channels is provided by using armoured cables which have 3.5 mm ends, 3 colour code (red, green, and blue) and labelled contacts (L, F, and R), as shown in Figure 2.

Our experiments consist of 3 parts. In the first part, 8 repetitions and 1 set of alternate dumbbell curl (ADBC) training was performed using a maximum load of 60–70%. In this section, firstly, it is investigated whether the analogue filter data obtained from the circuit in the training reflect the biopotential activity changes that occur during the training. In the sequel, the analogue filter data obtained from the circuit are processed by means of Kalman and threshold cut Haar wavelet filter (TCHW) to eliminate noise sources and to investigate the perceptibility of the isotonic contractions.

In the second part, the accuracy of the developed system was compared with the biomedical system (Viking on Nicolet EDX) used in Karaman State Hospital (See Table 1). In this comparison, the RMS values obtained from both systems were used.

In the third part, the availability of moving RMS and %MVC values as the screen output of the system was investigated in terms of performance feedback. For this purpose, first, the moving RMS values obtained by asking users to perform a second ADBC (8 repetitions 1 set) training were recorded. In addition, a %MCV measurement was made by asking all users in the training environment to lift 5 kg dumbbell and maximum weight (Men 17.5 kg, 20 kg, and 25 kg dumbbell; women 12.5 kg and 15 kg dumbbell) they can.

2.4. Kalman and TCHW Filters. Kalman filter is used to estimate the system status from input and output information with the previous information of a model in a dynamic system indicated by the state-space model [55, 56].

Table 2: Information about age, gender, weight, and height of the subjects.

Participant no.	Age	Gender	Weight (kg)	Height (cm)
1	21	Male	80	163
2	25	Male	82.3	178
3	29	Male	87	180
4	33	Male	85	177
5	37	Male	104.6	193
6	24	Female	70	180
7	27	Female	68	172

Figure 2: Example view of electrodes and shielded cables.

When the system is modelled, it was aimed to minimize the distortions in data by estimating the k parameter specified by x in SEMG data array at a particular time as X_k:

$$\widehat{X}_k = K_k \cdot Z_k + (1-)K_k \cdot \widehat{X}_{k-1}. \tag{1}$$

Here, Z_k expresses the measuring data wanted to be absolutized, K_k the Kalman gain and X_{k-1} the measuring data belonging to the previous stage. If the system is modelled through this information, a model consisting of calculation (2) and update (3) is obtained.

$$x_k = Ax_{k-1} + Bu_k + w_{k-1}, \tag{2}$$

$$z_k = Hx_k + v_k. \tag{3}$$

In (2), any x_k is expressed as a linear combination of the next control signal k of its previous value and the noise of the process. In (3), any measurement value making certain of the accuracy of which we are not sure is accepted to be a linear combination of the signal value and the noise of the measurement.

In HW, the main wavelet acts as the wavelet transform but is scaled and shifted during this procedure of wavelet transform [35]. Scaling corresponds to the widening and constriction of the signal ($f(t)$) and the shift to the wave shift (τ) in the timescale axis (t) in the following equation [57, 58]:

$$F(\omega, \tau) = \int f(t)w(t - \tau)e^{-j\omega t}dt. \tag{4}$$

HW is a wavelet-based, scaled, "square-shaped" array of functions. $\psi(t)$, the main function of HW (5), and also $\varphi(t)$,

a scaling function (6), are defined in t time interval given as follows:

$$\psi(t) = \begin{cases} 1, & 0 \le t \le \dfrac{1}{2}, \\ -1, & \dfrac{1}{2} < t \le 1, \\ 0, & \text{otherwise}, \end{cases} \tag{5}$$

$$\varphi(t) = \begin{cases} 1, & 0 \le t \le \dfrac{1}{2}, \\ 0, & \text{otherwise}, \end{cases} \tag{6}$$

The Haar function $\psi_{n,k}$ is defined as shown in

$$\psi_{n,k}(t) = 2^{n/2}\psi(2^n t - k), \quad t \in \Re. \tag{7}$$

Since the SEMG signals are user-based, SEMG signals between isotonic muscle contractions may vary according to the individual. In the method we use with HW, the individual waits for approximately 2–4 seconds with the weight in his hand before starting training and in the meantime, the procedure of threshold cutting in the system can be carried out. The threshold cutting is based on the calculation of the average value (8), the standard deviation (9), and the signal slope (10):

$$A = \frac{1}{n} * \sum_{i=1}^{n} x_i, \tag{8}$$

$$\sigma = \sqrt{\frac{1}{N} \sum_{i=1}^{N} (x_i - \mu)^2}, \tag{9}$$

$$s = \frac{\sum (x - \overline{x})(y - \overline{y})}{\sum (x - \overline{x})^2}. \tag{10}$$

Here, x_i is the value added to the average, μ is the average value and N is the number of the total value. After the values of the average, standard deviation and slope are calculated and all SEMG signals complying with this condition are equalled to zero. Thus, the signals between the voluntary contractions can be eliminated.

2.5. RMS, MA, and %MVC. After the SEMG signal is captured, the commonly used RMS or MA values are analysed by using [59]. In RMS analysis, the SEMG signal is subjected to a set of mathematical operations designed to measure the power of change. Thus, the intensity and duration of events like muscle contractions can be investigated. Therefore, the RMS value is a parameter chosen during contraction and reflects the level of physiological activity in the body. Mathematically, the RMS value of a continuous-time waveform is the square root of a function defining the continuous waveform shown in $f(t)$ in the following, defined in the range $T_1 \le t \le T_2$:

$$f_{\text{rms}} = \sqrt{\frac{1}{T_2 - T_1} \int_{T_1}^{T_2} [f(t)]^2 dt}, \tag{11}$$

$$f_{\text{rms}} = \lim_{T \to \infty} \sqrt{\frac{1}{T} \int_{0}^{T} [f(t)]^2 dt}. \tag{12}$$

Another method we use as MA is the technique of analysing changes in a data set to estimate long-term trends. For a given N time window, if the values $s_1, s_2, s_3, \ldots, s_n$ corresponding to this time interval of the S variable shown in the times $t_1, t_2, t_3, \ldots, t_n$ are known, the MA window size is defined as $N = 2k + 1$ and processed as specified in

$$\text{MA} = \frac{1}{N} \sum_{j=-k}^{+k} s_{i-j}. \tag{13}$$

Thus, changes in the time window given at the j moment are obtained by averaging the time series of the k time in the j moment. Instead of using the above-mentioned RMS and MA methods separately, the moving RMS method was used in our system by calculating the RMS value in a moving window, which is a combination of these methods. In this method, the operation can be performed at any t time interval of the moving window; therefore, it acts as a filter in a certain time interval, as shown in (14). In this way, the processing of the data obtained according to the variable speed of the replays in the training sets gets easier. In this equation, n refers to the length of the window, while $x(k)$ refers to the data within the window:

$$x_{\text{RMS}}[i] = \left(\frac{1}{n_0} \sum_{j=(i-N+1)}^{i} x^2[k] \right)^{1/2}. \tag{14}$$

So, it can be measured how much power is obtained from the muscle through the moving RMS value.

The MVC (maximum voluntary contraction-maximum amplitude of the signal) normalization is widely used in SEMG signals as an amplitude analysis technique. The results are shown as a percentage (%MVC) of the MVC value that can be used to create a common background when comparing data between subjects [60, 61]. SEMG signals depend on the user and have a structure that can cause records to change even when measured from the same position with the same motion. Therefore, MVC normalization is used to eliminate this difference and to enable data comparison between subjects [61]. MVC expresses the highest value obtained in a repeat during this measurement to normalize SEMG signals obtained for a specific purpose, while SMVC (submaximal voluntary contraction) refers to the voluntarily recorded SEMG data. %MVC corresponds to the multiplication of the normalized value of according to SMVC's MVC with 100 [62, 63]:

$$\%\text{MVC} = \left(\frac{\text{SMVC}}{\text{MVC}} \right) * 100. \tag{15}$$

FIGURE 3: Overview of the system. (a) Connecting electrodes before training (Photoshoot by Orucu). (b) Block diagram of the SEMG circuit. (c) Block diagram of the analysis software. (d) User interface of the analysis software.

Thus, it can be scaled how much power is obtained from the muscle or muscle groups investigated in repetitions in each set of training.

2.6. Proposed System.

Our system has the ability to follow the biopotential changes of four different superficial muscle groups at the same time. The reason why the system is designed with 4 channels is that most movements used in bodybuilding and weight training activate at least 1 or 3 muscle groups at the same time. The system takes the biopotential signals of the muscles that are activated during training through surface electrodes (Figure 3(a)), and then, first it amplifies them in the instrumentation and amplifier parts in the SEMG circuit, after it filters them with the 1st-degree high pass and 2nd-degree Sallen–Key low-pass filters. These analogue-filtered signals are sent to the computer via Bluetooth after a 12 bit analogue-to-digital conversion (Figure 3(b)). By the software we developed in C# language, all SEMG channel data received by the computer are digitally filtered and then they calculated the moving RMS values in time windows that vary according to the training speed (Figure 3(c)). After this process, the SMVC value of each repetition in each set of the training is processed according to the previously saved MVC values. Then, %MVC values are displayed on the screen in separate graphs according to the channels from which the data are taken. Finally, they are saved to the database in ".csv," ".dat," and ".xlsx" formats (Figure 3(d)).

3. Results and Discussion

3.1. Analogue + Digital Filtered Data from the System.

The analogue-filtered data of the first 4 repetitions of ADBC training performed by participant number two is shown in Figure 4(a), marked as 4(a) and 4(b) for each repetition.

The left BB (LBB-Left Biceps Brachii) data are obtained from CH1 (first channel of the SEMG circuit), and the right BB (RBB-Right Biceps Brachii) data are obtained from CH2 (the second channel of the SEMG circuit). From the data obtained, some decrease in Rep2b, Rep3a, Rep3b, and Rep4a (between 100 and 200 μV) and a data change during pushing the weight down (relaxation period of the muscle) in Rep 4b were observed. As we consulted with the professor of
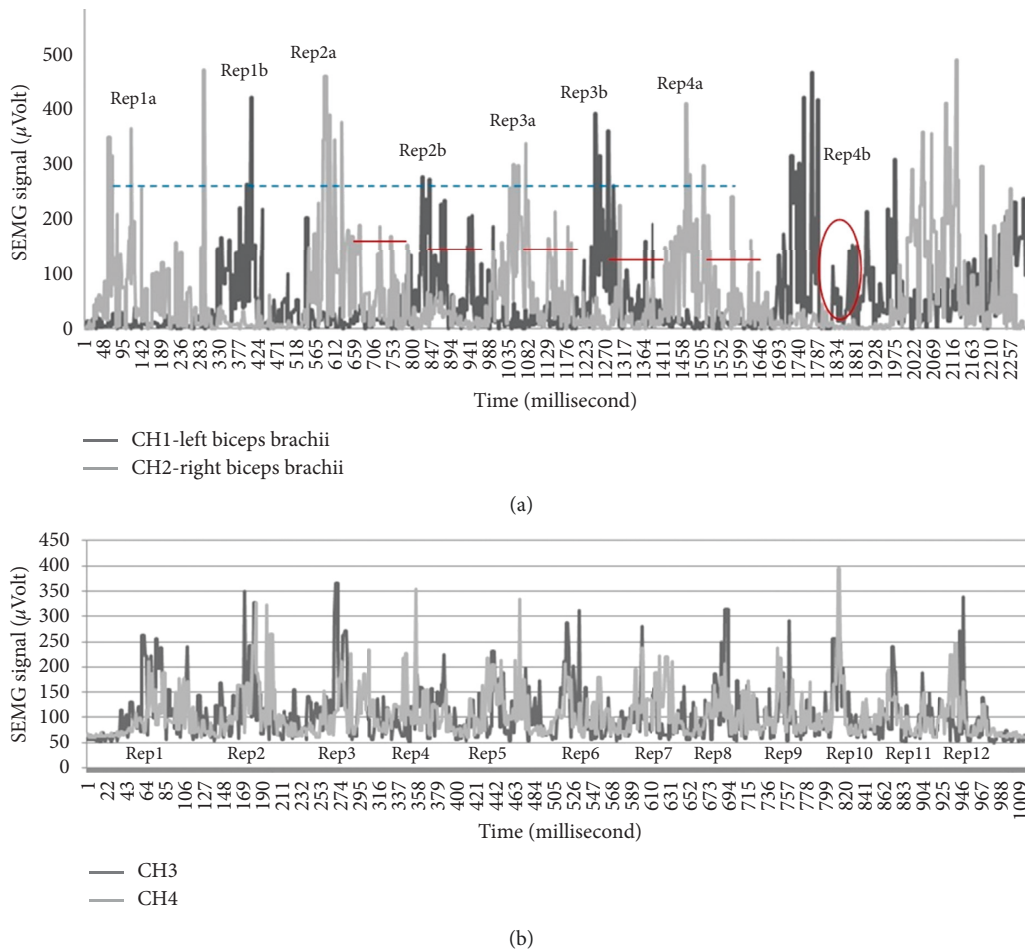
(a)

(b)

FIGURE 4: Sample analogue filtered data obtained from the SEMG circuit during training: (a) Sample results of participant number two, (b) sample results of participant number six.

Physical Education and Sports Teaching (Karamanoğlu Mehmetbey University), he stated that the fall was caused by the distortion of movement. According to the consultant professor, this change appeared to have been caused by the prolongation of the activation period of the muscle as a result of pushing the weight down more slowly as specified in [64, 65].

Other data of training performed by participant number four are shown in Figure 4(b). In this training, LBB data were obtained from CH3 (the third channel of the SEMG circuit) and RBB data were obtained from CH4 (the fourth channel of the SEMG circuit). When the results obtained are investigated in accordance with contraction and relaxation situations as specified in [65, 66] which consultant professor pointed, it is observed that BB muscles contract and relax normally in Rep1, Rep5, Rep7, and Rep9 and BB muscles contract fast and relax normally in Rep2. It is observed that the left BB contracts more than the right BB does and both relax normally in Rep3, that the required support is taken from other regions and movement is ruined in Rep4 and that the left BB muscle contracts more, the right BB muscle contracts normally and both relax normally in Rep6 and Rep8. It is observed that the left BB contracts normally and the right BB contracts more and

both relax normally in Rep10, in which distortion in movement appears as a result of fatigue in Rep11 and Rep12. In addition, the data of other participants obtained from these trainings are presented in Figure 5.

In Figure 6, the data, processed with TCHW and Kalman filters, of two repetitions in training, belonging to the right BB muscle, conducted by the participant numbered 4, are shown. In this Figure, 6(a) shows the analogue filtered state of the SEMG signal, and 6(b) shows the preliminary measurement of the threshold cut-out. The average and standard deviation measured here were found as $61.11 \pm 51.61\ \mu V$, and the slope was found as 0.005°. The signal filtered with TCHW after this procedure is shown in 6(c), and the signal processed through Kalman filter is shown in 6(d). Filtering results indicate that the TCHW method produces better results in filtering unwanted signals and contraction detection compared to the method of Kalman filter. As a result of these processes, it was decided to use TCHW filter in our system.

3.2. Comparison Results with the Existing Biomedical System. The accuracy of the data obtained from our system was compared through the data belonging to two men and two
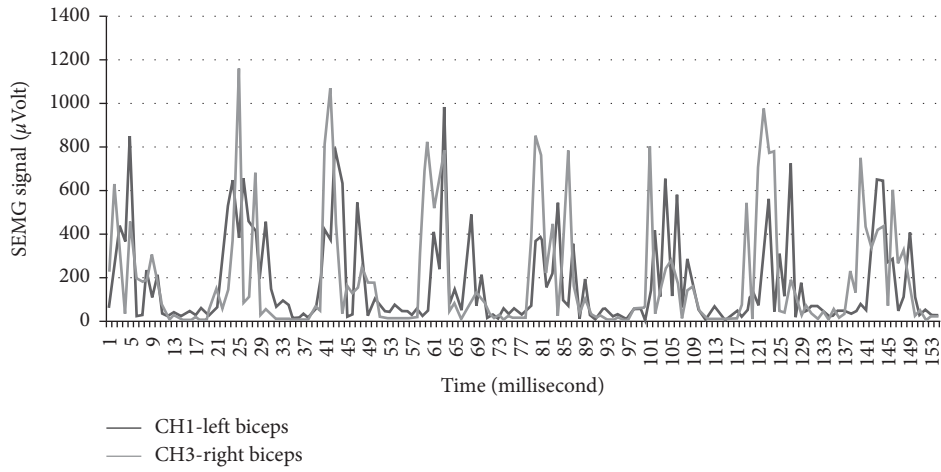
(a)
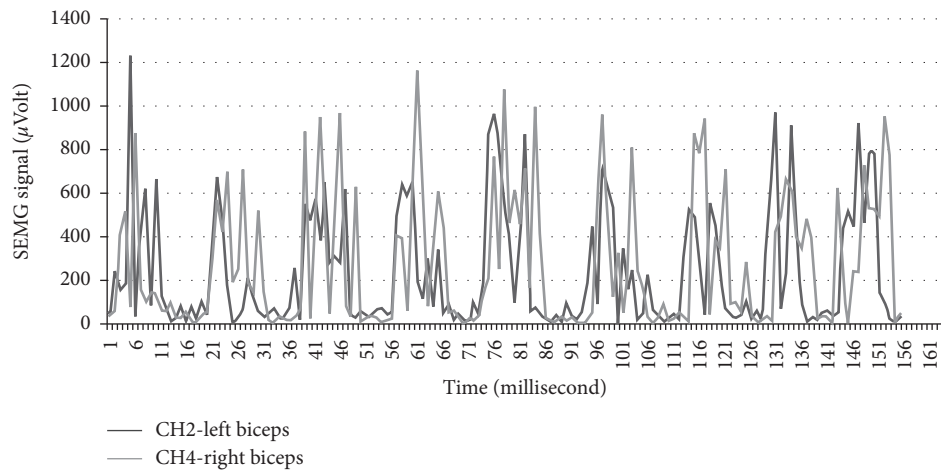
(b)
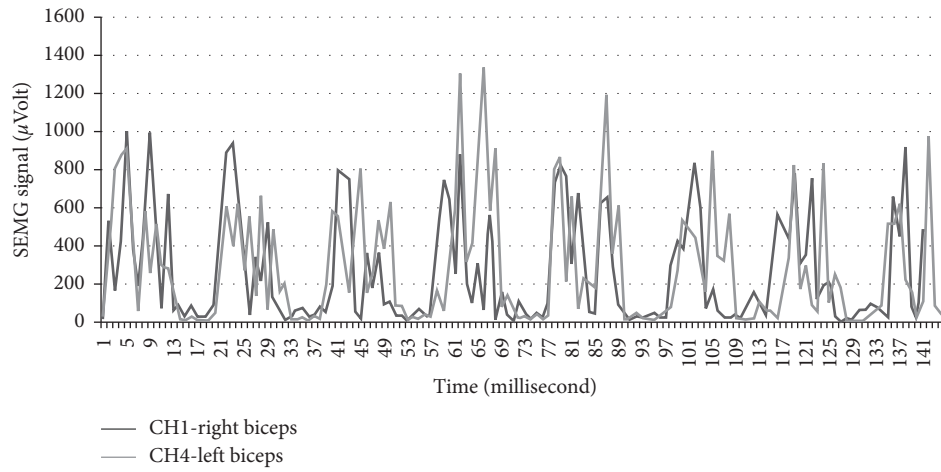
(c)

Figure 5: Continued.
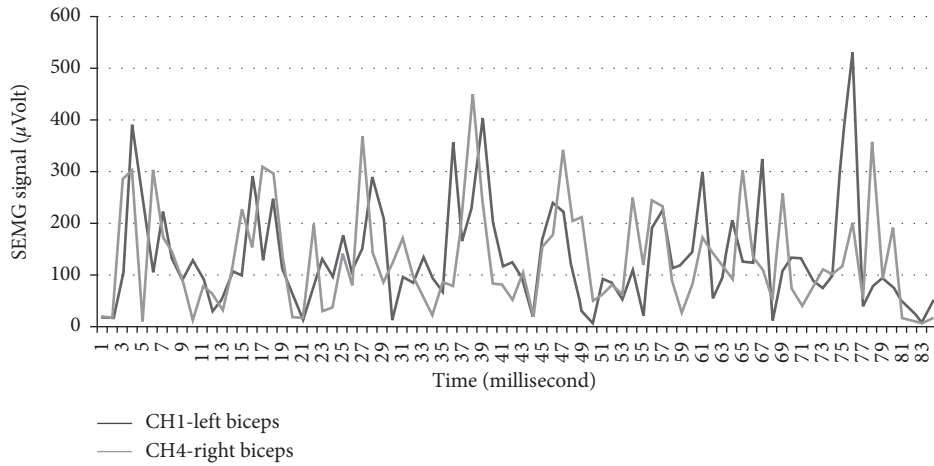
(d)
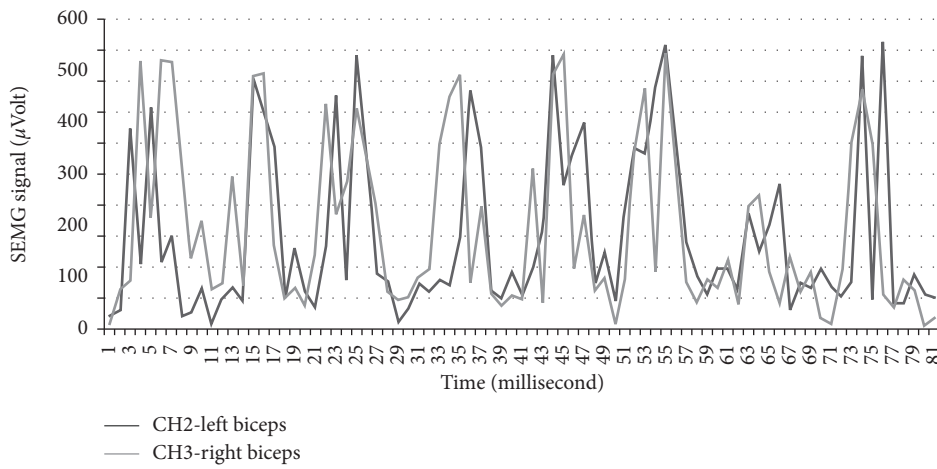
(e)

FIGURE 5: Data of other participants obtained from these trainings. (a) Results of participant number one. (b) Results of participant number three. (c) Results of participant number five. (d) Results of participant number six. (e) Results of participant number seven.
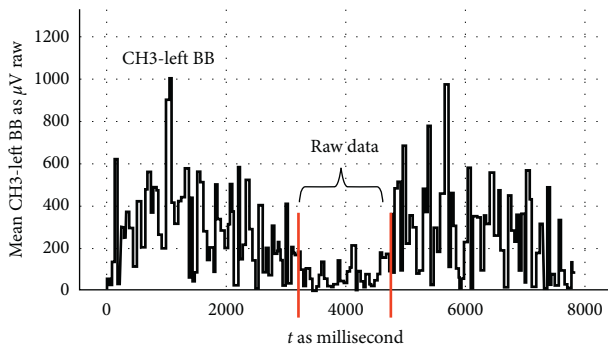
(a)
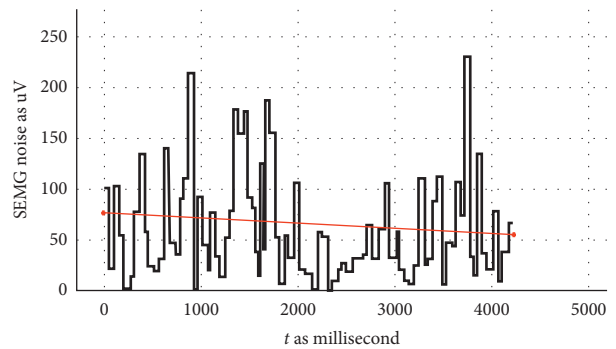
(b)

FIGURE 6: Continued.

(c)

(d)
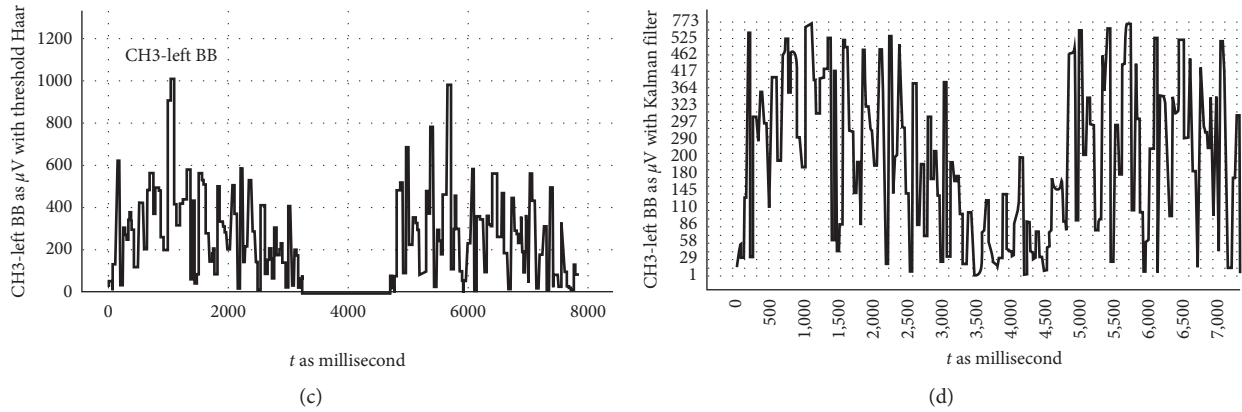
Figure 6: Comparison of the filtering results. (a) SEMG data without the filter. (b) Premeasurement for threshold filter. (c) SEMG signal with threshold + HW filter. (d) SEMG signal with Kalman filter.

(a)

(b)
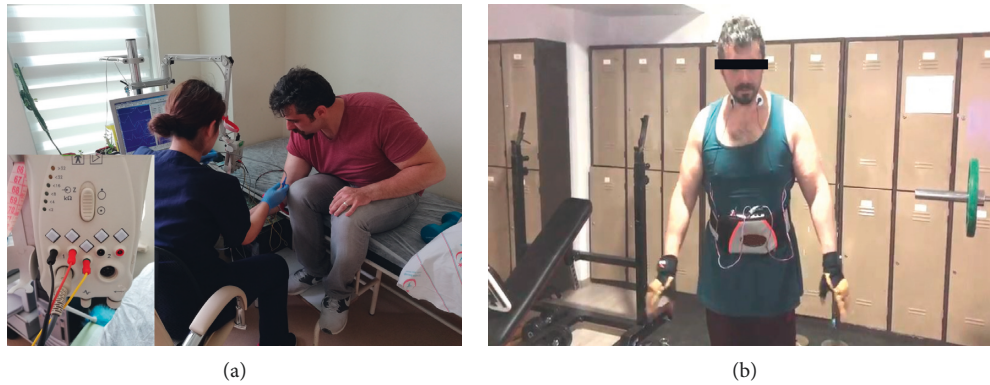
Figure 7: (a) A measurement taken in the hospital environment and a photograph of the current biomedical system. (b) A photograph taken at the gym before training.

Table 3: Moving RMS Results in Gym and Hospital. Note that "M" denotes the measurement number; "BB" denotes biceps brachii; "S" denotes system; "H" denotes hospital, "MN" denotes muscle name.

| M	MN	Type	1/idle	2/idle	3/idle	4/idle	1/5	2/5	3/5	4/5	1/25	2/25	3/15	4/12.5
							Participants/weight (no./kg)							
I	Left BB	S	70.69	69.72	51.18	43.82	123.69	129.54	97.54	93.64	914.7	935.98	566.98	547.64
		H	67.13	72.31	47.24	45.9	137.42	141.94	108.66	101.05	950.94	1112.53	616.53	604.36
	Right BB	S	71.4	69.75	49.66	42.45	119.11	127.41	96.86	93.95	960.71	937.69	565.69	515.43
		H	69.64	70.51	50.22	43.93	135.57	143.13	107.93	97.14	943.82	1117.15	615.15	545.64
II	Left BB	S	69.86	68.84	52.03	43.15	121.82	128.9	95.71	93.8	907.35	934.5	563.5	518.06
		H	70.39	69.61	51.76	43.75	138.87	139.69	105.78	101.55	942.14	1116.89	614.89	595.59
	Right BB	S	69.84	71.34	49.01	46.68	122.96	126.95	96.5	93.61	950.6	932.61	562.61	526.48
		H	71.82	67.83	50.25	43.27	136.52	142.8	106.73	102.46	1002.4	1110.94	612.94	598.81
III	Left BB	S	69.45	70.89	50.96	46.22	124.61	128.91	97.88	89.07	907.15	934.34	564.34	511.19
		H	68.57	69.97	50.24	46.71	138.81	139.69	106.74	105.67	1000.8	1115.11	614.11	583.55
	Right BB	S	71.64	67.65	52.01	43.55	122.97	129.74	95.38	92.52	948.63	930.36	562.36	539.49
		H	68.56	69.63	49.72	44.79	135.94	145.8	107.5	104.28	1000.9	1110.61	612.61	543.35

women with the SEMG device in Karaman State Hospital (Figure 7).

As shown in Table 3, this procedure was carried out through the data of 108 measurements in total, obtained through volunteers being unattached, lifting dumbbells of 5 kg and the maximum weight they could lift isometrically (1 RM) first in the gym, then in the hospital system for three times with breaks of 90 seconds. In this procedure, first the data given from the hospital system were recorded and then the moving RMS was calculated on the analogue and digital filter data obtained from the system.

In the system designed as a result of this measurement, accuracies of 90.95% ± 3.35 for the left BB and 90.75% ± 3.75 for the right BB were obtained.

TABLE 4: Moving RMS results in gym as training feedback.

Muscles and participants	Rep1	Rep2	Rep3	Rep4	Rep5	Rep6	Rep7	Rep8
LBB 1	862	798	738	683	782	556	715	741
LBB 2	845	779	852	786	590	812	796	766
LBB 3	757	725	721	560	712	699	645	736
LBB 4	810	841	840	804	828	832	791	830
LBB 5	704	802	651	670	604	354	558	701
LBB 6	387	413	395	354	367	403	381	370
LBB 7	316	328	372	346	377	302	328	319
RBB 1	876	833	811	790	815	846	704	653
RBB 2	823	817	847	834	649	747	621	770
RBB 3	821	793	766	696	566	884	685	785
RBB 4	832	853	856	821	819	808	809	815
RBB 5	815	763	750	753	718	707	725	714
RBB 6	389	422	418	350	371	402	361	378
RBB 7	331	380	365	351	372	348	314	341
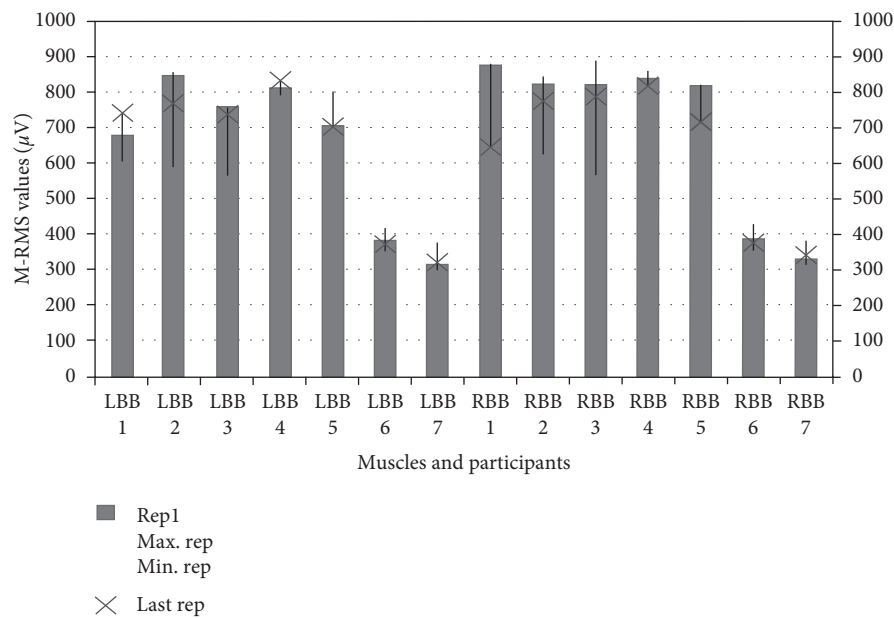
FIGURE 8: ADBC results of participants.

3.3. Moving RMS and %MVC Values. During the training, the volunteers were asked to perform a second training in order to obtain the moving RMS values given back to the user as feedback. The results are presented in Figure 8 and Table 4 in terms of ease of investigation.

Thus, it can be seen that the system can achieve minimum and maximum values of biopotential changes in muscles during training as in [66, 67].

Finally, the users were asked to lift 5 kg of dumbbell and the maximum weight they could lift. Thus, the %MVC was measured to be used in performance feedback through the obtained moving RMS values. The results obtained are presented in Table 5.

If Table 5 is analysed, it can be seen that the system can measure efficiency during training with the success rate of $96.87\% \pm 2.74$ based on %MVC.

When data obtained from the designed SEMG system are compared with data obtained from the systems used in the biomedical field, it is seen that it has 90.85%

accuracy. As digitally filtered data are compared, it is seen that TCHW method produces better results compared to Kalman filter. TCHW can soften data as processable and can also completely filter out unwanted signals between muscle contractions. It also eliminates the distortions in data expressed as artifact. Kalman filter appears to soften the data but not to be able to completely filter the signal between muscle contractions. Moreover, it is seen that the system can scale the strength obtained as moving RMS during the training on the basis of % MVC with the success rate of $96.87\% \pm 2.74$ in terms of efficiency. This allows the data obtained to be used in the simultaneous performance monitoring and analysis of athletes.

4. Conclusion

Thanks to this system, it is thought that athletes will be able to examine their performances instantly for each

TABLE 5: %MVC results in gym.

Muscle name	Part. no.	kg	SMVC (μV)	MVC (μV)	% MVC
LBB	1	5	138.3	850.26	16.26
		17.5	845.47	850.26	99.43
	2	5	138.30	992.6	13.93
		25	987.15	992.6	99.45
	3	5	152.6	960.13	15,89
		20	898.25	960.13	93,55
	4	5	155.4	963.30	16.13
		20	929.1	963.30	96.44
	5	5	158.9	967.5	16.42
		20	956.76	967.5	98.88
	6	5	89.5	615.7	14.53
		15	614.74	615.7	99.84
	7	5	93.5	545.2	17.14
		12.5	538.9	545.2	98.84
RBB	1	5	136.5	875.9	15.58
		17.5	854.15	875.9	97.51
	2	5	140.22	996.4	14.07
		25	985.92	996.4	98.94
	3	5	154.42	972.4	15.88
		20	893.56	972.4	91.89
	4	5	156.8	968.7	16.18
		20	930.76	968.7	96.08
	5	5	164.45	972.65	16.90
		20	910.5	972.65	93.61
	6	5	97.1	614.4	15.80
		15	609.9	614.4	99.26
	7	5	92.2	515.16	17.89
		12.5	506.3	515.16	98.28

training and make their training more efficient. It is possible to create intelligent training corners by using the system in gyms. It is thought that the system can easily be used by athletes, trainers, kinesiologists, and rehabilitation experts in bodybuilding trainings and rehabilitation processes. It is possible to improve system features by increasing the number of channels, further reducing the PCB size and adding extra sensor. It can be possible to follow more complicated movements (deadlift, barbell row, etc.) by increasing the number of channels. By making the size of system smaller, it can be possible to place it into textile product. In addition, by adding the pulse oximetry sensor to the system, oxygen consumption can be observed during the training. In our future studies, it is being thought of supporting the system with an image processing system in order to determine movement distortions in addition to use it for monitoring training performance and efficiency.

Data Availability

The data used to support the findings of this study are included within the article.

Conflicts of Interest

The authors declare that there are no conflicts of interest regarding the publication of this paper.

References

[1] R. M. Howard, R. Conway, and A. J. Harrison, "Muscle activity in sprinting: a review," *Sports Biomechanics*, vol. 17, no. 1, pp. 1–17, 2018.

[2] D. R. Clark, M. I. Lambert, and A. M. Hunter, "Contemporary perspectives of core stability training for dynamic athletic performance: a survey of athletes, coaches, sports science and sports medicine practitioners," *Sports Medicine-Open*, vol. 4, no. 1, pp. 32–42, 2018.

[3] J. Hussain, K. Sundaraj, Y. F. Low, L. C. Kiang, S. Sundaraj, and M. A. Ali, "A systematic review on fatigue analysis in triceps brachii using surface electromyography," *Biomedical Signal Processing and Control*, vol. 40, pp. 396–414, 2018.

[4] R. Lovell, M. Knox, M. Weston, J. C. Siegler, S. Brennan, and P. W. M. Marshall, "Hamstring injury prevention in soccer: before or after training?," *Scandinavian Journal of Medicine and Science in Sports*, vol. 28, no. 2, pp. 658–666, 2018.

[5] S. Skals, J. Vinstrup, E. Sundstrup, M. D. Jakobsen, C. H. Andersen, and L. L. Andersen, "Shoulder and arm muscle activity during elastic band exercises performed in a hospital bed," *The Physician and Sportsmedicine*, vol. 46, no. 2, pp. 233–241, 2018.

[6] M. Cardinale and M. C. Varley, "Wearable training-monitoring technology: applications, challenges, and opportunities," *International Journal of Sports Physiology and Performance*, vol. 12, no. s2, pp. S2–S55, 2017.

[7] A. D. Vigotsky, I. Halperin, G. J. Lehman, G. S. Trajano, and T. M. Vieira, "Interpreting signal amplitudes in surface electromyography studies in sport and rehabilitation sciences," *Frontiers in Physiology*, vol. 8, pp. 1–15, 2018.

[8] E. Zemková and D. Hamar, "Sport-specific assessment of the effectiveness of neuromuscular training in young athletes," *Frontiers in Physiology*, vol. 9, pp. 1–27, 2018.

[9] M. Vromans and P. Faghri, "Electrical stimulation frequency and skeletal muscle characteristics: effects on force and fatigue," *European Journal of Translational Myology*, vol. 27, no. 4, pp. 239–245, 2017.

[10] M. Kos and I. Kramberger, "A wearable device and system for movement and biometric data acquisition for sports applications," *IEEE Access*, vol. 5, pp. 6411–6420, 2017.

[11] O. Ozkaraca, A. Hakan Isik, and I. Guler, "Biological signals sensing with wearable technologies and an ECG athlete design," *Recent Patents on Biomedical Engineeringe*, vol. 4, no. 2, pp. 74–83, 2011.

[12] R. T. Li, S. R. Kling, M. J. Salata, S. A. Cupp, J. Sheehan, and J. E. Voos, "Wearable performance devices in sports medicine," *Sports Health: A Multidisciplinary Approach*, vol. 8, no. 1, pp. 74–78, 2015.

[13] S. Saponara, "Wearable biometric performance measurement system for combat sports," *IEEE Transactions on Instrumentation and Measurement*, vol. 66, no. 10, pp. 2545–2555, 2017.

[14] I. S. Dhindsa, R. Agarwal, and H. S. Ryait, "Performance evaluation of various classifiers for predicting knee angle from

electromyography signals," *Expert Systems*, vol. 36, no. 3, pp. e12381–14, 2019.

[15] Y. Yin, Y. Zeng, X. Chen, and Y. Fan, "The internet of things in healthcare: an overview," *Journal of Industrial Information Integration*, vol. 1, pp. 3–13, 2016.

[16] V. Bonaiuto, N. Lanotte, C. Romagnoli, N. Silvaggi, and G. Annino, "Design of a wireless wearable DAQ system for the evaluation of sports performances," *Proceedings*, vol. 2, no. 6, pp. 290–295, 2018.

[17] S. Heywood, Y. H. Pua, J. McClelland et al., "Low-cost electromyography—validation against a commercial system using both manual and automated activation timing thresholds," *Journal of Electromyography and Kinesiology*, vol. 42, pp. 74–80, 2018.

[18] G. Yang, J. Deng, G. Pang et al., "An IoT-enabled stroke rehabilitation system based on smart wearable armband and machine learning," *IEEE Journal of Translational Engineering in Health and Medicine*, vol. 6, pp. 1–10, 2018.

[19] A. Ranavolo, G. Chini, A. Silvetti, S. Mari, M. Serrao, and F. Draicchio, "Myoelectric manifestation of muscle fatigue in repetitive work detected by means of miniaturized sEMG sensors," *International Journal of Occupational Safety and Ergonomics*, vol. 24, no. 3, pp. 464–474, 2018.

[20] A. Cisnal, R. Alonso, J. P. Turiel, J. C. Fraile, V. Lobo, and V. Moreno, "EMG based bio-cooperative direct force control of an exoskeleton for hand rehabilitation: a preliminary study," in *Converging Clinical and Engineering Research on Neurorehabilitation III. ICNR 2018. Biosystems & Biorobotics*, L. Masia, S. Micera, M. Akay, and J. Pons, Eds., vol. 21, Springer, Cham, Switzerland, 2019.

[21] T. D. Williams, D. V. Tolusso, M. V. Fedewa, and M. R. Esco, "Comparison of periodized and non-periodized resistance training on maximal strength: a meta-analysis," *Sports Medicine*, vol. 47, no. 10, pp. 2083–2100, 2017.

[22] R. A. Panariello, T. J. Stump, and F. A. Cordasco, "The lower extremity athlete: postrehabilitation performance and injury prevention training," *Operative Techniques in Sports Medicine*, vol. 25, no. 3, pp. 231–240, 2017.

[23] J. Gondin, P. J. Cozzone, and D. Bendahan, "Is high-frequency neuromuscular electrical stimulation a suitable tool for muscle performance improvement in both healthy humans and athletes?," *European Journal of Applied Physiology*, vol. 111, no. 10, pp. 2473–2487, 2011.

[24] S. Grosprêtre, P. Gimenez, L. Mourot, and G. Coratella, "Elastic band exercise induces greater neuromuscular fatigue than phasic isometric contractions," *Journal of Electromyography and Kinesiology*, vol. 47, pp. 113–120, 2019.

[25] S. C. F. A. Von Werder, T. Kleiber, and C. Disselhorst-Klug, "A method for a categorized and probabilistic analysis of the surface electromyogram in dynamic contractions," *Frontiers in Physiology*, vol. 6, no. 30, pp. 1–8, 2015.

[26] U. Imtiaz, L. Bartolomeo, Z. Lin et al., "Design of a wireless miniature low cost EMG sensor using gold plated dry electrodes for biomechanics research," in *Proceedings of the 2013 IEEE International Conference on Mechatronics and Automation*, pp. 957–962, Takamatsu, Japan, August 2013.

[27] G. R. Jones, N. A. Neubauer, B. O'Connor, and J. M. Jakobi, "EMG Functional tasks recordings determines frailty phenotypes in males and females," *Experimental Gerontology*, vol. 77, pp. 12–18, 2016.

[28] S. Sadeghi Esfahlani, B. Muresan, A. Sanaei, and G. Wilson, "Validity of the Kinect and Myo armband in a serious game for assessing upper limb movement," *Entertainment Computing*, vol. 27, pp. 150–156, 2018.

[29] Delsys, Natick, MA, USA, "Trigno lab," 2017, http://www.delsys.com/products/wireless-emg/trigno-lab/.

[30] bitalino, Lisbon, Portugal, "EMG 151015," 2017, http://bitalino.com/datasheets/EMG_Sensor_Datasheet.pdf/.

[31] Muscle Monitor, Kuopio, FINLAND, "myontec," 2019, https://www.myontec.com/musclemonitor/manuals/Old/3_1/Muscle%20Monitor%20-%20User%20Guide.pdf12.

[32] Mpower, Vimpeli, Finland, "Mpower," 2019, http://mpower-bestrong.com/manual/MPOWER_user_manual.pdf.

[33] MyoTrac, Montreal, Quebec, Canada, "MyoTrac3," 2019, http://www.thoughttechnology.com/pdf/mar870-00%20myotrac3%20rehab.pdf.

[34] H. P. Da Silva, "Physiological sensing now open to the world: new resources are allowing us to learn, experiment, and create imaginative solutions for biomedical applications," *IEEE Pulse*, vol. 9, no. 2, pp. 9–11, 2018.

[35] A. Burns, B. R. Greene, M. J. McGrath et al., "SHIMMER™—A wireless sensor platform for noninvasive biomedical research," *IEEE Sensors Journal*, vol. 10, no. 9, pp. 1527–1534, 2010.

[36] Viking On Nicolet, Planegg, Germany, "Viking on nicolet," 2019, https://www.neuroswiss.ch/view/data/5962/Nicolet-Viking-EDX.pdf.

[37] K. Biron, K. Englehart, and P. Parker, "A study of kalman filtering applied to myoelectric signal state tracking," *CMBES*, vol. 35, pp. 1–4, 2012.

[38] T. Boaventura, L. Hammer, and J. Buchli, "Interaction force estimation for transparency control on wearable robots using a kalman filter," in *Converging Clinical and Engineering Research on Neurorehabilitation II. Biosystems & Biorobotics*, J. Ibáñez, J. González-Vargas, J. Azorín, M. Akay, and J. Pons, Eds., vol. 15, Springer, Cham, Switzerland, 2017.

[39] B. J. Schoenfeld, "The mechanisms of muscle hypertrophy and their application to resistance training," *Journal of Strength and Conditioning Research*, vol. 24, no. 10, pp. 2857–2872, 2010.

[40] B. J. Wallace, H. C. Bergstrom, and T. A. Butterfield, "Muscular bases and mechanisms of variable resistance training efficacy," *International Journal of Sports Science and Coaching*, vol. 13, no. 6, pp. 1177–1188, 2018.

[41] E. Barreiro, "Models of disuse muscle atrophy: therapeutic implications in critically ill patients," *Annals of Translational Medicine*, vol. 6, no. 2, p. 29, 2018.

[42] J. Kilby, K. Prasad, and G. Mawston, "Multi-channel surface electromyography electrodes: a review," *IEEE Sensors Journal*, vol. 16, no. 14, pp. 5510–5519, 2016.

[43] D. Devaprakash, G. J. Weir, J. J. Dunne, J. A. Alderson, and C. J. Donnelly, "The influence of digital filter type, amplitude normalisation method, and co-contraction algorithm on clinically relevant surface electromyography data during clinical movement assessments," *Journal of Electromyography and Kinesiology*, vol. 31, pp. 126–135, 2016.

[44] Texas instrument, May 2018, http://www.ti.com/lit/ds/symlink/ina128.pdf.

[45] Texas instrument, June 2018, http://www.ti.com/lit/ds/symlink/tl072.pdf.

[46] N. Miljković, N. Popović, O. Djordjević, L. Konstantinović, and T. B. Šekara, "ECG artifact cancellation in surface EMG signals by fractional order calculus application," *Computer Methods and Programs in Biomedicine*, vol. 140, pp. 259–264, 2017.

[47] Analog devices, September 2018, https://www.analog.com/en/analog-dialogue/articles/practical-filter-design-precision-adcs.html.

[48] A. Widmann, E. Schröger, and B. Maess, "Digital filter design for electrophysiological data - a practical approach," *Journal of Neuroscience Methods*, vol. 250, pp. 34–46, 2015.

[49] A. F. T. Ibrahim, V. R. Gannapathy, L. W. Chong, and I. S. M. Isa, "Analysis of electromyography (EMG) signal for human arm muscle: a review," in *Lecture Notes in Electrical Engineering*, pp. 567–575, 2016.

[50] M. B. I. Raez, M. S. Hussain, and F. Mohd-Yasin, "Techniques of EMG signal analysis: detection, processing, classification and applications," *Biological Procedures Online*, vol. 8, p. 11, 2006.

[51] SENIAM, March 2017, http://www.seniam.org/.

[52] F. Negro, K. Keenan, and D. Farina, "Power spectrum of the rectified EMG: when and why is rectification beneficial for identifying neural connectivity?," *Journal of Neural Engineering*, vol. 12, no. 3, article 036008, 2015.

[53] K. Praveen, A. D. Arun, and M. Sivaramakrishna, "EMI/EMC qualification of differential pressure monitoring system for PFBR—A case study," in *Proceedings of the 2016 International Conference on ElectroMagnetic Interference & Compatibility (INCEMIC)*, pp. 1–4, Bangalore, India, December 2016.

[54] J. Zhang, L. Wang, L. Yu, Y. Yang, Y. Zhang, and B. Li, "A low-offset analogue front-end IC for multi-channel physiological signal acquisition," in *Proceedings of the 2009 Annual International Conference of the IEEE Engineering in Medicine and Biology Society*, pp. 4473–4476, Minneapolis, MN, USA, September 2009.

[55] C. K. Chui and G. Chen, "Kalman filter: an elementary approach," in *Kalman Filtering*, Springer, Cham, Switzerland, 2017.

[56] A. Toprak and İ. Güler, "Angiograph image restoration with the use of rule base fuzzy 2D Kalman filter," *Expert Systems with Applications*, vol. 35, no. 4, pp. 1752–1761, 2008.

[57] M. Schimmack, S. Nguyen, and P. Mercorelli, "Anatomy of haar wavelet filter and its implementation for signal processing," *IFAC-PapersOnLine*, vol. 49, no. 6, pp. 99–104, 2016.

[58] S. Roldan-Vasco, E. Perez-Giraldo, and A. Orozco-Duque, "Continuous wavelet transform for muscle activity detection in surface EMG signals during swallowing," in *Applied Computer Sciences in Engineering. WEA 2018. Communications in Computer and Information Science*, J. Figueroa-García, J. Villegas, J. Orozco-Arroyave, and P. Maya Duque, Eds., vol. 916, Springer, Cham, Switzerland, 2018.

[59] S. Ranaldi, C. De Marchis, and S. Conforto, "An automatic, adaptive, information-based algorithm for the extraction of the sEMG envelope," *Journal of Electromyography and Kinesiology*, vol. 42, pp. 1–9, 2018.

[60] S. Mazumdar, A. Saikia, N. Sahai, S. Paul, and D. Bhatia, "Determination of significant muscle in movement of upper limb using maximum voluntary contraction of EMG signal," in *Proceedings of the 2017 4th International Conference on Signal Processing and Integrated Networks (SPIN)*, pp. 96–99, Noida, India, February 2017.

[61] B. N. Cahyadi, I. Zunaidi, S. A. Bakar et al., "Upper limb muscle strength analysis for movement sequence based on maximum voluntary contraction using EMG signal," in *Proceedings of the 2018 International Conference on Computational Approach in Smart Systems Design and Applications (ICASSDA)*, pp. 1–5, Kuching, Malaysia, August 2018.

[62] J. Paquin and G. A. Power, "History dependence of the EMG-torque relationship," *Journal of Electromyography and Kinesiology*, vol. 41, pp. 109–115, 2018.

[63] E. N. Rousanoglou, A. E. Oskouei, and W. Herzog, "Force depression following muscle shortening in sub-maximal voluntary contractions of human adductor pollicis," *Journal of Biomechanics*, vol. 40, no. 1, pp. 1–8, 2007.

[64] D. Roman-Liu and P. Bartuzi, "Influence of type of MVC test on electromyography measures of biceps brachii and triceps brachii," *International Journal of Occupational Safety and Ergonomics*, vol. 24, no. 2, pp. 200–206, 2018.

[65] J. J. D. Van der Gon, B. M. ter Haar Romeny, and E. J. van Zuylen, "Behaviour of motor units of human arm muscles: differences between slow isometric contraction and relaxation," *The Journal of Physiology*, vol. 359, no. 1, pp. 107–118, 1985.

[66] R. U. Newton, W. J. Kraemer, K. Häkkinen, B. J. Humphries, and A. J. Murphy, "Kinematics, kinetics, and muscle activation during explosive upper body movements," *Journal of Applied Biomechanics*, vol. 12, no. 1, pp. 31–43, 1996.

[67] S. Maeo, Y. Yoshitake, Y. Takai, T. Fukunaga, and H. Kanehisa, "Neuromuscular adaptations following 12-week maximal voluntary co-contraction training," *European Journal of Applied Physiology*, vol. 114, no. 4, pp. 663–673, 2014.

Research Article

Classification and Assessment of the Patelar Reflex Response through Biomechanical Measures

Yolocuauhtli Salazar-Muñoz [ID],[1] **G. Angelina López-Pérez,**[1,2] **Blanca E. García-Caballero,**[1] **Refugio Muñoz-Rios,**[1] **Luis A. Ruano-Calderón,**[3] **and Leonardo Trujillo** [ID][4]

[1]*Tecnológico Nacional de México/Instituto Tecnológico de Durango, C.P. 34080, Durango, DGO, Mexico*
[2]*Universidad Politécnica de Durango, C.P. 34300, Durango, DGO, Mexico*
[3]*Servicios de Salud del Estado de Durango, Hospital General 450, C.P. 34206, Durango, DGO, Mexico*
[4]*Tecnológico Nacional de México/Instituto Tecnológico de Tijuana, C.P. 22430, Tijuana, B.C., Mexico*

Correspondence should be addressed to Yolocuauhtli Salazar-Muñoz; ysalazar@itdurango.edu.mx

Clinical evaluation of the patellar reflex is one of the most frequent diagnostic methods used by physicians and medical specialists. However, this test is usually elicited and diagnosed manually. In this work, we develop a device specifically designed to induce the patellar reflex and measure the angle and angular velocity of the leg during the course of the reflex test. We have recorded the response of 106 volunteers with the aim of finding a recognizable pattern in the responses that can allow us to classify each reflex according to the scale of the National Institute of Neurological Disorders and Stroke (NINDS). In order to elicit the patellar reflex, a hammer is attached to a specially designed pendulum, with a controlled impact force. All volunteer test subjects sit at a specific height, performing the Jendrassik maneuver during the test, and the medical staff evaluates the response in accordance with the NINDS scale. The data acquisition system is integrated by using a tapping sensor, an inertial measurement unit, a control unit, and a graphical user interface (GUI). The GUI displays the sensor behavior in real time. The sample rate is 5 kHz, and the control unit is configured for a continuous sample mode. The measured signals are processed and filtered to reduce high-frequency noise and digitally stored. After analyzing the signals, several domain-specific features are proposed to allow us to differentiate between various NINDS groups using machine learning classifiers. The results show that it is possible to automatically classify the patellar reflex into a NINDS scale using the proposed biomechanical measurements and features.

1. Introduction

The observation of the patellar reflex is one of the clinical trials performed most frequently for neurological tests, making it an essential tool for the diagnosis of many neuromuscular diseases [1].

The patellar reflex is a deep tendon reflex, mediated by the spinal nerves from the levels L2, L3, and L4 in the spinal cord, predominantly in the root L4. The patellar reflex test is performed to determine the integrity of the neurological function, which is accomplished by hitting the patellar tendon below the knee cap with a test hammer [2].

The patellar reflex occurs when an abrupt change arises in muscle length; in this case, it is produced by the tendon stretching, which is caused when the hammer stroke is applied [3, 4]. The normal response must be a sudden leg extension. A reduction or exaggeration of the response is indicators of damage or interruption in the innervation of the quadriceps muscle [5].

The result of the test is commonly rated using the scales of the National Institute of Neurological Disorders and Stroke (NINDS) and the Mayo Clinic [6]; in this work, we use the former one. This scale measures the response magnitude assigning a different number of "crosses" (+), whereby zero crosses (0+) indicate an exam with no visible answer; one cross (1+) corresponds to a slight reflex; two crosses (2+) indicate a reflex in the lower half of the normal range; three crosses (3+) are a reflex in the upper half of the

normal range; and four crosses (4+) mean the reflex is significantly enhanced [6].

An alteration of the patellar reflex response may be caused by several different factors, which can range from tumors in the spinal cord [7] to diseases, such as the Guillain–Barre syndrome [8] that affects the peripheral nervous system [9]. Likewise, there are other factors that can disturb the test result, such as the intensity of the stroke [10], the nervousness that the patient may experiment during the test, and the age of the patient [11].

The development of an objective quantification for the test is a goal that has arisen in recent years [10, 12–14]. Some work has attempted to quantify the test by performing motion analysis [15] in cerebral palsy children [16] and also proposed a new iPhone application to measure the reflex response [17]. Other studies have attempted to model the patellar reflex as a response from a theoretical second-order system [18].

In a previous work, this research team designed a device to measure, digitally store, and display the patellar reflex response [19], capturing the relation between velocity and the magnitude of the response [20]. The aim of this study is to analyze the captured biomechanical variables, including the angle of the knee, the velocity of the knee movement, the applied force, and the magnitude of the reflex response, in order to develop an automatic classification algorithm using digital signal processing and machine learning algorithms.

2. Materials and Methods

2.1. Setup of the Measurement System.
According to the previous works of Salazar-Muñoz et al. [19, 20] and Moreno-Estrada et al. [21], the designed device uses an impact sensor as the start time marker of the test and an inertial measurement unit (IMU) to measure both the angular velocity and angular position of the leg after it receives the hammer stroke on the tendon. The measurement system consists of the following two parts.

2.1.1. Mechanical Controlled Force System.
The mechanical controlled force system consists of a hammer designed as a Charpy pendulum. The mechanical system consists of an aluminium pendulum rubber tip attached to a toothed gear angle with an adjustable height for the hammer initial position, which allows you to select the impact force on the patellar tendon as a function of the elevation angle of the pendulum. The tip is the same as the clinical hammer used by a physician. The physician shall place the arm in the desired position and release it manually. The force applied will be the same for all test subjects to generate their own flexion. The prototype was designed such that the elevation angle can increase from 30° to 165° in steps of 15°. In these experiments, the hammer arm was elevated to 135° and the hammer mass was 195 gr, resulting in an impact force of 0.82 N, which was validated by the Charpy pendulum equation at the mechanical engineering laboratory [21].

2.1.2. Data Acquisition System (DAS).
The DAS is composed of the following elements:

(i) *Tapping Sensor*. The LDT0-028K piezoelectric sensor manufactured by Measurement Specialities was used, connected to a charge amplifier circuit and an instrumentation amplifier to obtain a 5 V pulse, thus detecting the instant of impact on the tendon to synchronize the other measured variables.

(ii) *Angular Displacement and Rate Sensor*. The Sparkfun IMU number SEN-11072 was used, which has 5 degrees of freedom. It contains IDG500 2-axis gyroscope with the sensitivity set to 2 mV/°/s and ADXL335 3-axis accelerometer.

(iii) *Control Unit*. The signals from the sensors are captured by the NI USB6009 acquisition board, using two analogue channels and a power source of 5 V for the electronic system.

(iv) *Graphical User Interface (GUI)*. The GUI was designed in LabView to display the sensor readings in real time and save the captured signals of each test in an lvm file. Each new test generates a new file that is then imported into Matlab for later analysis. The selected sample rate is 5 kHz, and the board is configured for a continuous sample mode. The GUI shows the following indicators in real time: the angular displacement, the angular velocity, and the moment of impact on the tendon.

2.2. Volunteer Selection.
In this work, we use a group of 106 healthy volunteers to evaluate our proposed system. All of them are students from the Faculty of Medicine at the "Universidad Juárez del Estado de Durango," and they include both men and women. The mean age, height, and body mass for subjects were 21.5 ± 1.2 years, 1.73 ± 0.09 m, and 72 ± 13 kg, respectively. A volunteer is considered to be healthy for this study if he is not suffering from any diagnosed neurological or neuromuscular disease when the test is realized [22]. The clinical trial was carried out under the direction of the Neurology Department of the "Hospital General 450" of Durango City, Mexico. The study was approved by the Ethics and Research Committee from the hospital.

2.3. Measurement Procedure.
Experimental tests were performed under the supervision of the physician. Two reflex tests are applied to every volunteer to develop an automatic classification algorithm using digital signal processing and machine learning algorithms. We compare the NINDS scale with the biomechanical variables registered by the designed measurement system. The volunteer must be seated in a high chair, this way his right foot never touches the floor. In order to get a high relaxation of the quadriceps muscle, the volunteer is requested to perform the Jendrassik maneuver [23]. All the tests were performed under the same conditions.

(i) *Test A*. A physician gives a sharp tap on the patellar tendon with a standard clinical hammer. The

physician evaluates the reflex response using the NINDS scale. Dafkin et al. [10] established using stepwise multiple regression analysis that different groups of subjective raters all relied on the change of the knee angle to assess the reflex. Therefore, the trained physician was asked to focus on this feature to provide his rating for the analyzed patients.

(ii) *Test B.* After Test A, the sensors are placed on the leg of the volunteer as shown in Figure 1, and the procedure is as follows: (a) the taping sensor (impact sensor) is adhered to the patellar tendon with tape, below the patella to avoid any undesired movements and (b) the IMU is placed on the ankle using a belt. The distance between the knee centre of rotation and location of the sensor in all subjects was maintained small following the reference [24]. The IMU must be positioned parallel to the leg and perpendicular to the floor. The controlled force system hits the patellar tendon. The data acquisition system stores all sensor readings using the GUI that was designed for this experiment. After this procedure, the measurement system is withdrawn from the leg. This test was performed under the physician who verifies that the reflex response was equivalent to Test A. No test was rejected because it ranked differently from the Test A.

2.4. Data Treatment and Features.

The data stored by the system contain three time series. The first one is the impact signal, which marks the exact moment when the pendulum hits the tendon, denoted by t_o. The second time series is the angular position signal, which measures the angle of the leg during the reflex response. The third time series is the angular velocity of the leg movement during the test. All the signals are trimmed to only extract the 4 seconds following the hammer impact, after t_o, because the signal power has decreased by 97% and all the vector lengths were equal. A low pass 3rd degree Chebyshev filter with a cutoff frequency of 100 Hz was used to eliminate high-frequency noise.

Afterward, the signals of the angular position and angular velocity are characterized by extracting the following set of descriptive features. The extracted features are summarized in Figure 2 for the angular position and in Figure 3 for the angular velocity, each case showing a typical signal captured by the system for each measurement.

From the angular position signal, the extracted features are as follows. First, Δa represents the difference between the maximum and minimum peaks of the signal. Second, $\Delta 1/3$ is the ratio between the first (P1) and third peak (P3) of the signal. Third, Δt_1 is the time interval between the maximum and the minimum peaks. Fourth, Δt_2 is the time interval between the first peak and the third peak of the signal. Finally, T_s is the settling time, which is the moment when the signal power has decreased by 97%.

In the case of the angular velocity, a single feature is extracted called V_{max}, which is the maximum value of the signal, shown in Figure 3 as the highest peak.

2.5. Classification.

To achieve the classification of the realized patellar reflex tests based on the number of crossings in the NINDS scale, basic pattern recognition and machine learning methods are used [25, 26]. Specifically, the following four classifiers are used:

(i) Naive Bayes

(ii) Tree BAGGER

(iii) k-nearest neighbors (KNN)

(iv) Support vector machine (SVM)

Classifiers are tested with different combinations of the extracted features. Because the size of the dataset is relatively small, each classifier is tested using leave-one-out cross validation. Moreover, the data are preprocessed for feature reduction using principal component analysis (PCA).

3. Results and Discussion

According to the assessment given by the hospital staff at the "Hospital General 450," the collected samples are distributed in the NINDS scale as follows: 8 samples belong to the 0+ level, 20 samples were from 1+ level, 48 samples from 2+ level, and 30 samples belong to 3+ level. The 4+ level is omitted because none of the volunteers exhibited such a response.

First, we analyze the recorded signals from each response level, to determine if there are any general similarities between them. In Figures 4 and 5, we can see the average angular position and angular velocity, grouped based on the corresponding NINDS levels.

Figure 4 shows that the movement of the leg after the impact has a wavelike behavior, which decreases with time until it stabilizes to the rest position. The maximum amplitude reached by the corresponding average signal of the 3+ group is 47 degrees. This peak corresponds to the maximum elevation of the leg. The minimum average value of the same group is −37.85 degrees, corresponding to the retraction of the leg after the lift. This value, which is the Δa feature, is decreased by 36% in the corresponding average signal of the 2+ group, by 74% in the corresponding mean signal of the 1+ group, and by 97% in the corresponding mean signal of 0+ group, with respect to the mean signal of the 3+ group.

In Figure 5, the maximum value reached by the average of the velocity signals of 3+ is 38 degrees per second. This value is the V_{max} feature and is attenuated by 31% in the mean signal of the 2+ group, by 76% for the 1+ group, and by 95% for the 0+ group [20].

In Table 1, we can observe the mean and standard deviation of the grouped features according to the NINDS scale.

To make sure the separation between groups is significant, the Kruskal–Wallis statistical test is applied to every feature. The test is chosen because the data distribution is not Gaussian. The test gives a p value $\ll 0.05$ in every test, allowing us to reject the null hypothesis that all samples share the same median. Figure 6 shows the boxplots for each NINDS level for the Δa feature, and Figure 7
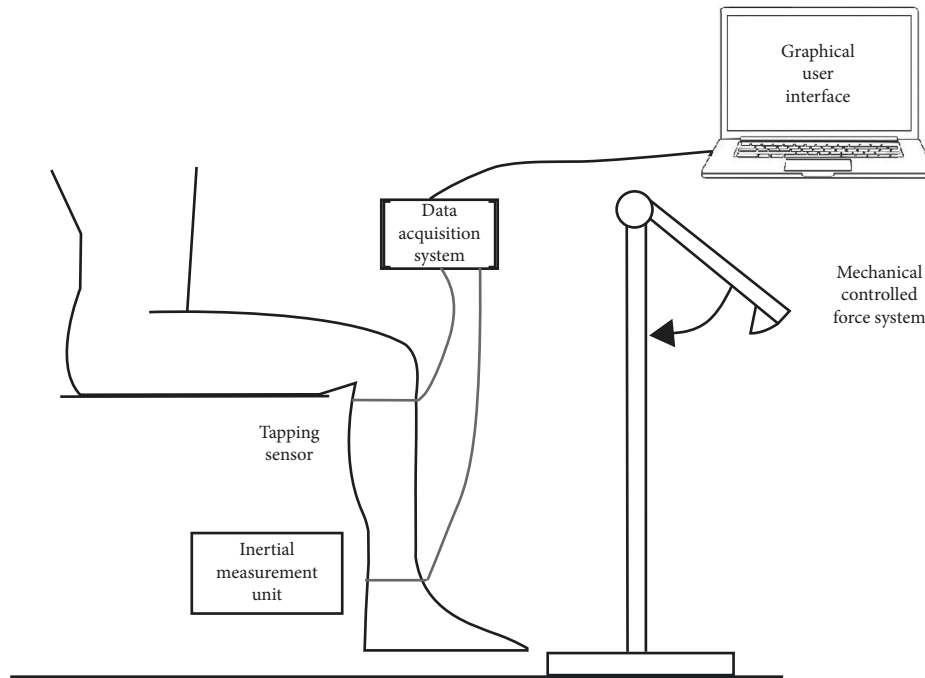
FIGURE 1: Schematic representation of the experimental system to obtain the patellar reflex response, showing the physical setup and sensor locations.
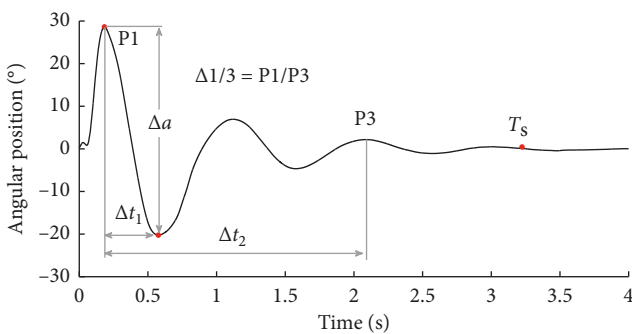
FIGURE 2: Features extracted from the angular position signal.

FIGURE 4: Mean signals of each NINDS group for angular position readings.

FIGURE 3: Feature extracted from the angular velocity signal.

shows the same box plot for V_{max} feature. These features are the ones that show the most separation between all the NINDS groups.

Different combinations of features are selected based on the statistical results and used as the input data for the machine learning classifiers. The tests are carried out using leave-one-out cross validation (LOO CV), given the relatively low number of samples in the database. Table 2 shows all of the tested combinations and the classification accuracy of each classifier. In each case, principal component analysis (PCA) is applied to the input features to perform feature transformation (but results are only shown for the case in which PCA improved the performance of at least one classifier). Best performance is achieved when using the Δa and V_{max} features with the naive Bayes classifier without PCA, with only 11 of 106 misclassifications, representing a classification accuracy of 89.62%.
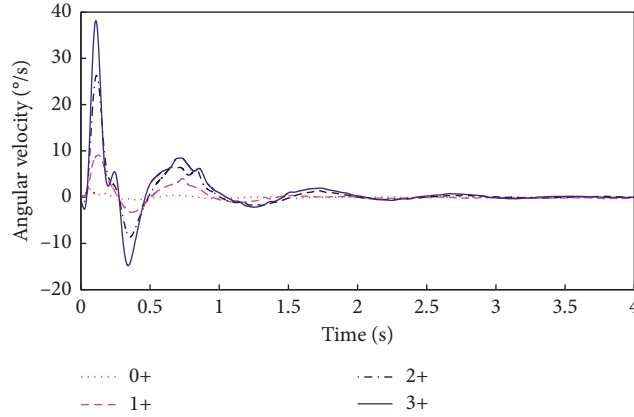
FIGURE 5: Mean signals of each NINDS group for angular velocity readings.

TABLE 1: Mean and standard deviation (mean ± std) of the features for each NINDS group.

NINDS scale	Δa	$\Delta 1/3$	Δt_1 (ms)	Δt_2 (ms)	T_s (sec)	V_{max}
0+	3.45 ± 1.93	0.82 ± 0.3	108 ± 71	1.78 ± 0.244	0.89 ± 0.318	2.73 ± 1.96
1+	24.52 ± 8.4	0.144 ± 0.12	354 ± 68	1.57 ± 0.164	1.97 ± 0.766	10.34 ± 5.06
2+	59.57 ± 12.41	0.156 ± 0.16	414 ± 64	1.73 ± 0.173	2.41 ± 0.785	26.97 ± 9.66
3+	93.83 ± 18.39	0.135 ± 0.16	440 ± 52	1.79 ± 0.222	2.53 ± 0.773	38.71 ± 9.53
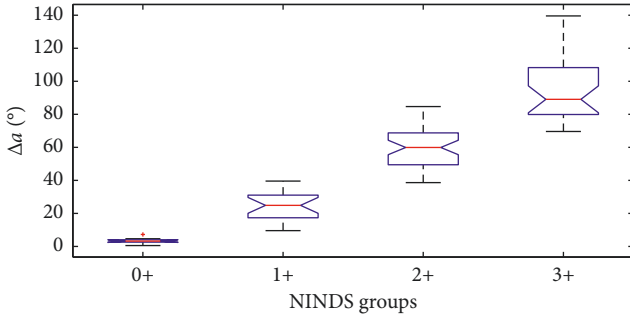
FIGURE 6: Boxplots of the Δa feature for each NINDS group.

TABLE 2: Classification accuracy for different feature combinations, showing the LOO CV testing performance.

|	Naive Bayes (%)	Tree BAGGER (%)	KNN (%)	SVM (%)
Δa, V_{max}	89.62	82.07	86.79	67.92
Δa, V_{max} (with PCA)	88.64	83.96	86.79	66.98
Δa, V_{max}, $\Delta 1/3$	84.9	86.79	83.96	69.81
Δa, T_s	86.79	84.9	35.84	71.69
$\Delta 1/3$, Δt_1, Δt_2	40.56	53.77	53.77	34.9
$\Delta 1/3$, Δt_1, Δt_2 (with PCA)	57.54	55.66	52.86	40.56
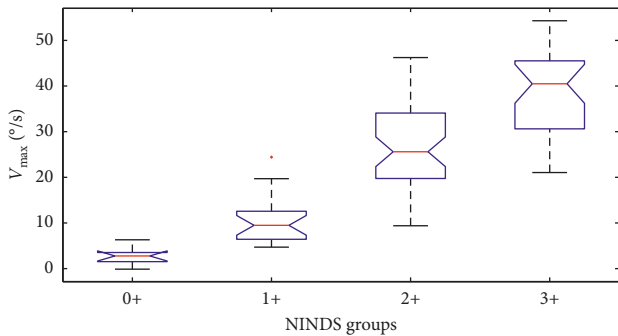
FIGURE 7: Boxplots of the V_{max} feature for each NINDS group.

Figure 8 shows all of the data samples plotted in the Δa and V_{max} feature space. The points are labeled to show the correctly classified sample from each group, using a different mark for each NINDS level and the misclassified samples as well. Notice that most of the classification errors can be found on the boundary between the 2+ and 3+ groups.
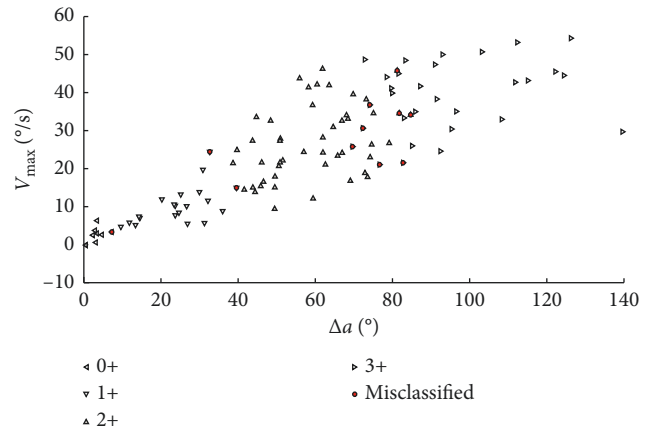
FIGURE 8: Δa and V_{max} feature space, showing all the samples collected in the dataset. The dark round markers shows misclassified tests by naive Bayes classifier, and all other points were correctly classified into their respective groups.

4. Conclusion

The dynamic behavior of the leg during the patellar reflex creates movement patterns that can be automatically classified in the NINDS scale with a useful degree of accuracy. This is shown to be possible using a straightforward feature extraction procedure and pattern recognition techniques. The classification methods used in this study achieved a LOO CV test accuracy of 89.62% in the best case, using only two feature dimensions and the naive Bayes classifier. However, despite the good performance by the proposed system, discordance between clinical measurements and the current measurements might still be considered high in some scenarios. Moreover, the proposed approach should be verified using observations from different neurologists to determine how well this approach generalized across experts. Nonetheless, the proposed system might lead to the full automatization of this test by integrating these future improvements, along with other promising technical enhancements, such as wireless sensors to increase a patient's comfort or edge computing to simplify the data processing and transmission process.

Data Availability

The data used to support the findings of this study are available from the corresponding author upon request.

Disclosure

The preliminary results of the manuscript are presented in 13th International Conference on Power Electronics (CIEP), 2016.

Conflicts of Interest

The authors declare that there are no conflicts of interest regarding the publication of this article.

Acknowledgments

References

[1] Merck & Co., *Merck Manual of Medical Information*, Merck & Co., Kenilworth, NJ, USA, 2012, https://www.merckmanuals.com/professional/neurologic-disorders/approach-to-the-neurologic-patient/evaluation-of-the-neurologic-patient.

[2] R. François, *Tratamiento Osteopático de las Lumbalgias y Lumbociáticas por Hernias Discales*, Medica Panamericana, Madrid, Spain, 2003.

[3] G. J. Tortora and B. Derrickson, *Principios de Anatomia y Fisiologia*, Medica Panamericana, Madrid, Spain, 11th edition, 2011.

[4] J. Waterhouse and I. Campbell, "Reflexes: principles and properties," *Anaesthesia & Intensive Care Medicine*, vol. 9, no. 5, pp. 210–215, 2008.

[5] M. L. Palmer and M. E. Epler, *Fundamentos de las Tecnicas de Evaluación Musculo Esqueletica (Bicolor)*, vol. 1, 1st edition, 2003.

[6] S. Manschot, L. van Passel, E. Buskens, A. Algra, and J. van Gijn, "Mayo and NINDS scales for assessment of tendon reflexes: between observer agreement and implications for communication," *Journal of Neurology, Neurosurgery & Psychiatry*, vol. 64, no. 2, pp. 253–255, 1998.

[7] M. Mendioroz Iriarte and J. J. Poza Aldea, "Mielopatía y radiculopatía por cervicoartrosis: tumores de la médula espinal," *Medicine—Programa de Formación Médica Continuada Acreditado*, vol. 8, no. 99, pp. 5339–5344, 2003.

[8] F. Micheli, *Tratado de Neurología Clinica*, Medica Panamericana, Madrid, Spain, 2002.

[9] E. B. Kelly, *Encyclopedia of Human Genetics and Disease*, vol. 1, ABC-CLIO, Greenwood, Santa Barbara, CA, USA, 2012.

[10] C. Dafkin, A. Green, S. Kerr, D. Veliotes, and W. Mckinon, "The accuracy of subjective clinical assessments of the patellar reflex," *Muscle & Nerve*, vol. 47, no. 1, pp. 81–88, 2013.

[11] A. Chandrasekhar, A. O. Noor Azuan, L. K. Tham, K. S. Lim, and W. A. B. Wan Abas, "Influence of age on patellar tendon reflex response," *PLoS One*, vol. 8, no. 11, Article ID e80799, 2013.

[12] M. K. Lebiedowska, S. Sikdar, A. Eranki, and L. Garmirian, "Knee joint angular velocities and accelerations during the patellar tendon jerk," *Journal of Neuroscience Methods*, vol. 198, no. 2, pp. 255–259, 2011.

[13] S. G. Chung, E. M. van Rey, Z. Bai, M. W. Rogers, E. J. Roth, and L.-Q. Zhang, "Aging-related neuromuscular changes characterized by tendon reflex system properties," *Archives of Physical Medicine and Rehabilitation*, vol. 86, no. 2, pp. 318–327, 2005.

[14] V. A. Safronov, "Patellar reflex: I—studies in healthy subjects," *Human Physiology*, vol. 32, no. 2, pp. 157–160, 2006.

[15] L. Tham, N. Abu Osman, W. Wan Abas, and K. Lim, "The validity and reliability of motion analysis in patellar tendon reflex assessment," *PLoS One*, vol. 8, no. 2, Article ID e55702, 2013.

[16] R. O'Sullivan, D. Kiernan, M. Walsh, T. O'Brien, and Y. Elhass, "Characterisation of the patellar tendon reflex in cerebral palsy children using motion analysis," *Irish Journal of Medical Science*, vol. 185, no. 4, pp. 813–817, 2016.

[17] R. Lemoyne, T. Mastroianni, W. Grundfest, and K. Nishikawa, "Implementation of an iPhone wireless accelerometer application for the quantification of reflex response," in *Proceedings of the 2013 35th Annual International Conference of the IEEE Engineering in Medicine and Biology Society (EMBC)*, pp. 4658–4661, Osaka, Japan, July 2013.

[18] B. D. Steineman, P. Karra, and K. Park, "Assessment of patellar tendon reflex responses using second-order system characteristics," *Applied Bionics and Biomechanics*, vol. 2016, Article ID 7172948, 4 pages, 2016.

[19] Y. Salazar-Muñoz, L. A. Ruano-Calderon, J. A. Leyva, and O. S. Martinez, "Patellar reflex measurement system with tapping force controlled," in *Proceedings of the XIII Mediterranean Conference on Medical and Biological Engineering and Computing 2013*, Seville, Spain, September 2013.

[20] Y. Salazar-Muñoz, B. García-Caballero, R. Muñoz-Ríos, G. A. López-Pérez, and L. A. Ruano-Calderon, "Angular rate measurement in the assessment of patellar reflex," in *Proceedings of the 13th International Conference on Power Electronics (CIEP)*, Guanajuato, Mexico, June 2016.

[21] J. R. Moreno-Estrada, O. García-Cano, and Y. Salazar-Muñoz, *Diseño de un Mecanismo Percutor Rotuliano*, TECNM/Instituto Tecnológico de Durango-Dpto. de Metal-Mecánica, Durango, Mexico, 2016.

[22] U.S. Department of Health and Human Services, "Food and Drug Administration," E 10 Choice of Control Group and Related Issues in Clinical Trials, Washington, DC, USA, 2001.

[23] R. Llanio and G. Perdomo, "Propedéutica Clínica y Semiología Médica," vol. 1, University of Medical Sciences, Cienfuegos, Cuba, 2003.

[24] R. Avila-Chaurand, L. Prado-León, and E. González-Muñoz, Dimensiones antropométricas de la población latinoamericana: México, Cuba, Colombia, Chile, México, 2nd edition, 2007.

[25] S. Theodoridis and K. Koutroumbas, "Pattern Recognition," Academic Press, Cambridge, MA, USA, 4th edition, 2008.

[26] W. J. Freeman and R. Q. Quiroga, *Imaging Brain Function With EEG*, Springer, New York, NY, USA, 1st edition, 2013.

Research Article

Consistency of Outputs of the Selected Motion Acquisition Methods for Human Activity Recognition

Magdalena Smoleń [ID]

AGH University of Science and Technology, Kraków 30-059, Poland

Correspondence should be addressed to Magdalena Smoleń; msmolen@agh.edu.pl

The aim of this paper is to choose the optimal motion sensor for the selected human activity recognition. In the described studies, different human motion measurement methods are used simultaneously such as optoelectronics, video, electromyographic, accelerometric, and pressure sensors. Several analyses of activity recognition were performed: recognition correctness for all activities together, matrices of the recognition errors of the individual activities for all volunteers for the individual sensors, and recognition correctness of all activities for each volunteer and each sensor. The experiments enabled to find a range of interchangeability and to choose the most appropriate sensor for recognition of the selected motion.

1. Introduction

Telemetric recording and automatic interpretation of motion activities play a significant role in home monitoring. From a variety of applications, we can distinguish a few most common ones: prevention and detection of falls, detection of abnormal or dangerous situations, rehabilitation monitoring, and activity assessment and quantification. An automatic system usually consists of sensors, specific signal or image processing methods, and recognition module for the selected activity. Selection of sensors seems to be the most important issue and must take into account useable sensor properties: wearing ability, sensitivity to disturbances, occurrence of outsiders, etc. Out of the many propositions of sensors, it is difficult to choose the best universal one because each sensor works best in a certain range of recognized activities. This fact motivates us to study that topic.

In [1], electromyographic (EMG) analysis of four lower limb muscles was performed during seven classes of preventive exercises against loss of balance or falling. Other researchers integrated EMG and inertial measurement unit (IMU) to construct a balance evaluation system for recording the body in a dynamic and static posture [2]. In [3], seven hand movements were classified (by neural networks with backpropagation and Gustafson–Kessel algorithm) on the basis of EMG signal of four forearm muscles. An EMG- and augmented reality- (AR-) based rehabilitation system for the upper limbs was proposed in [4]. In [5], an EMG biofeedback device for forearm physiotherapy was constructed to discriminate 6 classes of movements.

Novak et al. [6] proposed a system for automatic detection of gait phases using acceleration and pressure sensors and supervised learning algorithm. For gait abnormalities detection in [7], the authors built a prototype of pressure force sensing resistor (FSR), bend sensor, and IMU. Principal component analysis (PCA) was used for the features generation and support vector machine (SVM) for multiclass classification. Shu et al. [8] presented a time-space measurement tool in the form of insoles of conductive fabric sensors placed around the midfoot and the heel. The wireless capacitive pressure sensors were introduced in [9]. Other studies [10] were related to equilibrium measurements with an instrumented insole with 3 pressure sensors per foot.

An accelerometric (ACC) system for monitoring the daily motor activity (sitting, standing, lying, and periods of natural walking) was proposed in [11]. An ACC sensor was placed on the subject's sternum. Detection of gait parameters by means of a detector composed of gyrometric, accelerometric, and magnetic sensors was proposed in [12]. Rong et al. [13] presented the use of 3D accelerometric sensor

located at the waist to identify people based on their characteristic gait patterns. Identification was prepared with discrete wavelet transform (DWT). Jafari et al. [14] proposed ACC-based detection of accidental fall. The selected signal features were used for distinction of four transitions (sitting-standing, standing-sitting, lying-standing, and standing-lying) with the use of neural network and k-nearest neighbour (k-NN) classification. In [15], researchers developed ACC-based fall detection for smartphones. The proposed system enabled fall event detection, location tracking of the person, and notifications of emergency situations.

Juang et al. [16] introduced a system for detection of four body postures (standing, bending forward, sitting, or lying) and sudden falls. For classification purposes, the silhouette was segmented from each image frame. The feature vector was composed of Fourier transform coefficients and a ratio of body silhouette length and width. Real-time system was implemented in [17]. It consisted of three main modules: segmentation of silhouette, recognition, and identification of posture. The authors introduced decision rules based on body parameters. It was possible to detect four postures: standing, sitting, squatting, and bending. In [18], authors performed analysis by means of supervised and non-supervised learning for classification of the body position on images sequence. Other researchers [19] presented the posture detection method which took into account information about the body shape and the skin colour. Song and Chen [20] proposed vision-based activity recognition on the basis of information of pose, location, and elapsed time.

In the mentioned papers, the selection of particular sensors was not so clearly justified. This raises a natural question about the optimal choice. The aim of our research was based on the use of various sensors applied to simultaneously capture the signs in basic activities and study the correlation of information obtained from them. This approach enabled the choice of the proper sensor depending on the situation and the current need. The experiments aimed at determining how well the simple measuring devices can approximate the information obtained from the specialized medical equipment. Our measurements were performed by means of three-dimensional motion capture system, wireless EMG amplifier and wireless feet pressure system (as reference equipment), and accelerometer and video camera (as currently available consumer-grade sensors).

2. Materials and Methods

2.1. Plan of the Experiment.
A total number of 20 volunteers (8 women, 12 men, age—22 to 61, average age—27) were examined. Each subject was instructed to do about 30 (19 to 46) repetitions of 12 different activities:

(i) Squatting from a stand position (1a) and getting up from a squat (1b)

(ii) Sitting on a chair from a stand position (2a) and getting up from a chair (2b)

(iii) Reaching (3a) and returning from reaching the upper limb forward in the sagittal plane (standing) (3b)

(iv) Reaching (4a) and returning from reaching the upper limb upwards in the sagittal plane (standing) (4b)

(v) Bending from a stand position (5a) and straightening the trunk forward in the sagittal plane (5b)

(vi) Single step for the right (6a) and left lower limb (6b).

The measurements were performed simultaneously with the following:

(i) A, a motion capture system: Optotrak Certus (NDI) with NDI First Principles software

(ii) B, a wireless biopotential amplifier: ME6000 (Mega Electronics) with MegaWin software

(iii) C, a wireless feet pressure measurement system: ParoLogg with Parologg software

(iv) D, a digital video camera: Sony HDR-FX7E

(v) E: ACC recorder (Revitus system) with dedicated software.

2.2. Characteristics of the Examined Signals.
The three-dimensional motion trajectories of 30 infrared markers M1 to M30 located on the body were measured from the left side of the observed person (Figure 1). The acquisition was performed with the sampling frequency 100 Hz, accuracy 0.1 mm, and resolution 0.01 mm.

Surface EMG signals were recorded (2 kHz) from 8 muscles of both lower limbs: (1) quadriceps (vastus lateralis), (2) biceps femoris, (3) tibialis anterior, and (4) gastrocnemius (medial head).

Feet pressure signals were captured with 64 piezoresistive sensors (32 for each feet) with 100 Hz. Triaxial acceleration signal was recorded by sensors integrated in Revitus device located on the sternum. The recorder enabled online measurement via Bluetooth (100 Hz).

Video signals (720 × 576 pixels, 25 frames per second) were obtained from silhouette measurement using a digital camera placed from the volunteer's left side.

2.3. Processing of the Measurement Data.
To calculate feature vectors for classification, the processing of data recorded with sensors B to E was performed in MATLAB.

The three-dimensional motion trajectories were used for determining the precise time moments of start and end of activities. The exception was the gait (6a, 6b), which cannot be performed in a natural way in the distance as short as 4 m (the maximal width of registration space of the motion capture system). Therefore, for the gait (6a, 6b), the start and end points of duration were determined from visual analysis of video frames.

The difference of performance time between analyzed movements and acting volunteers requires normalization of the data length with a window W. In order to make the optimal selection of its width, a set of histograms of activities performance were calculated:

(i) Histograms of minimal, maximal, and average (MIN, MAX, AVG) performance time for all people
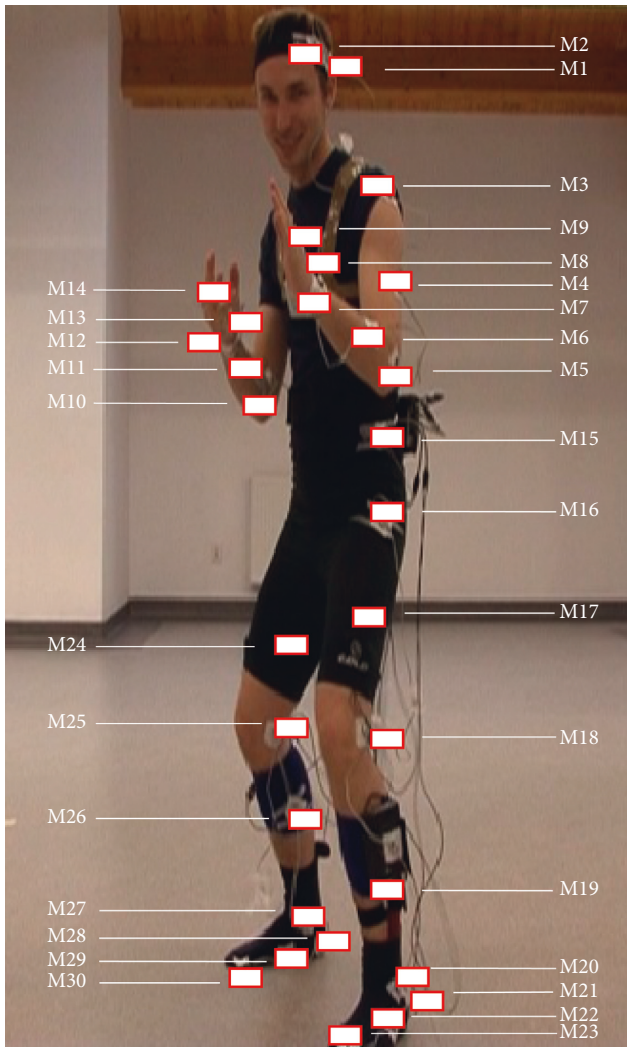
FIGURE 1: Placement of the markers M1 to M30.

and all activities together; the ALL histogram—for all values of duration time together and for all volunteers and activities (Figure 2)

(ii) Histograms of all performance time for all volunteers, for each activity separately from 1a to 6b (Figure 3).

Based on the ALL histogram, the length of time window was set to $W = 1.6$ s, as the shortest of all window-covering activities of various types. Above this value, the other histograms (except for MAX) do not show a significant activity.

The electromyographic signals were processed as follows:

(i) Calculating the absolute value of the signal

(ii) Averaging the signal in a moving time window (0.1 s)

(iii) Normalizing the amplitude separately for each volunteer—dividing the signal by the maximal value from all measurements of all activities for each volunteer

(iv) Creating the vector data (which are then used as a component of the input classifier vector) consisting

of the prepared (as above) EMG signal of each muscle of the left (L) and right (R) lower limb: $[\, EL1 \ \ EL2 \ \ EL3 \ \ EL4 \ \ ER1 \ \ ER2 \ \ ER3 \ \ ER4 \,]$

(v) Normalizing the amplitude to (0 1) interval

(vi) Resampling the signal to the frequency of 25 Hz.

The feet pressure signals were processed as follows:

(i) Averaging the signal values from the sensors in the three selected areas—the heel (1), the center (2), and the front (3) for the left (L) and the right (R) foot: $[\, L1 \ \ L2 \ \ L3 \ \ R1 \ \ R2 \ \ R3 \,]$

(ii) Averaging the signal in a moving time window of 0.3 s

(iii) Normalizing the amplitude for each volunteer separately

(iv) Creating the vector data: $[\, L1 \ \ L2 \ \ L3 \ \ R1 \ \ R2 \ \ R3 \,]$

(v) Normalizing the amplitude to (0 1) interval

(vi) Resampling the signal to the frequency of 25 Hz.

The accelerometric signals were processed as follows [21]:

(i) Subtracting the offset value from the signal (offset—average of the 10 s length signal, when a person is in a stationary upright position) separately for each channel (x, y, z) and for each person

(ii) Averaging the signal in a moving time window of 0.2 s

(iii) Normalizing the amplitude for each volunteer separately

(iv) Creating the vector data consisting of a prepared acceleration signal in the axes x, y, z: $[\, X \ \ Y \ \ Z \,]$

(v) Normalizing the amplitude to (0 1) interval

(vi) Resampling the signal to the frequency of 25 Hz.

The video signal was prepared as follows [22]:

(i) Converting a colour image to a grayscale.

(ii) Calculating the vector motion field with 2 coordinates—optical flow (OF) using Horn–Schunck algorithm [23].

(iii) Median filtering of the motion field components (5×5 pixels).

(iv) Detecting the moving objects—binarization of the motion field module with a T threshold constant for all people and all activities; the threshold has been chosen experimentally in [24].

(v) Calculating an area of the moving silhouette S_{n-1} on the $(n-1)$-th frame (yellow area in Figure 4(b)) as a joint part from areas $OF_{n-1/n-2}$ (blue) and $OF_{n/n-1}$ (turquoise), where $OF_{n-1/n-2}$ is the motion field calculated on the basis of $(n-1)$-th and $(n-2)$-th frame and $OF_{n/n-1}$ is the motion field calculated on the basis of n-th and $(n-1)$-th frame.

(vi) Filling the holes in the area S_{n-1}.
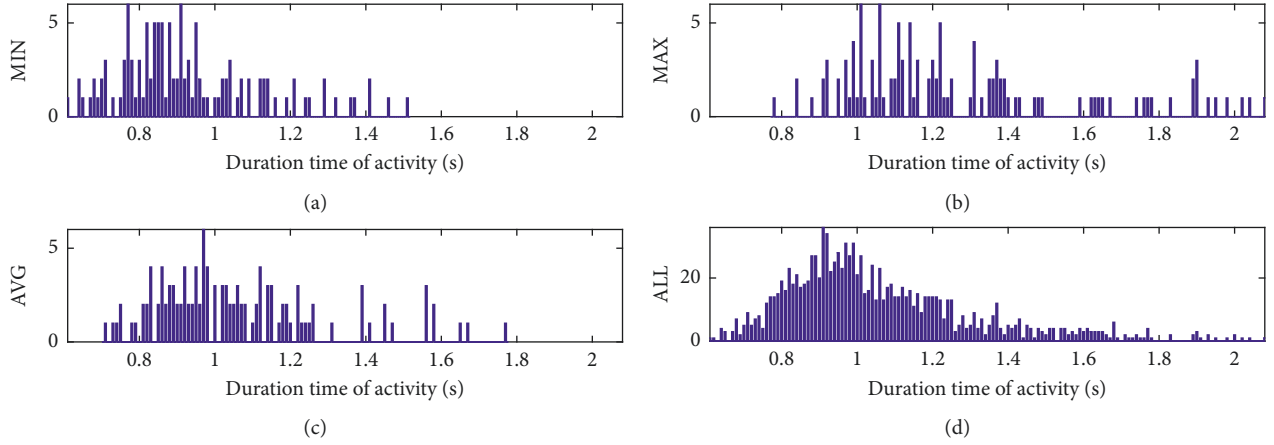
(a)

(b)

(c)

(d)

FIGURE 2: Histograms of performance time for all volunteers and all activities together: (a) minimal MIN, (b) maximal MAX, (c) average AVG duration, and (d) collective ALL.

(vii) Thickening the contour mask of the movable silhouette part S_{n-1} (inside to approximately four pixels (Figure 4(c)).

(viii) Determining the histograms of motion field directions—aggregation of motion field vectors from the bold contour to 8 directions; each direction corresponds to the following angle ranges $[-337.50° \; 22.50°]$, $[22.50° \; 67.50°]$, …, $[292.50° \; -337.50°]$.

(ix) Normalizing the histograms.

(x) Creating the data vector consisting of the histograms with bins B1, B2, B3, B4, B5, B6, B7, B8—each bar corresponds to one of eight directions: $[\, B1 \; B2 \; B3 \; B4 \; B5 \; B6 \; B7 \; B8 \,]$.

2.4. Identification of the Activities.

To identify the selected activities, a supervised classification was performed. The set of all measurement data from each sensor was divided into learning and test sets. The former contained 2400 randomly selected representatives of all 10 activities, while the latter all 4874 remaining cases.

For classification of the selected activities, k-NN algorithm and Manhattan metrics were used. Before the classification step, the classifier was tested using the LOO (Leave-One-Out) method. On the basis of these analyses, k equal to 1 was the optimal value for all sensors and sets of sensors.

For each activity a and each sensor s, the correctness of recognition for all volunteers R_{s_a} (1) and its calculation error U_{s_a} (2) were calculated. U_{s_a} is a measure of the results dispersion coming from intersubject differences. Due to different numbers of activity repetitions for each volunteer, we used weighted standard deviation (2):

$$R_{s\_a} = \frac{P_{s\_a}}{W_{s\_a}}, \tag{1}$$

where P_{s_a} is the sum of correctly identified repetitions of the activity a for all volunteers for the sensor s and W_{s_a} is the

sum of all repetitions of the activity a performed by all volunteers for the sensor s:

$$U_{s\_a} = \sqrt{\frac{\sum_{i=1}^{n} w_i \left(x_i - R_{s\_a}\right)^2}{(n - 1/n)\sum_{i=1}^{n} w_i}}, \tag{2}$$

where $n = 20$ is the number of weights, equal to the number of volunteers; w_i is the weight for the i-th volunteer, equal to the number of the activity a repetitions performed by the i-th volunteer; and x_i is the percentage of correct recognition for specific activity calculated for the i-th volunteer.

In order to represent an additional variable, $R_{s\_a\_ALL}$ (and its calculation error U_{s_ALL}) was employed. It illustrates the percentage of correct recognition for all activities and all volunteers for each sensor:

$$R_{s\_a\_ALL} = \frac{P_{s\_a\_ALL}}{W_{s\_a\_ALL}}, \tag{3}$$

where $P_{s\_a\_ALL}$ is the sum of correctly identified repetitions of all activities ALL performed by all volunteers for the sensor s and $W_{s\_a\_ALL}$ is the sum of all performed repetitions of all activities ALL for all volunteers.

$$U_{s\_a\_ALL} = \sqrt{\frac{\sum_{i=1}^{n} u_i \left(y_i - R_{s\_a\_ALL}\right)^2}{(n - 1/n)\sum_{i=1}^{n} u_i}}, \tag{4}$$

where u_i is the weight for the i-th volunteer, equal to the total number of repetitions of all activities performed by the i-th volunteer, and y_i is the percentage of correct recognition for all activities calculated for volunteer i.

For each volunteer V and sensor s, the percent recognition for all activities R_{s_V} (5) and its calculation error U_{s_V} (6) were determined. U_{s_V} is a measure of the results value dispersion arising from differences between different activities.

$$R_{s\_V} = \frac{P_{s\_V}}{W_{s\_V}}, \tag{5}$$
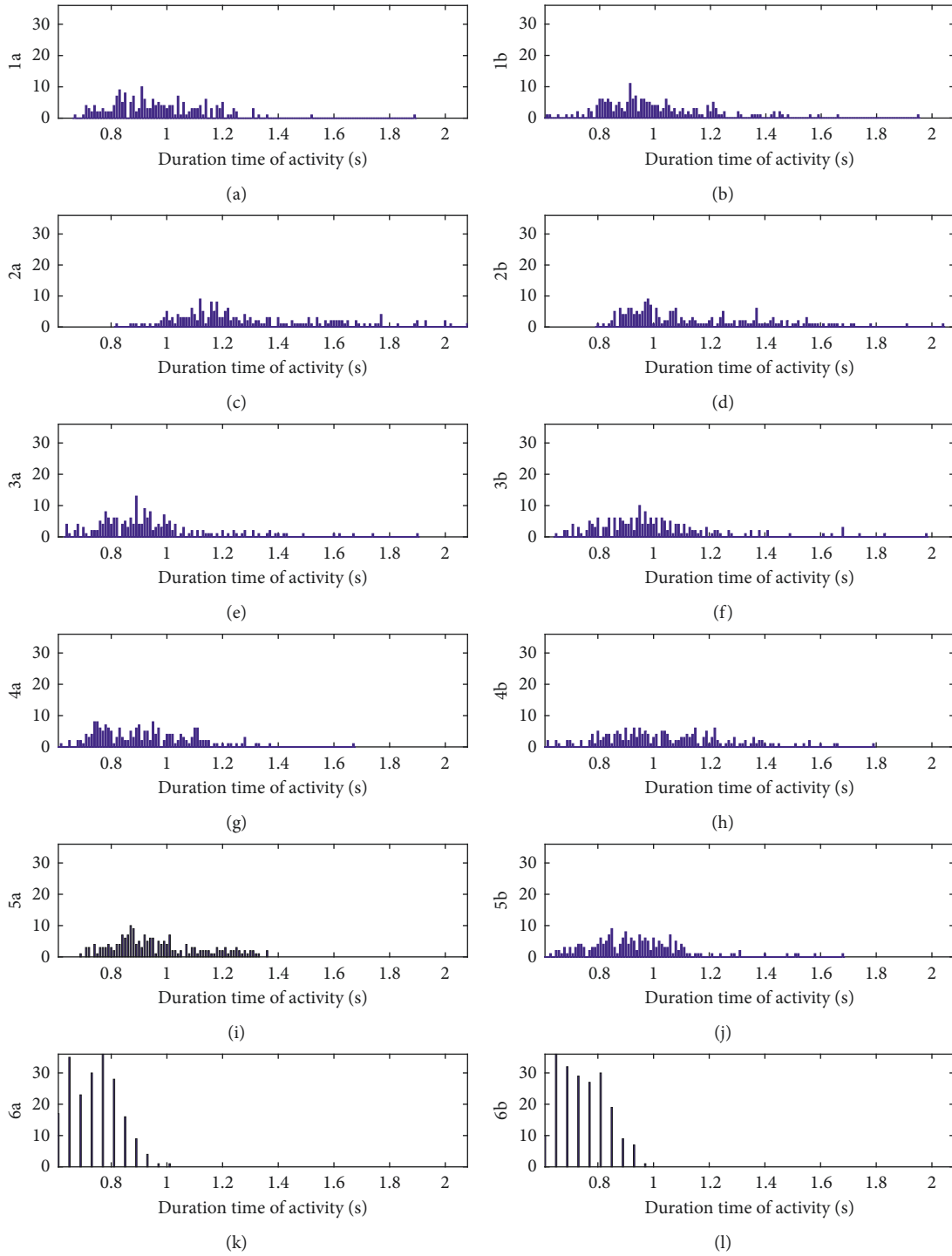
FIGURE 3: Histograms 1a to 6b of all performance time for all volunteers, for each activity separately 1a to 6b.

where P_{s_V} is the sum of correctly identified repetitions of all activities with the sensor s performed by the volunteer V and W_{s_V} is the sum of repetitions of all activities performed by the volunteer V.

$$U_{s\_V} = \sqrt{\frac{\sum_{j=1}^{m} p_j (z_j - R_{s\_V})^2}{(m-1/m)\sum_{j=1}^{m} p_j}}, \qquad (6)$$

where $m = 12$ is the number of weights, equal to the number of activity types, p_j is the weight for the j-th activity, equal to the number of its repetitions performed by the volunteer, and z_j is the percentage of correct recognition for the j-th activity for the specific subject.

In addition, the calculation error $U_{s\_V\_ALL}$, was determined as an activity-related dispersion:
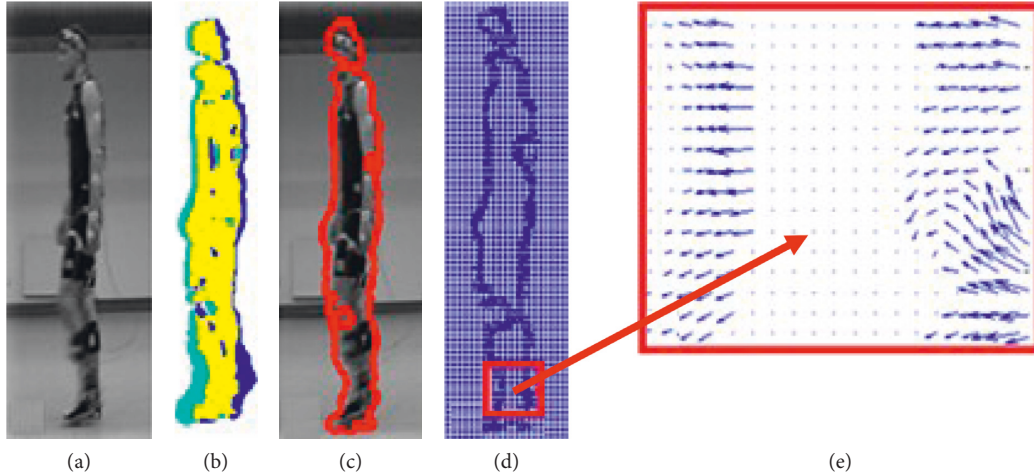
Figure 4: Optical flow algorithm [25]. (a) $(n-1)$-th frame representing the silhouette during free gait. (b) Joint part (yellow) of the areas: $OF_{n-1/n-2}$ (blue) and $OF_{n/n-1}$ (turquoise). (c) $(n-1)$-th frame representing the free gait with detected silhouette contour. (d) Optical flow calculated on bold contour of the moving silhouette and (e) optical flow of the zoomed silhouette part from red frame in (d).

$$U_{s\_V\_ALL} = \sqrt{\frac{\sum_{j=1}^{m} q_j \left(r_j - R_{s\_a\_ALL}\right)^2}{(m - 1/m)\sum_{j=1}^{m} q_j}}, \quad (7)$$

where q_j is the weight for the j-th activity equal to the number of all the repetitions performed by all volunteers and r_j is the percentage of correct recognition for the j-th activity calculated for all volunteers.

3. Results

The correctness of recognition R_{s_a} (1) of activities 1a to 6b for all persons for sensors B to E is presented in Table 1.

Matrices of the recognition errors (in %) of the individual activities 1a to 6b for all volunteers for the individual sensors B to E are shown in Tables 2–5. The percentage of correct recognition R_{s_a} for the individual activities is therefore placed on a diagonal matrix.

The correctness of recognition R_{s_V} of all activities for volunteers $V1$ to $V20$ and $R_{s\_a\_ALL}$ for ALL volunteers for sensors B to E is presented in Table 6.

4. Discussion

The correctness of recognition R_{s_a} (1) is negatively correlated with the dispersion of the value U_{s_a} (2) (Table 1). Therefore, less reliable recognition of the activity carried out by all volunteers does not mean worse recognition of the activity for each individual volunteer, but rather it is the implication of the individual way of performing the activity by the volunteer.

Some types of activities such as free gait or the return from reaching in the vertical and horizontal plane showed much less reliable recognition than others, regardless of the sensor type. Reliability of gait recognition is low probably due to high diversity in walking rhythm. Reaching is difficult to recognize, as it is characterized by low degree of dynamics of the whole body.

It was found that, among the single sensors, the best classifier for different activities is sensor B, followed successively by sensors D, E, and C.

The correctness of recognition R_{s_V} (5) is negatively correlated with the value of dispersion U_{s_V} (7) (Table 6). It means that less reliable recognition for a single volunteer (taking into account all activities) does not come from an inferior recognition reliability of every single activity for that volunteer, but rather it is a result of the existing inconsistency of individual activities recognitions.

Our research is focused on the recognition of only 12 types of daily life activities. The motivation of that choice is mainly based on the following aspects:

(i) Since the chosen activities are done quite often and are easy to repeat, we limit as much as possible the errors coming from different volunteer performance of the activity and thus the comparison of the sensors is more reliable

(ii) It can be presumed that any activity (even more complex) can be presented by means of the simple (elementary) poses [26].

Although the choice of a proper sensor is a very complex issue, in our studies, we simplify it only to the comparison of motion items. Nevertheless, the final choice of the sensors is precisely related with the application. The following requirements should then be taken into consideration:

(i) Individual characteristics of the sensor signal

(ii) Size of the registration space

(iii) Sensor accuracy

(iv) Sensor portability and unobtrusiveness

(v) Cost of the sensor device and reliable software

(vi) Privacy of the supervised person.

The reason for the performance differences for each activity and for each sensor has the source in differences in:

(i) Speed, range, and way of doing the particular motion

Table 1: Correctness of recognition R_{s_a} (in %) of activities 1a to 6b and $R_{s\_a\_ALL}$ of ALL activities for all volunteers for sensors B to E.

	1a	1b	2a	2b	3a	3b	4a	4b	5a	5b	6a	6b	All
B	96.9	100.0	99.5	98.5	99.0	99.3	99.1	98.6	97.9	98.2	96.0	97.6	98.4
	3.9	*0.0*	*1.5*	*3.7*	*3.4*	*1.8*	*3.2*	*3.1*	*3.7*	*3.5*	*12.7*	*7.5*	*1.8*
C	90.8	91.8	95.7	96.7	94.9	92.4	95.3	93.6	87.0	88.2	94.9	97.1	93.1
	10.0	*10.8*	*12.4*	*15.5*	*6.9*	*6.4*	*10.2*	*7.6*	*15.0*	*14.6*	*14.1*	*8.2*	*5.7*
D	95.2	97.2	95.5	94.2	96.6	95.1	98.4	97.6	97.9	99.3	96.5	96.0	96.7
	17.2	*11.2*	*15.8*	*15.4*	*6.6*	*8.8*	*3.2*	*4.1*	*2.8*	*1.9*	*12.3*	*12.1*	*5.2*
E	99.7	99.5	95.5	95.5	99.3	97.6	96.0	79.8	99.3	99.3	91.7	92.3	95.5
	1.1	*1.6*	*17.7*	*18.8*	*1.8*	*4.4*	*7.9*	*25.0*	*1.7*	*1.7*	*9.1*	*8.4*	*4.4*

Calculation errors U_{s_a} and $U_{s\_a\_ALL}$ are in italics.

Table 2: Matrix of recognition errors (in %) of activities 1a to 6b for all volunteers for sensor B.

B		Performed activity											
		1a	1b	2a	2b	3a	3b	4a	4b	5a	5b	6a	6b
Recognized activity	1a	**96.9**		0.5	0.8								
	1b		**100**										
	2a	2.0		**99.5**	0.8	0.2							
	2b				**98.5**								
	3a					**99.0**			0.2				
	3b						**99.3**		0.5				
	4a	0.5				0.2		**99.1**	0.7	1.1			
	4b						0.7	0.7	**98.6**	0.9	1.8		
	5a	0.5				0.5		0.2		**97.9**			
	5b										**98.2**		
	6a											**96.0**	2.4
	6b											4.0	**97.6**

Table 3: Matrix of recognition errors (in %) of activities 1a to 6b for all volunteers for sensor C.

C		Performed activity											
		1a	1b	2a	2b	3a	3b	4a	4b	5a	5b	6a	6b
Recognized activity	1a	**90.8**	0.3			4.1		0.5		0.5			
	1b		**91.8**				3.9		0.9				
	2a	0.3	0.8	**95.7**	1.5				0.7	0.2	0.7		
	2b	1.8		1.3	**96.7**				0.2	0.9	1.4		
	3a	3.1				**94.9**	0.2			0.5			
	3b		2.0				**92.4**			0.5			
	4a	2.8	0.5	0.8	1.0	1.0	0.2	**95.3**	4.0	4.6	1.6		
	4b	0.3	3.3	1.5	0.5		1.7	3.8	**93.6**	1.6	5.5		
	5a	1.0		0.3				0.5		**87.0**	2.7	0.3	0.3
	5b		1.3	0.5	0.3		1.5		0.5	4.3	**88.2**		
	6a											**94.9**	2.7
	6b											4.8	**97.1**

(ii) Anatomy and biomechanics of the volunteer body (physical fitness, strength, endurance, flexibility, way of loading the body weight, etc.).

The above factors have an impact on all of the sensors (B to E).

5. Conclusions

The paper presents results of recognition of 12 motor activities in human based on individual interpretation of simultaneous recordings from various sensors. The main finding is that some sensors are more appropriate to the selected activities, while the other sensors show higher performance compared with the others. Consequently, we specified both areas where sensors show distinctive properties and a common range of activities where the sensors show similar metrological properties and may be selected based on other criteria (e.g., cost and commodity).

Additionally, we found that some recognition results generalized for all volunteers as well as those generalized for all activities showed surprisingly low values. This suggests that the recognition performance is dependent on particular

TABLE 4: Matrix of recognition errors (in %) of activities 1a to 6b for all volunteers for sensor D.

D		1a	1b	2a	2b	3a	3b	4a	4b	5a	5b	6a	6b
						Performed activity							
Recognized activity	1a	**95.2**	1.0	0.3						0.9			
	1b	2.0	**97.2**	0.3	0.8						0.7		
	2a	0.5	0.5	**95.5**	3.5			0.2	0.2	0.9			0.3
	2b	1.0		2.3	**94.2**					0.2			
	3a					**96.6**		0.7					
	3b						**95.1**		1.2				
	4a			0.3	0.3	2.9	0.2	**98.4**	0.9			0.5	0.5
	4b		0.3	0.3	0.3	0.5	4.6	0.7	**97.6**				
	5a	1.3	0.3	1.0	1.0					**97.9**			
	5b		0.8	0.3							**99.3**		
	6a											**96.5**	3.2
	6b											2.9	**96.0**

TABLE 5: Matrix of recognition errors (in %) of activities 1a to 6b for all volunteers for sensor E.

E		1a	1b	2a	2b	3a	3b	4a	4b	5a	5b	6a	6b
						Performed activity							
Recognized activity	1a	**99.7**								0.5			
	1b		**99.5**								0.7		
	2a			**95.5**			0.2	0.2	0.2				
	2b				**95.5**	0.2	0.2		0.9				
	3a				0.5	**99.3**		3.8	0				
	3b			0.8			**97.6**		2.8				
	4a			3.8	3.8	0.5	0.2	**96.0**	16.2	0.2			
	4b	0.3					1.7		**79.8**				
	5a				0.3					**99.3**			
	5b		0.5								**99.3**		
	6a											**91.7**	7.7
	6b											8.3	**92.3**

TABLE 6: Correctness of recognition R_{s_V} (in %) of all activities for volunteers $V1$ to $V20$ and $R_{s\_a\_ALL}$ for ALL volunteers for sensors B to E.

	V1	V2	V3	V4	V5	V6	V7	V8	V9	V10	V11	V12	V13	V14	V15	V16	V17	V18	V19	V20	All
B	99.1	94.8	98.4	98.3	98.7	99.1	99.6	97.7	98.3	98.0	98.4	99.6	92.6	100.0	99.6	99.1	97.3	99.6	99.6	100.0	98.4
	2.0	*7.8*	*2.4*	*4.6*	*3.1*	*1.9*	*1.5*	*4.1*	*3.3*	*4.5*	*3.7*	*1.4*	*15.8*	*0.0*	*1.4*	*2.9*	*4.3*	*1.1*	*1.1*	*0.0*	*1.1*
C	98.2	94.8	98.0	97.9	92.3	97.4	97.3	94.9	95.7	91.2	94.4	88.0	85.3	97.1	87.3	88.9	75.2	94.7	93.5	98.4	93.1
	2.5	*5.6*	*3.3*	*2.2*	*11.6*	*5.9*	*5.0*	*7.8*	*4.1*	*12.5*	*7.2*	*17.2*	*15.9*	*3.3*	*13.4*	*13.6*	*22.7*	*13.1*	*11.8*	*4.4*	*3.3*
D	96.9	93.1	99.2	96.9	98.3	98.7	100.0	76.2	93.1	97.6	99.2	99.2	91.1	98.2	100.0	98.3	94.6	100.0	100.0	100.0	96.7
	3.9	*11.1*	*1.9*	*6.5*	*2.5*	*3.2*	*0.0*	*33.8*	*11.3*	*4.1*	*2.7*	*1.9*	*17.2*	*2.9*	*0.0*	*2.5*	*9.1*	*0.0*	*0.0*	*0.0*	*1.5*
E	97.4	95.3	95.9	88.8	97.9	99.1	99.6	97.7	94.4	93.6	99.2	81.0	96.5	94.9	99.2	98.3	92.3	97.3	97.7	94.8	95.5
	6.4	*9.7*	*7.4*	*23.4*	*3.6*	*1.9*	*2.0*	*3.1*	*10.5*	*14.7*	*1.9*	*31.8*	*5.3*	*16.2*	*1.9*	*3.9*	*16.1*	*4.7*	*4.5*	*11.2*	*5.8*

Calculation errors U_{s_V} and $U_{s\_V\_ALL}$ are in italics.

volunteer (i.e., subject-specific) and also on particular action. Accordingly, the hierarchy of expected recognition results for particular actions is not universal, and to produce optimal results, it should be individually adjusted with regard to particular user behavior.

The prospective ways of future extension of our studies are as follows:

(i) Expanding the list of activities with more complex ones

(ii) Evaluating and adapting the proposed solutions in home environment

(iii) Extending video processing algorithm with a detection of individual body parts.

Data Availability

Research data are not openly available because of the volunteers' privacy.

Conflicts of Interest

Acknowledgments

References

[1] A. Phinyomark, G. Chujit, P. Phukpattaranont, C. Limsakul, and H. Hu, "A preliminary study assessing time-domain EMG features of classifying exercises in preventing falls in the elderly," in *Proceedings of the 9th International Conference on Electrical Engineering & Electronics, Computer, Telecommunications and Information Technology*, pp. 1–4, Phetchaburi, Thailand, May 2012.

[2] Y. C. Wang, C. K. Huang, W. K. Lee et al., "The convenient balance evaluation system," in *Proceedings of the International Conference on Information Science, Electronics and Electrical Engineering*, pp. 914–917, Sapporo City, Hokkaido, Japan, April 2014.

[3] U. Baspinar, H. Selcuk Varol, and K. Yildiz, "Classification of hand movements by using artificial neural network," in *Proceedings of the International Symposium on Innovations in Intelligent Systems and Applications*, pp. 1–4, Trabzon, Turkey, July 2012.

[4] Y. Mon Aung and A. Al-Jumaily, "Rehabilitation exercise with real-time muscle simulation based EMG and AR," in *Proceedings of the 11th International Conference on Hybrid Intelligent Systems*, pp. 641–646, Melacca, Malaysia, December 2011.

[5] H. Converse, T. Ferraro, D. Jean et al., "An EMG biofeedback device for video game use in forearm physiotherapy," in *Proceedings of the IEEE Sensors*, pp. 1–4, Baltimore, MD, USA, November 2013.

[6] D. Novak, P. Rebersek, T. Beravs et al., "Early recognition of gait initiation and termination using wearable sensors," in *Proceedings of the 4th IEEE RAS & EMBS International Conference on Biomedical Robotics and Biomechatronics (BioRob)*, pp. 1937–1942, Rome, Italy, June 2012.

[7] M. Chen, B. Huang, and Y. Xu, "Intelligent shoe for abnormal gait detection," in *Proceedings of the IEEE International Conference on Robotics and Automation*, pp. 2019–2024, Pasadena, CA, USA, May 2008.

[8] L. Shu, T. Hua, Y. Wang, Q. Li, D. D. Feng, and X. Tao, "In-shoe plantar pressure measurement and analysis system based on fabric pressure sensing array," *IEEE Transactions on Information Technology in Biomedicine*, vol. 14, no. 3, pp. 767–775, 2009.

[9] O. Mazunder, A. S. Kundu, and S. Bhaumik, "Development of wireless insole foot pressure acquisition device," in *Proceedings of the International Conference on Communications, Devices and Intelligent Systems*, pp. 302–305, Kolkata, India, December 2012.

[10] H. Abou Ghaida, S. Mottet, and J. M. Goujon, "A real time study of the human equilibrium using an instrumented insole with 3 pressure sensors," in *Proceedings of the 36th Annual International Conference of the IEEE Engineering in Medicine and Biology Society (EMBC 2014)*, pp. 4968–4971, Chicago, IL, USA, August 2014.

[11] B. Najafi, K. Aminian, A. Paraschiv-Ionescu, F. Loew, C. J. Bula, and P. Robert, "Ambulatory system for human motion analysis using a kinematic sensor: monitoring of daily physical activity in the elderly," *IEEE Transactions on Biomedical Engineering*, vol. 50, no. 6, pp. 711–723, 2003.

[12] S. W. Lee, K. Mase, and K. Kogure, "Detection of spatio-temporal gait parameters by using wearable motion sensors," in *Proceedings of the IEEE Engineering in Medicine and Biology 27th Annual Conference*, pp. 6836–6839, Shanghai, China, January 2006.

[13] L. Rong, D. Zhigu, Z. Jianzhong, and L. Ming, "Identification of individual walking patterns using gait acceleration," in *Proceedings of the 1st International Conference on Bioinformatics and Biomedical Engineering*, pp. 543–546, Wuhan, China, July 2007.

[14] R. Jafari, W. Li, R. Bajcsy, S. Glaser, and S. Sastry, "Physical activity monitoring for assisted living at home," in *Proceedings of the 4th International Workshop on Wearable and Implantable Body Sensor Networks (IFMBE)*, pp. 213–219, Aachen, Germany, March 2007.

[15] B. Aguiar, T. Rocha, J. Silva, and I. Sousa, "Accelerometer-based fall detection for smartphones," in *Proceedings of the IEEE International Symposium on Medical Measurements and Applications (MeMeA)*, pp. 1–6, Lisboa, Portugal, July 2014.

[16] C.-F. Juang and C.-M. Chang, "Human body posture classification by a neural fuzzy network and home care system application," *IEEE Transactions on Systems, Man, and Cybernetics—Part A: Systems and Humans*, vol. 37, no. 6, pp. 984–994, 2007.

[17] C. C. Li and Y. Y. Chen, "Human posture recognition by simple rules," in *Proceedings of the IEEE International Conference on Systems, Man, and Cybernetics*, pp. 3237–3240, Taipei, Taiwan, October 2006.

[18] K. K. Htike and O. O. Othman, "Comparison of supervised and unsupervised learning classifiers for human posture recognition," in *Proceedings of the International Conference on Computer and Communication Engineering*, pp. 1–6, Kuala Lumpur, Malaysia, May 2010.

[19] C.-F. Juang, C.-M. Chang, J.-R. Wu, and D. Lee, "Computer vision-based human body segmentation and posture estimation," *IEEE Transactions on Systems, Man, and Cybernetics—Part A: Systems and Humans*, vol. 39, no. 1, pp. 119–133, 2009.

[20] K. T. Song and W. J. Chen, "Human activity recognition using a mobile camera," in *Proceedings of the 8th International Conference on Ubiquitous Robots and Ambient Intelligence*, pp. 3–8, Incheon, Korea, November 2011.

[21] P. Augustyniak, M. Smoleń, Z. Mikrut, and E. Kańtoch, "Seamless tracing of human behavior using complementary wearable and house-embedded sensors," *Sensors*, vol. 14, no. 5, pp. 7831–7856, 2014.

[22] A. Adamski, Z. Bubliński, Z. Mikrut, and P. Pawlik, "The image-based automatic monitoring for safety traffic lanes intersections," in *Transactions on Transport Systems*

Telematics—Emerging Technologies, J. Piecha, Ed., pp. 92–102, Wydawnictwo Politechniki Śląskiej, Gliwice, Poland, 2004.

[23] B. K. P. Horn and B. G. Schunck, ""Determining optical flow": a retrospective," *Artificial Intelligence*, vol. 59, no. 1-2, pp. 81–87, 1993.

[24] Z. Mikrut and K. Pałczyński, "Segmentacja sekwencji obrazów z wideodetektora na podstawie przepływu optycznego," *Automatyka AGH*, vol. 7, no. 3, pp. 371–384, 2003, in Polish.

[25] P. Augustyniak, K. Barczewska, A. Broniec et al., *Systemy Techniczne Formujące Inteligentne Otoczenie Osoby Niepełnosprawnej*, Akademicka Oficyna Wydawnicza EXIT, Warszawa, Poland, 2015, in Polish.

[26] P. Augustyniak and G. Ślusarczyk, "Graph-based representation of behavior in detection and prediction of daily living activities," *Computers in Biology and Medicine*, vol. 95, pp. 261–270, 2018.

Research Article

Wearable Sensors Integrated with Virtual Reality: A Self-Guided Healthcare System Measuring Shoulder Joint Mobility for Frozen Shoulder

Jianjun Cui,[1] Shih-Ching Yeh [ID],[1] and Si-Huei Lee [ID][2]

[1]*Fudan University, Shanghai 200433, China*
[2]*Taipei Veterans General Hospital, Taipei 11217, Taiwan*

Correspondence should be addressed to Si-Huei Lee; leesihuei@gmail.com

Frozen shoulder is a common clinical shoulder condition. Measuring the degree of shoulder joint movement is crucial to the rehabilitation process. Such measurements can be used to evaluate the severity of patients' condition, establish rehabilitation goals and appropriate activity difficulty levels, and understand the effects of rehabilitation. Currently, measurements of the shoulder joint movement degree are typically conducted by therapists using a protractor. However, along with the growth of tele-rehabilitation, measuring the shoulder joint mobility on patients' own at home will be needed. In this study, wireless inertial sensors were combined with the virtual reality interactive technology to provide an innovative shoulder joint mobility self-measurement system that can enable patients to measure their performance of four shoulder joint movements on their own at home. Pilot clinical trials were conducted with 25 patients to confirm the feasibility of the system. In addition, the results of correlation and differential analyses compared with the results of traditional measurement methods exhibited a high correlation, verifying the accuracy of the proposed system. Moreover, according to interviews with patients, they are confident in their ability to measure shoulder joint mobility themselves.

1. Introduction

Frozen shoulder is the common name for impaired shoulder movement caused by injury to the shoulder capsule and soft tissues. Clinically, frozen shoulder is a common shoulder condition. The symptoms of this condition include restriction of active or passive joint motion, stiffness, aching, and loss of muscular strength in the shoulder. Such symptoms typically manifest for 2 years [1–5], although in severe cases, they can persist for more than 5 years. Generally, patients cannot move their shoulder because of injury to the soft tissue surrounding the shoulder. The accompanying pain causes them to avoid all movements, which further exacerbates the condition. The prevalence of frozen shoulder in the general population is between 2% and 5%. This condition is typically experienced between the ages of 40 and 65 years, with a higher occurrence rate for women compared with that for men (at a ratio of 58 : 42) [6]. People diagnosed with diseases such as diabetes and

hyperthyroidism also exhibit a higher than average occurrence rate [7].

Regarding medication treatments, medicines such as Panadol and nonsteroid anti-inflammatory drugs can be considered. In addition, steroid injections into the shoulder joint can also be administered to ease pain. Medication treatments are generally provided to alleviate pain and reduce inflammation. However, for certain patients with severe symptoms, the effect of such treatments is limited. Therefore, alternative physical therapies are necessary to effectively restore shoulder joint function [8]. Measurements of shoulder joint mobility are crucial to the rehabilitation process. By measuring shoulder joint mobility before rehabilitation, the goals and difficulty levels of the rehabilitation activities can be set according to the severity of the patient's condition, which is determined based on the maximum angle of shoulder joint motion when performing various rehabilitation movements, to accommodate each

patient's rehabilitation needs. These measurements also allow patients to recognize the effects of rehabilitation, thereby increasing their motivation and compliance. Currently, measurements of shoulder joint mobility are conducted by therapists and using protractors. Along with the growth of telerehabilitation [9–11], there is increasing need for patients to measure shoulder joint mobility on their own at home in order to understand the progress of rehabilitation. However, it is difficult for patients to operate protractors alone at home.

With recent advancements in microelectromechanical systems, the size and cost of various types of sensors have declined considerably, leading to increased applications. Inertial measurement units (IMUs) are primarily used to measure the movement direction and orientation of a physical object. Incorporating wireless transmission technologies, the wireless IMU (WIMU) sensor was proposed as a wearable sensor and its applications in motor rehabilitation have increased [12, 13]. In this research, by integrating wireless IMU sensors with VR interactive technology, an innovative self-measurement system combined with a set of shoulder joint mobility exercises was developed, facilitating home-based objective assessments of patients' shoulder mobility. The research objectives of this study were as follows: (1) to combine wireless IMU sensors with VR interactive technology to produce an innovative shoulder joint mobility self-measurement system; (2) to verify the feasibility and accuracy of the developed system via clinical trials; and (3) to investigate patients' usage intentions for this system.

2. Methods

2.1. System Design. The two essential elements to define virtual reality are immersion and interaction. The system architecture comprised two units: a WIMU and a VR-based interactive self-guided program (VRISG). The system architecture design is shown in Figure 1. In our design, projector is used to display the virtual environment in order to provide the immersion. WIMU is applied that the user is able to interact with the virtual environment.

The WIMU is primarily used to detect the shoulder joint position. Physically, the WIMU is attached to the user's affected side at wrist or elbow according to movement types, as shown in Figure 2. In addition, their performance of various shoulder joint mobility exercises could be assessed to determine the joint angle. Data of the shoulder joint angle and position are then transmitted wirelessly to the VRISG for processing. The proposed system comprised two parts: an IMU and a wireless transmission module (as shown in Figure 1). The IMU used in this study was a 9DOF Razor IMU. This IMU contains three sensor chips: triple-axis gyroscope, triple-axis accelerometer, and triple-axis magnetometer. Using these three sensor chips, the posture value (pitch, yaw, and row) of an object can be measured. After the IMU obtains posture data, the wireless transmission module XBee (manufactured by Digi International) transmits data signals to the XBee receiver connected to a computer. Finally, the game engine reads the signals and uses animations to present users' movement postures.

The VRISG uses the received data and animation functions to realistically simulate the human body. A projector is then used to project the simulated image onto a wall. The system uses a 3D Unity game engine and related software programs to produce a skeleton animation and user interface for measuring shoulder joint mobility when performing various movements. Corresponding activities were designed for self-guided measurement, with the movements including abduction, flexion, internal rotation, and external rotation, as shown in Figure 3. For measuring joint mobility during each movement, an instructional video is provided to assist users in understanding the correct way to perform each movement and the important steps they should be aware of during the measurement stage. Next, during the measurement process, the system guides users through skeleton animations based on shoulder joint angle measurements and presents user posture immediately as real-time visual feedback. This enables users to clearly understand the range and margin of their shoulder joint movements. Concurrently, an angle bar graph and angle value column appear on the right side of the computer screen and display shoulder joint angle measured by the IMU, informing users of their shoulder joint movement angle. Each movement should be performed three times, and the outcome is measured every time. Every movement cycle begins with users raising their upper limbs and gradually rotating the shoulder joint until the maximum movement angle is reached. The movement cycle ends when users relax their upper limbs. This movement cycle must be performed three times. The three angle measurements and the average of these measurements are displayed as a reference for patients and physical therapists. Furthermore, after each measurement is complete, the data are stored in a database to provide therapists with an understanding and analysis of each patient's rehabilitation status and progress.

2.2. Participants. The clinical trials conducted for this research were proactive, intervening, randomly assigned, and single blind. This study obtained consent for participation from 25 people, specifically, 10 men and 15 women, with an average age of 56.25 years. The average duration of the condition was 8.2 months. This study project was approved by the Institutional Review Board of Taipei Veterans General Hospital with VGHIRB: 2012-07-004A. The participant inclusion and exclusion criteria were as follows:

2.2.1. Inclusion Criteria

(1) At least 20 years of age
(2) No previous experience of physical therapy
(3) Normal cognition and able to follow the system use instructions
(4) Clinical diagnosis of frozen shoulder
(5) A signed consent form

2.2.2. Exclusion Criteria

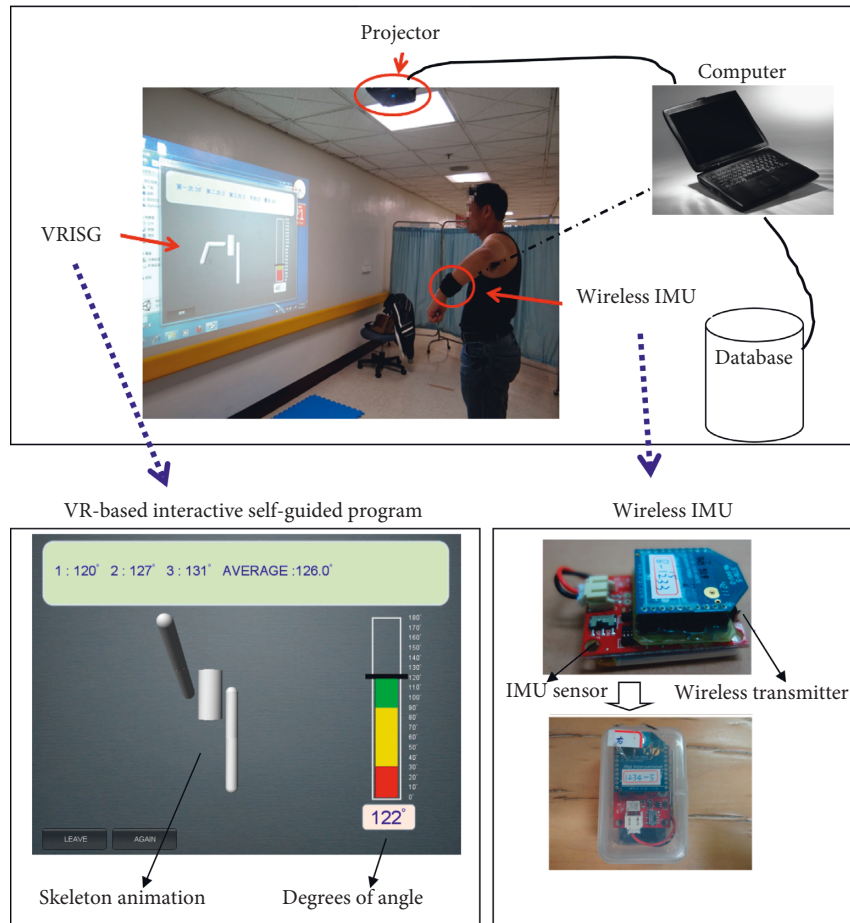(1) A history of injury, dislocation, or surgery to the shoulder or humerus
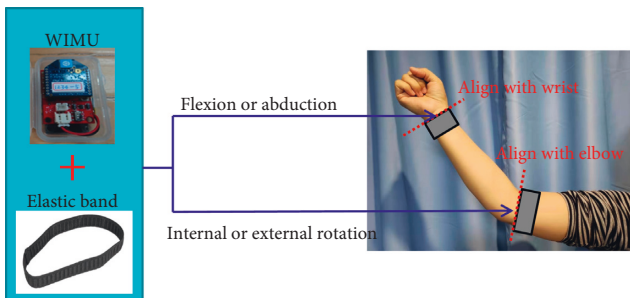
FIGURE 1: System architectures.

FIGURE 2: Physical setting of IMU.

mobility. The movements that were performed in the experiment to measure shoulder joint mobility were divided into the following four categories: flexion, abduction, internal rotation, and external rotation. Two types of measurement methods were employed, which are as follows:

(1) To use the innovative shoulder joint mobility self-measurement system proposed in this study for conducting measurements. During the experiment, the participants observed changes in the angle and mobility of their shoulder joint as well as the measurement results projected on the screen, as shown in Figure 1.

(2) To use the traditional method, which involved physical therapists using a protractor for measurement, the patients were not provided any information regarding the measurements, as shown in Figure 4.

In this study, every participant was measured using both methods. During these measurements, they were required to perform the four shoulder joint mobility movements in sequence, and each movement was measured three times. Subsequently, the three measurements of each movement were averaged and recorded by a physical therapist. These data acquired from the first measurement method were classified as the experimental group, while data from the

(2) Prior treatment with hyaluronic acid injections in the shoulder

(3) A history of cervical spondylotic radiculopathy or degenerative arthritis of the shoulder

(4) A history of terminal malignant disease

(5) Pregnancy

2.3. Experimental Procedure. Before the experiment, the participants were required to sign an experiment consent form and understand the research procedures. The experiment primarily measured the patients' shoulder joint

(a)   (b)
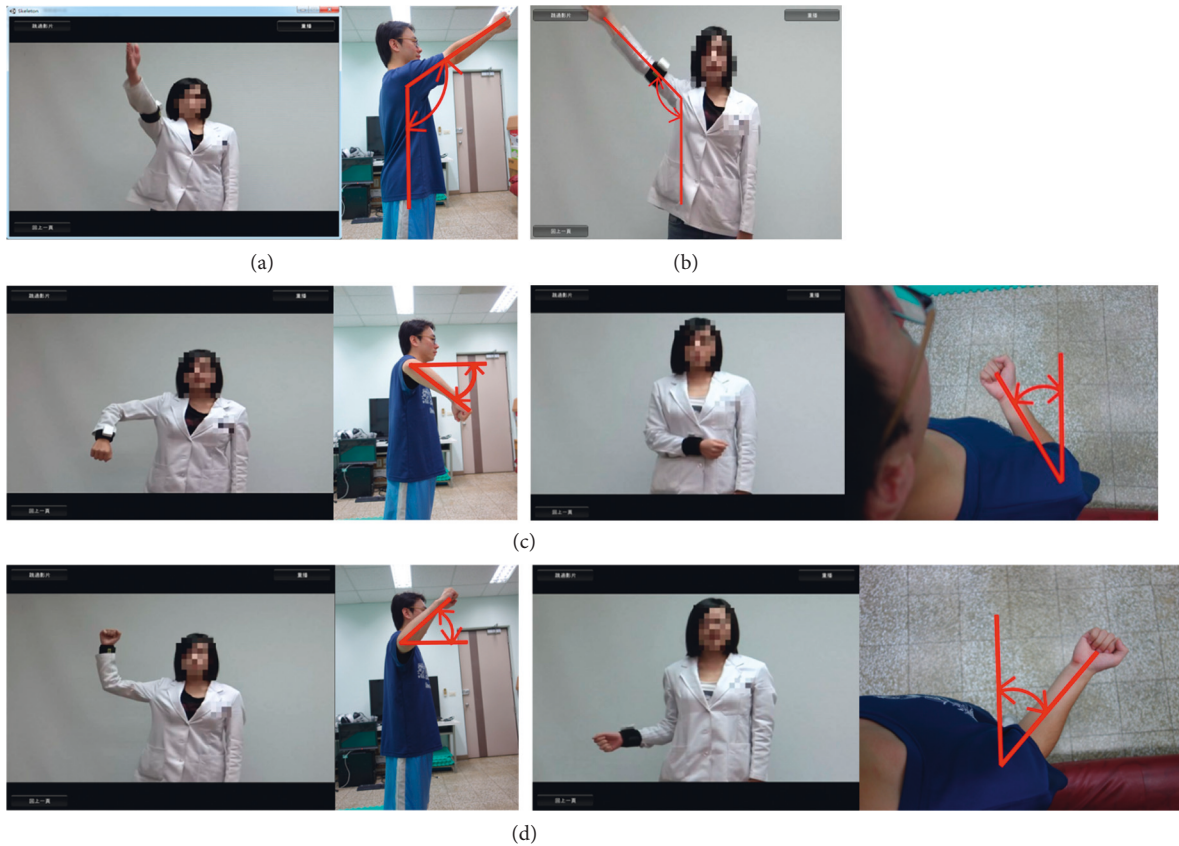
(c)

(d)

FIGURE 3: Movement types. (a) Flexion. (b) Abduction. (c) Internal rotation. (d) External rotation.

Protractor

FIGURE 4: Using a protractor for measurement.

second method were classified as the control group. The experimental group and control group were measured separately by two physical therapists.

The participants in the experimental group first followed the sequence of the movements to attach the WIMU to the specified location and then used the VRISG to conduct measurements. Please refer to Section 2.2 for more details regarding the measurement process and content.

For the control group, a different physical therapist than the one assigned to the experimental group employed the traditional measurement method, where shoulder joint mobility was primarily measured by using traditional tools

including a protractor. No software system was used to assist with the experimental process. The mobility measurement steps and movement sequence adopted for the control group were identical to those of the experimental group. Thus, the participants' shoulder joint mobility when performing each movement was measured three times by the physical therapist using a protractor combined with other traditional techniques. The measurement results were then averaged and recorded.

2.4. Measurement and Analysis. To verify the accuracy of the innovative shoulder joint mobility self-measurement system proposed in this study for clinical applications, the correlation and difference between the results of the experimental and control groups were further investigated by evaluating and comparing the analysis results of the Pearson's correlation coefficient and Wilcoxon signed-rank tests. The primary functions of a correlation coefficient are to identify the linear relationship between two random variables and to calculate the strength of their linear relationship. If the absolute value of the population correlation coefficient is near 1, the linear relationship between two variables increases in strength and correlation. The reason for conducting a Wilcoxon signed-rank test was because the experimental and control group samples were from the same population. Thus, this analysis method was adopted to investigate whether the difference between the results provided

by the two methods was significant. Using the two aforementioned analysis methods to examine the correlation and difference between the results of the two measurement methods, the accuracy of the proposed system was verified.

3. Results

The first analysis method involved using correlation coefficients to compare the data provided by the two measurement methods; the analysis results are shown in Table 1. The results show that the calculated correlation coefficients were close to 1, and the P values all reached the level of significance. This indicates that the results of the two measurement methods possessed a high correlation.

For the second measurement method, a Wilcoxon signed-rank test was adopted to perform a paired-samples t-test analyzing the difference between the results provided by the two measurement methods. The analysis results are shown in Table 2. The P values calculated according to the paired-samples t-test results for the four movement measurements all exceeded 0.05. Thus, the measurement results obtained for the experimental group and the control group showed no significant differences.

4. Discussion

For this experiment, clinical trials were conducted on 25 patients. When performing self-measurements using the system proposed in this paper, the participants were able to follow the system instructions and measure their joint mobility themselves, verifying the feasibility of the proposed system.

According to the findings of the two analyses conducted, as mentioned previously, the measurements obtained using the proposed shoulder joint mobility self-measurement system and those obtained using a traditional protractor exhibited a high correlation and no significant differences. The similarity of the two measurement results verifies the accuracy of the proposed shoulder joint mobility self-measurement system.

The system proposed in this study comprises two aspects, software and hardware. Because of recent technological advancements, the size and weight of the wireless IMU sensor hardware have become substantially more compact and light. In addition, the precision of such hardware has increased while the cost decreased. Therefore, from a user perspective, acceptance of this system should be high and distribution should be fairly easy. The corresponding software program guides patients in completing self-assessments of shoulder joint mobility. This system not only exhibits technical accuracy and consistency, but also satisfies demands for user-centered designs. Furthermore, this system can be used to reduce the clinical burdens of therapists and extend the treatment into the patients' home, facilitating home-based healthcare.

According to the results of interviews conducted with therapists and patients, the therapists believe that the proposed system can effectively measure patients' joint mobility with reliable accuracy. In addition, the system can reduce the

TABLE 1: Comparison of the correlation between the measurement results for the experimental and control groups.

Flexion	Abduction	External rotation	Internal rotation
0.997	0.978	0.897	0.984
$P = **$	$P = **$	$P = **$	$P = **$
Correlation level		Significance level = 0.05	
$0 \leqq |r| < 0.3$: low		$^* p < 0.05$	
$0.3 \leqq |r| < 0.7$: medium		$^{**} p < 0.01$	
$0.7 \leqq |r| < 1$: high			

TABLE 2: Results of the Wilcoxon signed-rank test for the experimental and control group measurements.

	Flexion	Abduction	External rotation	Internal rotation
P value	0.556	0.129	1.044	2.547

Significance level = 0.05; $^* p < 0.05$; $^{**} p < 0.01$.

human resources and time required to assess patients' joint mobility using traditional methods. According to the observations of the therapists, patients can easily operate the system by themselves to measure their shoulder joint mobility. However, they asserted that should this system be used to replace therapists completely, side effects and issues, particularly social psychological issues, may result. Therefore, further investigations are required to find the optimum use strategy for this system and therapist assistance, for example, how patients should periodically undergo measurements by therapists at medical therapy centers in addition to using the system at home for self-measurements. The results of the patient interviews showed that the patients were confident and willing to operate the proposed system to enhance their understanding of their rehabilitation progress. However, they also acknowledged that compared with using the system at home for self-measurements, the psychological support and encouragement provided by therapists during traditional measurements and face-to-face assessments was highly valued.

5. Study Limitations

The primary limitations of this study resulted from the wireless IMU sensor hardware, namely, the size, weight, and "wearability" of the device, which influence people's willingness to use the system. The sensors' precision and wireless transmission speed can directly influence the sensitivity of interactions between the user and guidance system, which indirectly affects the user's perceptions. The guidance software designed for this system cannot provide patients with the psychological aspects of support and trust that a real therapist can.

6. Conclusions

In this study, an IMU sensor was successfully combined with interactive VR technology to develop an innovative shoulder

joint mobility self-measurement system for patients diagnosed with frozen shoulder. Clinical trials were conducted with 25 patients; the results of which verified the feasibility of the system. The results of an analysis and comparison of the measurements provided by the proposed system and those obtained using traditional measurement methods show that a high correlation and no significant differences are exhibit between the two. This confirms that the proposed system can effectively and reliably measure patients' shoulder joint mobility. According to the results of interviews conducted with therapists and patients, the therapists believe that the system can effectively reduce the human resources and time required to assess patients' shoulder joint mobility while providing accurate and reliable results. The patients indicated that they were confident and willing to operate the system themselves to understand their rehabilitation progress.

In the future, additional novel MEMS technologies are expected to be employed to produce wireless IMU sensors that are comparatively smaller in size, lighter in weight, and higher in accuracy, thereby increasing the convenience of self-operated systems. Furthermore, large-scale clinical trials are set to be conducted to determine the reliability and validity of the proposed system. In the future, the application of advanced Internet technology and cloud technology combined with the concept of long-distance medical rehabilitation will popularize the system developed in this study for use at home.

Data Availability

The data used to support the findings of this study are available from the corresponding author upon request.

Conflicts of Interest

The authors declare that they have no conflicts of interest regarding the publication of this article.

Acknowledgments

References

[1] G. R. Clarke, L. A. Willis, W. W. Fish, and P. J. Nichols, "Preliminary studies in measuring range of motion in normal and painful stiff shoulders," *Rheumatology Rehabilitation*, vol. 14, no. 1, pp. 39–46, 1975.

[2] B. Reeves, "The natural history of the frozen shoulder syndrome," *Scandinavian Journal of Rheumatology*, vol. 4, no. 4, pp. 193–196, 1975.

[3] A. I. Binder, D. Y. Bulgen, B. L. Hazleman, and S. Roberts, "Frozen shoulder: a long-term prospective study," *Annals of the Rheumatic Diseases*, vol. 43, no. 3, pp. 361–364, 1984.

[4] M. A. Sattar and W. A. Luqman, "Periarthritis: another duration-related complication of diabetes mellitus," *Diabetes Care*, vol. 8, no. 5, pp. 507–510, 1985.

[5] B. Shaffer, J. E. Tibone, and R. K. Kerlan, "Frozen shoulder. A long-term follow-up," *Journal of Bone and Joint Surgery*, vol. 74, no. 5, pp. 738–746, 1992.

[6] D. Thierry, "Adhesive capsulitis," *Emedicine*, vol. 11, p. 7, 2005.

[7] J. E. Bateman and V. L. Fornasier, *The Shoulder and Neck*, 2nd edition, Saunders Limited, Philadelphia, PA, USA, 1978.

[8] H. F. Moseley, "Disorders of the shoulder," *Clinical Symptoms*, vol. 11, no. 3, pp. 75–102, 1959.

[9] M. K. Holden, T. A. Dyar, L. Schwamm, and E. Bizzi, "Virtual-environment-based telerehabilitation in patients with stroke," *Presence: Teleoperators and Virtual Environments*, vol. 14, no. 2, pp. 214–233, 2005.

[10] D. Anton, A. Goni, A. Illarramendi, J. J. Torres-Unda, and J. Seco, "KiReS: a kinect-based telerehabilitation system," in *Proceedings of the IEEE 15th International Conference on e-Health Networking, Applications and Services (Healthcom 2013)*, pp. 444–448, Lisbon, Portugal, March 2013.

[11] L. Paul, E. H. Coulter, L. Miller, A. McFadyen, J. Dorfman, and G. M. P. George, "Web-based physiotherapy for people moderately affected with multiple sclerosis; quantitative and qualitative data from a randomized, controlled pilot study," *Clinical Rehabilitation*, vol. 28, no. 9, pp. 924–935, 2014.

[12] C. Cifuentes, A. Braidot, L. Rodriguez, M. Frisoli, A. Santiago, and A. Frizera, "Development of a wearable ZigBee sensor system for upper limb rehabilitation robotics," in *Proceedings of the IEEE RAS & EMBS International Conference on Biomedical Robotics and Biomechatronics*, pp. 1989–1994, Rome, Italy, June 2012.

[13] Z. Luo, C. K. Lim, W. Yang et al., "An interactive therapy system for arm and hand rehabilitation," in *Proceedings of the Robotics Automation and Mechatronics*, pp. 9–14, Singapore, 2010.

Research Article

Registration and Analysis of Acceleration Data to Recognize Physical Activity

Marcin Kołodziej [iD], **Andrzej Majkowski, Paweł Tarnowski, Remigiusz J. Rak, Dominik Gebert, and Dariusz Sawicki**

Institute of Theory of Electrical Engineering, Measurements and Information Systems, Warsaw University of Technology, Warsaw, Poland

Correspondence should be addressed to Marcin Kołodziej; marcin.kolodziej@ee.pw.edu.pl

The purpose of the article is to check whether the acceleration signals recorded by a smartphone help identify a user's physical activity type. The experiments were performed using the application installed in a smartphone, which was located on the hip of a subject. Acceleration signals were recorded for five types of physical activities (running, standing, going up the stairs, going down the stairs, and walking) for four users. The statistical parameters of the signal were used to extract features from the acceleration signal. In order to classify the type of activity, the quadratic discriminant analysis (QDA) was used. The accuracy of the user-independent classification for five types of activities was 83%. The accuracy of the user-dependent classification was in the range from 90% to 95%. The presented results indicate that the acceleration signal recorded by the device placed on the hip of a user allows us to effectively distinguish among several types of physical activity.

1. Introduction

In today's world, it can be seen that more and more people are beginning to pay attention to their physical activity. A sedentary lifestyle, whether at home or at work, makes caring for our physical condition not just another addition to everyday activities but also a certain duty toward maintaining our health. Currently, the 10,000 steps per day recommended by specialists [1] take an average person just over an hour. Since cardiovascular diseases are now one of the main causes of death, each of us should sacrifice from 20 minutes to 2 hours a day for physical exercises as they help prevent many of these diseases. In the United States, diseases caused by the lack of physical exercises lead to the death of more people than all forms of cancer combined [2]. In view of the above mentioned aspects, newer solutions are emerging in the market that can be used to monitor daily physical activity, and companies producing devices for athletes are primarily involved in this. In addition, devices to monitor the type of activity performed are also available in the market for the average user.

Several researchers have invested a lot of effort to explore different sensing technologies and have proposed a number of methods to recognize human physical activities [3–5]. Researchers constructed various activity recognition systems that utilized accelerometers to infer the body position; accelerometers can provide acceleration and velocity data largely associated with various human physical activities [6–8].

However, having a specialized solution to monitor physical activity is not necessary. A smartphone can be successfully used for this purpose. Almost every smartphone has an accelerometer, also known as an acceleration transducer. As the name suggests, the accelerometer is used to measure the acceleration affecting a given object. An acceleration transducer allows the position of a device in space to be determined and enables the device to be controlled by motion.

The aim of this article is at analyzing the signal from a smartphone accelerometer, in order to use it to identify the user's physical activity type. To collect data, an Android application written in Java programming language was used.

Activity recognition typically consists of three stages. In the first step, the sensor data are divided into segments, typically using the sliding window technique [6, 9]. The next

step is to extract features from the segments. Finally, a classifier is trained over these extracted features. The last task is to use the classifier to associate the sensor data with a predefined activity.

In our research, we used the same approach. We tried to answer the following questions:

(1) Does the recorded acceleration signal (accelerometer placed on the user's hips) allow several typical physical activities to be distinguished?

(2) Does a set of simple statistical features allow you to distinguish between activities effectively?

(3) What types of physical activity are the most difficult to distinguish?

(4) Is it possible to create a system that recognizes activities based on data collected only from a specific user or it is better to use data from all users (user-dependent vs user-independent classification)?

Answers to these questions will allow you to assess whether there is a chance to develop an application to recognize user activity with just a smartphone. The presented results should be treated as preliminary. In order to fully estimate the effectiveness of the presented activity recognition system, a larger number of users should be tested.

2. Materials

The Huawei P10 smartphone equipped with an iNEMO module (LSM6DSM) was used to record the acceleration signals. The LSM6DSM module has a three-axis accelerometer and a gyroscope. The accelerometer can work in ranges $\pm 2\,g$, $\pm 4\,g$, $\pm 8\,g$, and $\pm 16\,g$. For each person, the phone was placed on the hip, with the display facing the outside (Figure 1). Physical activity was recorded for four people—two men aged 26 and 56 and two women aged 23 and 46. Each person was asked to perform simple physical activities:

(i) Running (R)

(ii) Standing (S)

(iii) Going up the stairs (U)

(iv) Going down the stairs (D)

(v) Walking (W)

Each individual user's data were recorded for each activity for several minutes. The acceleration signals were recorded in the three axes, with a sampling frequency fs = 50 Hz, and saved in text files. One line of the file corresponded to a single acceleration measurement and contained information about acceleration values in the x-, y-, and z-axes with respect to time. Files containing the recorded signals were analyzed with use of the PC.

3. Methods

3.1. Signal Processing. At first, the recorded acceleration signals were visually evaluated and fragments of these, associated with the physical activities of interest, were selected.
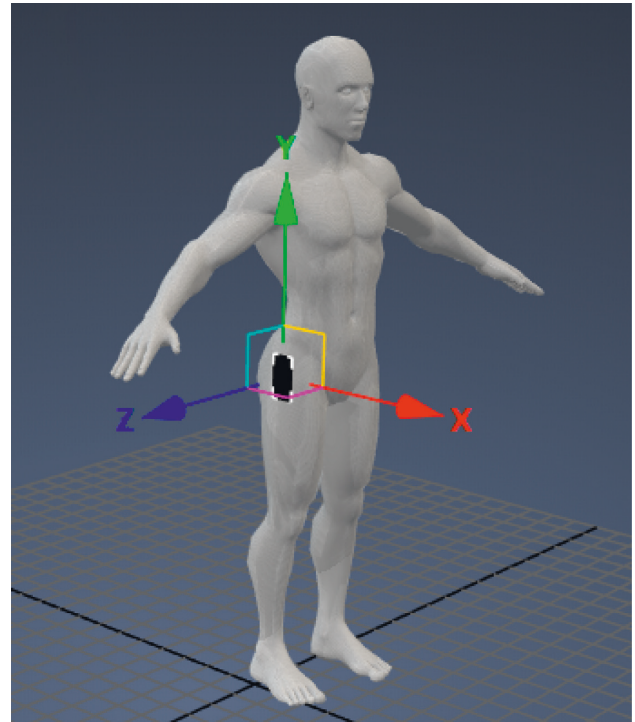

FIGURE 1: The location of the smartphone with the coordinate axes (X, Y, and Z).

The fragments in which the person had not yet started to perform the given physical activity were removed. It is worth noting that the recorded acceleration signals contain a gravitational component. During experiments, the smartphone can slightly change its position in relation to the original (in the x-, y-, and z-axis). In this way, the gravity component would decompose in various degrees into the acceleration components associated with the x, y, and z coordinate systems. To eliminate this problem, we decided to use the absolute value of the acceleration signal for further analysis. In this way single, independent of the change of the smartphone position, acceleration signal was obtained. The absolute value A of the acceleration signals A_X, A_Y, and A_Z (in the three axes) was calculated. The signal A, calculated for each activity, was divided into windows of the width $N = 200$ samples (4 seconds). The windows overlapped every $N/2$ samples.

3.2. Feature Extraction. A set of features was calculated from each signal window. We decided to use simple statistical features such as energy: VAR, maximum value: MAX, minimum value: MIN, skewness: SK, kurtosis: KU, and quantiles of order 0.025, 0.25, 0.5, 0.75, 0.095: $Q025$, $Q25$, $Q5$, $Q75$, $Q095$, respectively [10]. In this way, a set of 10 features was obtained for each window (trial). The number of trials for each activity type per user was 22. For all types of one-user activity, the number of trials was 110 (5 activities × 22 windows).

3.3. Classification. In order to assess the possibility of recognizing user physical activity on the basis of the

acceleration signal, the quadratic discriminant analysis (QDA) [11] classifier was implemented. We decided to use the QDA because we assumed that the features do not have to be separated in a linear way. Another advantage is the ease and speed of training such a classifier in comparison with, for example, neural networks.

The 10-CV test was used as a measure of classification accuracy [12]. In the 10-fold cross-validation test, the original set is randomly partitioned into 10 equal sized subsets. Of the 10 subsets, a single subset is retained as the validation data for testing the model, and the remaining nine subsets are used as data for training. The cross-validation process is then repeated 10 times, with each of the 10 subsets used exactly once as the validation data. The 10 results from the folds are then averaged to produce a single estimation [12].

4. Results

The results for the accuracy of classification of the five activity classes for individual users are presented in Table 1 (user-dependent classification). A confusion matrix for subject S1 is presented in Table 2.

The presented results indicate satisfactory recognition efficiency. For all subjects (Table 1), the recognition accuracy was 92%. For a classifier that acted in a random manner, the accuracy would be 20%. An example of a confusion matrix for the subject S1 (Table 2) indicates the existence of problems in recognition between the activity of going up the stairs (U) and down the stairs (D).

Next, features from all the subjects were used for training and testing the QDA classifier in the user-independent mode. As in the previous case, the 10 CV test was used. The accuracy of classification of the five types of activity for all users together was 82%. The confusion matrix is presented in Table 3. Also in this case, it turned out that problems were encountered in recognition of the activity of going up the stairs (U) and down the stairs (D). In addition, for some subjects, walking (W) was recognized as going down the stairs (D), and going up the stairs (U) was classified as walking (W).

Tests similar to real conditions were also performed. Furthermore, all trials were divided into 75% for training and 25% for testing. In this case, the classification accuracy was equal to 83%.

5. Discussion

Three seconds of the absolute value A of acceleration signal recorded for subject S1 is presented in Figure 2. The highest acceleration values, up to $60\,\mathrm{m/s^2}$, were recorded during running. The smallest accelerations were recorded obviously during the resting status of the user. For walking, we can observe the increases and decreases in acceleration caused by taking each step.

The features for the entire set of acceleration signals recorded for subject S1 were calculated (Table 4). The maximum value of acceleration for going down the stairs (D) was $26\,\mathrm{m/s^2}$, for running (R) was $83.9\,\mathrm{m/s^2}$, for rest (S) was

Table 1: Results of the accuracy of classification of five types of physical activity.

Subject	Accuracy
S1	0.95
S3	0.91
S3	0.90
S4	0.92
Mean	0.92

Table 2: Confusion matrix for subject S1.

		Predicted class				
		D	R	S	U	W
	D	18	0	0	3	0
	R	0	21	0	0	0
True class	S	0	0	21	0	0
	U	1	0	0	20	0
	W	0	0	0	0	21

Table 3: Confusion matrix.

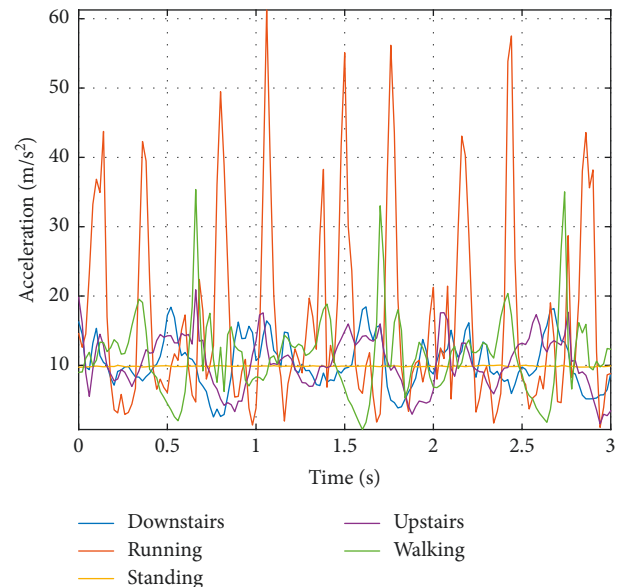|		Predicted class				
		D	R	S	U	W
	D	48	0	0	30	6
	R	0	84	0	0	0
True class	S	0	0	84	0	0
	U	13	0	0	69	2
	W	19	0	0	1	64

Figure 2: Acceleration signal obtained for subject S1 for three seconds for the various physical activities.

$10.6\,\mathrm{m/s^2}$, for going up the stairs (U) was $27.4\,\mathrm{m/s^2}$, and for walking (W) was $48.4\,\mathrm{m/s^2}$.

Histograms of samples of the acceleration signals recorded for different types of activities are presented in Figure 3. Figure 4 presents the distribution of features of the

TABLE 4: Features calculated for subject S1.

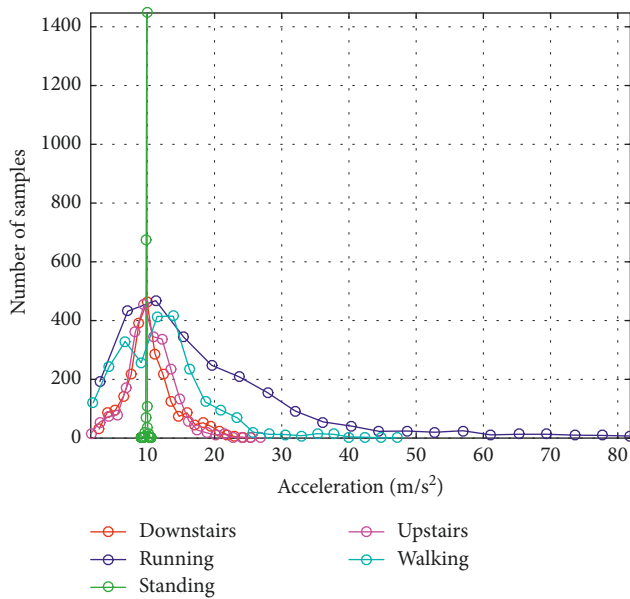| Feature	D	R	S	U	W
VAR	13.7	197.1	0.1	11.4	43.8
MAX	26.0	83.9	10.6	27.4	48.4
MIN	2.2	0.8	8.9	0.9	0.7
SK	0.7	1.8	−0.2	0.3	1.1
KU	3.8	7.1	32.4	4.2	5.8
Q025	3.8	3.3	9.5	3.3	2.3
Q25	8.3	8.9	9.8	8.3	7.1
Q50	9.9	14.4	9.8	10.1	11.8
Q75	12.1	23.4	9.9	12.4	15.1
Q095	6.0	5.2	9.8	6.3	4.0

FIGURE 3: Histograms of samples of the acceleration signals recorded for different types of activities.
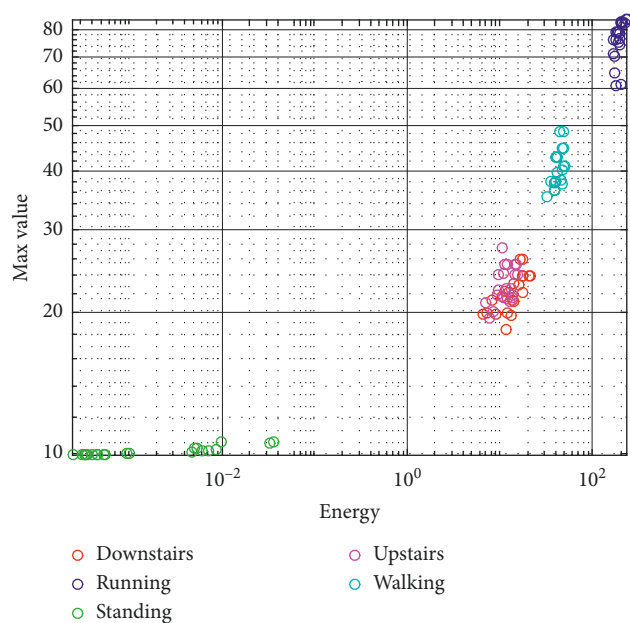

FIGURE 4: Distribution graph of the features of the acceleration signal for subject S1 (4-second window).

acceleration signal for subject S1. The presented results indicate that using only energy and the maximum value of the acceleration signal (calculated for a 4-second window), we can effectively separate activity classes. The problem may be the separation of the activity of going up and down the stairs. The features for these signals are very similar to each other.

Calculations were also carried out to select the best set of features. To this end, the Sequential Forward Selection (SFS) algorithm was used [13]. At this stage, the features collected for all subjects were used. The best features, selected in particular stages of the SFS algorithm, and the accuracy of recognition (ACC) obtained for these features are presented in Table 5. The $Q75$ feature turned out to be the best. The best classification accuracy (0.76) was obtained for three features (KU, $Q25$, and $Q75$).

For comparative purposes, short-time Fourier transform analysis of the recorded acceleration signals was performed [14]. Figure 5 presents the spectrogram for the case in which a user was going down the stairs.

You can observe changes in certain frequencies (5, 12, 21, 28, 34, and 42 seconds) to be dominant. Changes are also caused by the "short walk" on flat places between the building's half-floors.

Figure 6 presents a spectrogram for the case in which the subject was running. We can observe a basic frequency and subsequent harmonics, probably related to the frequency of foot strikes on the ground.

High accuracy of physical activities classification (Tables 1–5) prompts consideration of using the described device in real applications. The best approach seems to be training the recognition system for a specific subject (Table 1). The obtained accuracy of classification was in the range of 90–95%. Results for data collected from all subjects (Table 3) were little less accurate. In this case, the classification accuracy for the five classes was 83%. Simple statistical features and the use of one accelerometer allowed satisfactory results to be obtained.

We performed additional experiments to check whether the use of another classifier could improve the accuracy of movement recognition. For this purpose, commonly known classifiers were tested: decision tree, linear discriminant analysis (LDA), support vector machine (SVM) with linear and quadratic kernel, and nearest neighbor classifier 1-NN. The classification results are shown in Table 6. It turned out that the classification accuracy is better by 2% only when using the SVM classifier with quadratic kernel. Slightly worse results were obtained for the LDA classifier, which implements a linear separation of data. Thus, it seems that the use of the QDA classifier was a good solution.

The accuracy of classification obtained by us is consistent with the results of other studies. In [6], the authors recognize different types of activities (2–6 types) using (2–36) sensors. Most often, these activities include standing, walking, bicycling, running, and going upstairs. The obtained classification results have a very large spread of accuracy, from 42% to 96%. In [15], the dependence of the accuracy of classification on the location of the accelerometer on the subject's body was examined. For most activities, the location turned out to be unimportant, and the accuracy of the

Table 5: The best features: SFS algorithm.

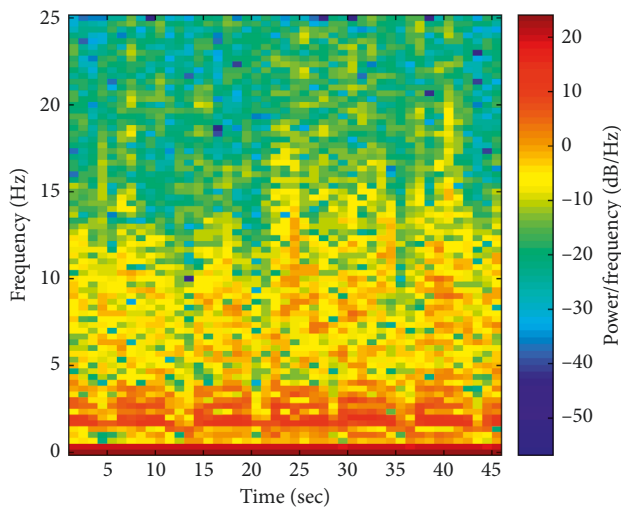| Number of best features	VAR	MAX	MIN	SK	KU	Q025	Q25	Q5	Q75	Q095	ACC
1									×		0.72
2							×		×		0.75
3				×			×		×		0.76
4				×	×		×		×		0.76
5	×			×	×		×		×		0.76
6	×	×		×	×		×		×		0.76
7	×	×		×	×		×	×	×		0.75
8	×	×		×	×	×	×	×	×		0.75
9	×	×	×	×	×	×	×	×	×		0.74
10	×	×	×	×	×	×	×	×	×	×	0.73

Figure 5: Spectrogram of the acceleration signal while descending the stairs.

Figure 6: Spectrogram of the acceleration signal during running.

Table 6: Comparison of classification results.

Classifier type	Classification accuracy (%)
QDA	82
Decision tree	83
LDA	73
SVM-LINEAR	80
SVM-QUADRATIC	84
1-NN	82

recognition accuracy by about 10%. In other studies, the possibility of using only one accelerometer to recognize the type of activity was checked. In [17], six types of activities were identified and statistical and frequency features of the signal were used. The best results (93%) were obtained for the decision tree classifier and time-domain and frequency-domain features (94%).

In summary, it is possible to develop a solution to recognize the user's physical activity using only a smartphone located on the hip. Smartphones are easily available and relatively cheap. In connection with the above, the acceleration classification may be used in fitness applications, which monitor user activity. This mechanism can also be used in the audit of employee activity during the working day. In regards to this topic, the above applications are certainly not exhaustive. With the development of technology, newer sensors are available, but the accelerometer will surely continue to be used in detecting activity.

6. Conclusion

Acceleration signals were recorded for the five basic types of user's physical activities. Based on the results of the classification obtained, we can answer the questions from the beginning of the article. (1) The accelerometer placed on the user's hip distinguishes between several types of the user's physical activity. (2) Simple statistical features of the acceleration signal are enough to recognize basic activities. (3) From the considered list of five types of activities, the most difficult to distinguish were going up the stairs (U) and down the stairs (D). (4) It is possible to create a system that recognizes activity based on data collected only from a specific subject (user-dependent), and the recognition then is much more accurate, over 90%. It is also possible to train system based on features from all subjects (user-independent), but the accuracy of classification is less, about 83%.

classification reached over 90%. In [16], the authors presented a system that used many types of sensors in a smartphone (accelerometer, gyroscope, magnetometer, and barometer) to recognize eight types of activities. For all classifiers, using a combination of four sensors performed better than using only the accelerometer. It improves the

Data Availability

Data used to support the findings of this study are available from the corresponding author upon request.

Conflicts of Interest

The authors declare that there are no conflicts of interest regarding the publication of this paper.

Acknowledgments

References

[1] A. Wattanapisit and S. Thanamee, "Evidence behind 10,000 steps walking," *Journal of Health Research*, vol. 31, no. 3, pp. 241–248, 2017.

[2] C. Tudor-Locke, C. L. Craig, W. J. Brown et al., "How many steps/day are enough? For adults," *International Journal of Behavioral Nutrition and Physical Activity*, vol. 8, no. 1, p. 79, 2011.

[3] A. Wang, G. Chen, J. Yang, S. Zhao, and C.-Y. Chang, "A comparative study on human activity recognition using inertial sensors in a smartphone," *IEEE Sensors Journal*, vol. 16, no. 11, pp. 4566–4578, 2016.

[4] L. Chen, J. Hoey, C. D. Nugent, D. J. Cook, and Z. Yu, "Sensor-based activity recognition," *IEEE Transactions on Systems, Man, and Cybernetics, Part C (Applications and Reviews)*, vol. 42, no. 6, pp. 790–808, 2012.

[5] L. Chen, C. D. Nugent, and H. Wang, "A knowledge-driven approach to activity recognition in smart homes," *IEEE Transactions on Knowledge and Data Engineering*, vol. 24, no. 6, pp. 961–974, 2012.

[6] L. Bao and S. S. Intille, "Activity Recognition from user-annotated acceleration data," in *Pervasive Computing*, A. Ferscha and F. Mattern, Eds., pp. 1–17, Springer, Berlin, Germany, 2004.

[7] A. M. Khan, Y. Young-Koo Lee, S. Y. Lee, and T. Tae-Seong Kim, "A triaxial accelerometer-based physical-activity recognition via augmented-signal features and a hierarchical recognizer," *IEEE Transactions on Information Technology in Biomedicine*, vol. 14, no. 5, pp. 1166–1172, 2010.

[8] Y. Zheng, W.-K. Wong, X. Guan, and S. Trost, "Physical activity recognition from accelerometer data using a multi-scale ensemble method," in *Proceedings of Twenty-Seventh AAAI Conference on Artificial Intelligence*, pp. 1575–1581, Bellevue, WA, USA, July 2013.

[9] X. Hong and C. D. Nugent, "Partitioning time series sensor data for activity recognition," in *Proceedings of 9th International Conference on Information Technology and Applications in Biomedicine*, pp. 1–4, Larnaka, Cyprus, November 2009.

[10] E. Langford, "Quartiles in elementary statistics," *Journal of Statistics Education*, vol. 14, no. 3, 2006.

[11] A. Nefedov, J. Ye, C. Kulikowski, I. Muchnik, and K. Morgan, "Comparative analysis of support vector machines based on linear and quadratic optimization criteria," in *Proceedings of International Conference on Machine Learning and Applications*, pp. 288–293, Miami, FL, USA, July 2009.

[12] R. Kohavi, "A study of cross-validation and bootstrap for accuracy estimation and model selection," in *Proceedings of International Joint Conference on Artificial Intelligence IJCAI*, pp. 1137–1143, Montreal, QC, Canada, 1995.

[13] S. J. Reeves and Z. Zhao Zhe, "Sequential algorithms for observation selection," *IEEE Transactions on Signal Processing*, vol. 47, no. 1, pp. 123–132, 1999.

[14] D. Griffin and J. Jae Lim, "Signal estimation from modified short-time fourier transform," *IEEE Transactions on Acoustics, Speech, and Signal Processing*, vol. 32, no. 2, pp. 236–243, 1984.

[15] U. Maurer, A. Smailagic, D. P. Siewiorek, and M. Deisher, "Activity recognition and monitoring using multiple sensors on different body positions," in *Proceedings of International Workshop on Wearable and Implantable Body Sensor Networks (BSN'06)*, vol. 4, p. 116, Cambridge, UK, April 2006.

[16] F. Gu, K. Khoshelham, and S. Valaee, "Locomotion activity recognition: a deep learning approach," in *Proceedings of IEEE 28th Annual International Symposium on Personal, Indoor, and Mobile Radio Communications (PIMRC)*, pp. 1–5, Montreal, QC, Canada, October 2017.

[17] A. S. A. Sukor, A. Zakaria, and N. A. Rahim, "Activity recognition using accelerometer sensor and machine learning classifiers," in *Proceedings of IEEE 14th International Colloquium on Signal Processing Its Applications (CSPA)*, pp. 233–238, Pulau Pinang, Malaysia, March 2018.